1

Theory of Micelle Formation

Quantitative Approach to Predicting Micellar Properties from Surfactant Molecular Structure

R. NAGARAJAN The Pennsylvania State University, University Park, Pennsylvania, U.S.A.

I. INTRODUCTION

The numerous, practical applications of surfactants have their basis in the intrinsic duality of their molecular characteristics, namely, they are composed of a polar headgroup that likes water and a nonpolar tail group that dislikes water. A number of variations are possible in the types of the headgroup and tail group of surfactants. For example, the headgroup can be anionic, cationic, zwitterionic, or nonionic. It can be small and compact in size or an oligomeric chain. The tail group can be a hydrocarbon, fluorocarbon, or a siloxane. It can contain straight chains, branched or ring structures, multiple chains, etc. Surfactant molecules with two headgroups (bola surfactants) are also available. Further, the headgroups and tail groups can be polymeric in character, as in the case of block copolymers. This variety in the molecular structure of surfactants allows for extensive variation in their solution and interfacial properties. It is natural that one would like to discover the link between the molecular structure of the surfactant and its physicochemical action so that surfactants can be synthesized or selected specific to a given practical application.

Pioneering contributions to our understanding of the general principles of surfactant self-assembly in solutions have come from the early studies of Tanford [1–3], Shinoda [4], and Mukerjee [5–9]. Utilizing their results, we have focused our effort in the last 25 years, on developing quantitative molecular thermodynamic models to predict the aggregation behavior of surfactants in solutions starting from the surfactant molecular structure

and the solution conditions. In our approach, the physicochemical factors controlling self-assembly are first identified by examining all the changes experienced by a singly dispersed surfactant molecule when it becomes part of an aggregate [10–16]. Relatively simple, explicit analytical equations are then formulated to calculate the contribution to the free energy of aggregation associated with each of these factors. Because the chemical structure of the surfactant and the solution conditions are sufficient for estimating the molecular constants appearing in these equations, the free energy expressions can be used to make completely a priori predictions.

In this chapter we describe in detail our quantitative approach to predicting the aggregation properties of surfactants from their molecular structures. In Section II we present the general thermodynamic equations that govern the aggregation properties of surfactants in solutions. Many conclusions about the aggregation behavior can be drawn from such analysis without invoking any specific models to describe the aggregates. In Section III we summarize the geometrical relations for various shapes of aggregates including spherical, globular, and rodlike micelles and spherical bilayer vesicles, consistent with molecular packing considerations as had been discussed many years ago by Tartar [17]. These considerations lead us to the concept of the packing parameter proposed by Israelachvili et al. [18] that has been widely cited in the literature. The molecular packing model, as it is currently used, is built on the free energy model of Tanford [1]. We examine its predictive power and then show that the model neglects some tail length-dependent free energy contributions; if these are included, they will lead to significantly different predictions of the aggregation behavior. In Section IV the molecular theory of micelle formation is described. The central feature of the theory is the postulation of explicit equations to calculate the free energy of formation of different types of aggregates invoking phenomenological concepts. We suggest how the molecular constants appearing in these equations can be estimated and describe the computational approach suitable for making predictive calculations. We then demonstrate the predictive power of the molecular theory via illustrative calculations performed on a number of surfactant molecules having a variety of headgroups and tail groups. This molecular theory presented in this section is the point of departure for all subsequent models described in this chapter and also for other aggregation phenomena involving solvent mixtures, solubilization, microemulsions, etc. that have been described elsewhere [19]. In Section V we extend the molecular theory to binary mixtures of surfactants and demonstrate its predictive ability for a variety of ideal and nonideal surfactant mixtures. The model is then applied to surfactants in the presence of nonionic polymers in Section VI. How the nonionic polymer changes the aggregate morphology, in addition to the critical concentrations

and aggregate microstructures, is explored in this section. The extension of the free energy model to block copolymers is done in Section VII, where the polymeric nature of the headgroup and the tail group of the molecule is taken into consideration in constructing the free energy expressions. The analogy between low-molecular-weight conventional surfactants and the block copolymer amphiphiles is discussed in this section. The last section presents some conclusions.

II. THERMODYNAMIC PRINCIPLES OF AGGREGATION

A. Aggregate Shapes

Figure 1 illustrates the shapes of surfactant aggregates formed in dilute solutions. The small micelles are spherical in shape. When large rodlike micelles form, they are visualized as having a cylindrical middle portion and parts of spheres as endcaps. The cylindrical middle and the spherical endcaps are allowed to have different diameters. When micelles cannot pack any more into spheres, and if at the same time the rodlike micelles are not yet favored by equilibrium considerations, then small, nonspherical globular aggregates form. Israelachvili et al. [18] have suggested globular shapes generated via ellipses of revolution for the aggregates in the sphere-to-rod transition region, after examining the local molecular packing requirements for various nonspherical shapes. The average surface area per surfactant molecule of the ellipses of revolution suggested by Israelachvili et al. [18] is practically the same as that of prolate ellipsoids, for aggregation numbers up to 3 times larger than the largest spherical micelles,. Therefore, the average geometrical properties of globular aggregates in the sphere-to-rod transition region can be computed as for prolate ellipsoids. Some surfactants pack into a spherical bilayer structure called a vesicle that encloses an aqueous cavity. In the outer and the inner layers of the vesicle, the surface area (in contact with water) per surfactant molecule, and the number of surfactant molecules need not be equal to one another and the thicknesses of the two layers can also be different.

In addition to the variety of shapes, it is also natural to expect that surfactant aggregates of various sizes will exist in solution. The size distribution can be represented in terms of a distribution of the number of surfactant molecules constituting the aggregate (i.e., the aggregation number g).

B. Size Distribution of Aggregates

Important results related to the size distribution of aggregates can be obtained from the application of general thermodynamic principles to surfactant solutions. The surfactant solution is a multicomponent system con-

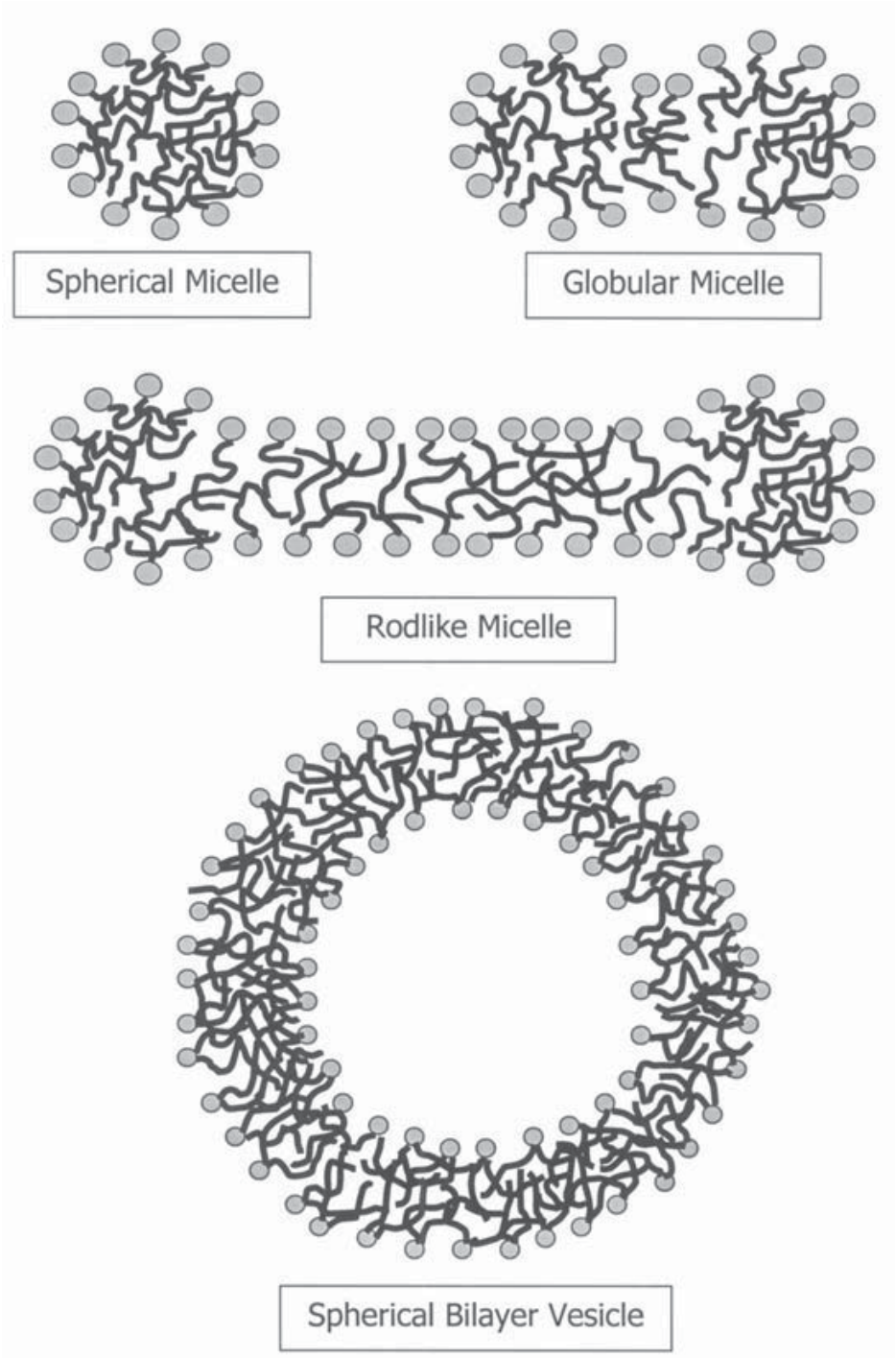

FIG. 1 Schematic representation of surfactant aggregates in dilute aqueous solutions. The structures formed include spherical micelles (a), globular micelles (b), spherocylindrical micelles (c), and spherical bilayer vesicles (d).

sisting of N_W water molecules, N_1 singly dispersed surfactant molecules, and N_g aggregates of aggregation number g, where g can take all values from 2 to ∞. (The subscript W refers to water, 1 to the singly dispersed surfactant, and g to the aggregate containing g surfactant molecules.) All shapes of

aggregates are considered. Each of the aggregates of a given shape and size is treated as a distinct chemical component described by a characteristic chemical potential. The total Gibbs free energy of the solution G, expressed in terms of the chemical potentials μ_i of the various species i, has the form

$$G = N_w\mu_w + N_1\mu_1 + \sum_{g=2}^{g=\infty} N_g\mu_g \tag{1}$$

The equilibrium condition of a minimum of the free energy leads to

$$\frac{\mu_g}{g} = \mu_1 \tag{2}$$

This equation stipulates that the chemical potential of the singly dispersed surfactant molecule is equal to the chemical potential per molecule of an aggregate of any size and shape. Assuming a dilute surfactant solution, one can write a simple expression for the chemical potential of an aggregate of size g (for all values of g including $g = 1$) in the form:

$$\mu_g = \mu_g^0 + kT \ln X_g \tag{3}$$

where μ_g^0 is the standard state chemical potential of the species g and X_g is its mole fraction in solution. The standard states of all the species other than the solvent are taken as those corresponding to infinitely dilute solution conditions. The standard state of the solvent is defined as the pure solvent. Introducing the expression for the chemical potential in the equilibrium relation [(Eq. 2)], one gets the aggregate size distribution equation:

$$X_g = X_1^g \exp -\left(\frac{\mu_g^0 - g\mu_1^0}{kT}\right) = X_1^g \exp -\left(\frac{g\Delta\mu_g^0}{kT}\right) \tag{4}$$

where $\Delta\mu_g^0$ is the difference in the standard chemical potentials between a surfactant molecule present in an aggregate of size g and a singly dispersed surfactant in water [1]. If an expression for $\Delta\mu_g^0$ is available, then from Eq. (4), the aggregate size distribution can be calculated. From the aggregate size distribution, all other important and experimentally accessible solution properties can be computed as described below.

C. Calculating CMC, Micelle Size, and Aggregate Polydispersity

1. Critical Micelle Concentration (CMC)

The critical micelle concentration can be calculated from the aggregate size distribution by constructing a plot of one of the functions X_1, $\sum X_g$, $\sum gX_g$, or $\sum g^2X_g$ (which are proportional to different experimentally measured

properties of the surfactant solution such as surface tension, electrical conductivity, dye solubilization, light scattering intensity, etc.) against the total concentration $X_{\text{tot}}(= X_1 + \sum gX_g)$ of the surfactant in solution [1,20–22]. In all cases, the summation extends from 2 to ∞. The CMC can be identified as that value of the total surfactant concentration at which a sharp change in the plotted function (representing a physical property) occurs. The CMC has also been estimated as that value of X_1 for which the concentration of the singly dispersed surfactant is equal to that of the surfactant present in the form of aggregates, namely, $X_1 = \sum gX_g = X_{\text{CMC}}$ [23]. For surfactants in aqueous solutions, the estimates of the CMC obtained by the different methods mentioned above are usually close to one another, though not identical [20].

2. Average Micelle Size

From the size distribution one can compute various average sizes of the aggregates based on the definitions

$$g_n = \frac{\sum gX_g}{\sum X_g}, \qquad g_w = \frac{\sum g^2 X_g}{\sum gX_g}, \qquad g_z = \frac{\sum g^3 X_g}{\sum g^2 X_g} \tag{5}$$

where g_n, g_w, and g_z denote the number average, the weight average, and the z average aggregation numbers, respectively, and the summations extend from 2 to ∞, as mentioned earlier. The different average aggregation numbers correspond to those determined by different experimental techniques; for example, g_n is obtained via membrane osmometry, g_w via static light scattering, and g_z via intrinsic viscosity measurements. If the summations in Eq. (5) extend from 1 to ∞ (i.e., include the singly dispersed surfactant molecules), then one obtains apparent (as opposed to true) average aggregation numbers $g_{n,\text{app}}$, $g_{w,\text{app}}$, and $g_{z,\text{app}}$.

3. Aggregate Size Polydispersity

For nonionic and zwitterionic surfactants, the standard state free energy difference $\Delta\mu_g^0$ appearing in Eq. (4) is not dependent on the concentration of the singly dispersed surfactant X_1 or on the total concentration of the surfactant. Consequently, by taking the derivative of the size distribution relation with respect to X_1 , one obtains [24–26]:

$$\begin{aligned}
\partial \ln \sum X_g &= \frac{1}{\sum X_g}\left[\sum gX_g \partial \ln X_1\right] = g_n \partial \ln X_1 \\
\partial \ln \sum gX_g &= \frac{1}{\sum gX_g}\left[\sum g^2 X_g \partial \ln X_1\right] = g_w \partial \ln X_1 \\
\partial \ln \sum g^2 X_g &= \frac{1}{\sum g^2 X_g}\left[\sum g^3 X_g \partial \ln X_1\right] = g_z \partial \ln X_1
\end{aligned} \tag{6}$$

where the average aggregation numbers defined by Eq. (5) have been introduced. Equation (6) shows that the average aggregation numbers g_n and g_w depend on the concentration $(X_{\text{tot}} - X_1)$ of the micellized surfactant as follows (note that $\sum gX_g = X_{tot} - X_1$):

$$\begin{aligned} \partial \ln g_n &= \left(1 - \frac{g_n}{g_w}\right) \partial \ln \sum gX_g \\ \partial \ln g_w &= \left(\frac{g_z}{g_w} - 1\right) \partial \ln \sum gX_g \end{aligned} \tag{7}$$

The variances of the size dispersion $\sigma^2(n)$ and $\sigma^2(w)$ are defined by the relations:

$$\begin{aligned} \sigma^2(n) &= \frac{\sum (g - g_n)^2 X_g}{\sum X_g} = g_n^2 \left(\frac{g_w}{g_n} - 1\right) \\ \sigma^2(w) &= \frac{\sum (g - g_w)^2 g X_g}{\sum g X_g} = g_w^2 \left(\frac{g_z}{g_w} - 1\right) \end{aligned} \tag{8}$$

Combining Eqs. (7) and (8), we can relate the variance of the size distribution to the concentration dependence of the average aggregation number as follows:

$$\begin{aligned} \left(\frac{\sigma(n)}{g_n}\right)^2 &= \frac{g_w}{g_n} - 1 = \left(1 - \frac{\partial \ln g_n}{\partial \ln \sum gX_g}\right)^{-1} - 1 \approx \frac{\partial \ln g_n}{\partial \ln \sum gX_g} \\ \left(\frac{\sigma(w)}{g_w}\right)^2 &= \frac{g_z}{g_w} - 1 = \frac{\partial \ln g_w}{\partial \ln \sum gX_g} \end{aligned} \tag{9}$$

Equation (9) states that the average aggregation numbers g_n and g_w must increase appreciably with increasing concentration of the aggregated surfactant if the micelles are polydispersed [$\sigma(n)/g_n$ and $\sigma(w)/g_w$ are large]; the average aggregation numbers must be virtually independent of the aggregated surfactant concentration if the micelles are narrowly dispersed.

For ionic surfactants, $\Delta\mu_g^0$ is dependent on the ionic strength of the solution (discussed in Section IV.A) and thus on the concentration of the surfactant, making Eq. (6) inapplicable to them. However, it has been shown that Eq. (9) derived for nonionic and zwitterionic surfactants based on general thermodynamic considerations is valid also for ionic surfactants [25,26].

D. Sphere-to-Rod Transition of Micelles

Micelles having spherical or globular shapes are usually small and narrowly dispersed. A different micellization behavior is, however, observed when

large rodlike micelles are generated [5–9]. These aggregates are visualized as having a cylindrical middle part with two spherical endcaps as shown in Fig. 1. The standard chemical potential of a rodlike aggregate of size g containing g_{cap} molecules in the two spherical endcaps and $(g - g_{cap})$ molecules in the cylindrical middle can be written [5–9,16,18,27] as

$$\mu_g^0 = (g - g_{cap})\mu_{cyl}^0 + g_{cap}\mu_{cap}^0 \tag{10}$$

where μ_{cyl}^0 and μ_{cap}^0 are the standard chemical potentials of the molecules in the two regions of the rodlike aggregate, respectively. Introducing the above relation in the aggregate size distribution [Eq. (4)] yields

$$X_g = \left[X_1 \exp - \left(\frac{\Delta\mu_{cyl}^0}{kT}\right)\right]^g \exp\left(-g_{cap}\,\frac{\Delta\mu_{cap}^0 - \Delta\mu_{cyl}^0}{kT}\right) \tag{11}$$

where $\Delta\mu_{cyl}^0$ and $\Delta\mu_{cap}^0$ are the differences in the standard chemical potentials between a surfactant molecule in the cylindrical middle or the endcaps of the spherocylindrical micelle and a singly dispersed surfactant molecule. Equation (11) can be rewritten as

$$\begin{aligned} X_g &= \frac{1}{K}\,Y^g, \qquad Y = \left[X_1 \exp\left(\frac{\Delta\mu_{cyl}^0}{kT}\right)\right], \\ K &= \exp\left(g_{cap}\,\frac{\Delta\mu_{cap}^0 - \Delta\mu_{cyl}^0}{kT}\right) \end{aligned} \tag{12}$$

where K is a measure of the free energy advantage for a molecule present in the cylindrical portion compared to that in the spherical endcaps. The possibility of occurrence of rodlike aggregates at a given concentration X_1 of the singly dispersed surfactant molecules is indicated by the proximity of the parameter Y to unity. The average aggregation numbers defined by Eq. (5) can be computed on the basis of the size distribution Eq. (12), by performing the analytical summation of the series functions [5–9,18]:

$$g_n = g_{cap} + \left(\frac{Y}{1 - Y}\right), \qquad g_w = g_{cap} + \left(\frac{Y}{1 - Y}\right)\left(1 + \frac{1}{Y + g_{cap}(1 - Y)}\right) \tag{13}$$

The total concentration of surfactant present in the aggregated state can be also calculated analytically [5–9,18] and is given by the expression

$$\sum gX_g = \frac{1}{K}\left(\frac{g_{cap}\,Y^{g_{cap}}}{1 - Y}\right)\left(1 + \frac{Y}{g_{cap}(1 - Y)}\right) \tag{14}$$

Equation (13) shows that for values of Y close to unity, very large aggregates are formed. In the limit of Y close to unity and $g_{cap}(1 - Y) \ll 1$, Eqs. (13) and (14) reduce to

$$\sum gX_g = \frac{1}{K}\left(\frac{1}{1-Y}\right)^2, \quad g_n = g_{cap} + \left(\frac{Y}{1-Y}\right), \quad g_w = g_{cap} + 2\left(\frac{Y}{1-Y}\right) \tag{15}$$

Noting that $\sum gX_g = X_{tot} - X_1$, the dependence of the average aggregation numbers on the surfactant concentration is obtained:

$$\begin{aligned} g_n &= g_{cap} + \left(\frac{1}{1-Y}\right) = g_{cap} + (K(X_{tot} - X_1))^{1/2} \\ g_w &= g_{cap} + \left(\frac{2}{1-Y}\right) = g_{cap} + 2(K(X_{tot} - X_1))^{1/2} \end{aligned} \tag{16}$$

It is evident from Eq. (16) that the weight average and the number average aggregation numbers must substantially deviate from one another if rodlike micelles form (i.e., g_n, $g_w \gg g_{cap}$), indicating large polydispersity in the micellar size. The polydispersity index g_w/g_n is close to 2 at sufficiently large surfactant concentrations. Further, the sphere-to-rod transition parameter K must be in the range of 10^8 to 10^{12}, if the rodlike micelles are to form at physically realistic surfactant concentrations [5–9,18,27]. The critical micelle concentration is calculated from Eq. (12) with the recognition that Y is close to unity:

$$X_1 = X_{CMC} = \exp\left(\frac{\Delta\mu^0_{cyl}}{kT}\right) \tag{17}$$

The thermodynamic results obtained so far are independent of any specific expression for the standard free energy change $\Delta\mu^0_g$ associated with aggregation and constitute general theoretical principles governing the aggregation behavior of surfactants. However, to perform quantitative predictive calculations of the aggregation behavior, specific expressions for $\Delta\mu^0_g$ are needed. In the following section, we will introduce the expression for $\Delta\mu^0_g$ formulated by Tanford [1–3] on a phenomenological basis and use it to examine the molecular packing model of aggregation that is widely cited in the literature on self-assembly.

III. MOLECULAR PACKING MODEL

A. Packing Constraint and Packing Parameter

The notion of molecular packing into various aggregate shapes has been recognized in the early work of Tartar [17] and Tanford [1-3], as can be seen, for example, from Figure 9.1 of Tanford's classic monograph (1). However, only after this concept was explored thoroughly in the work of Israelachvili et al. [18], taking the form of the packing parameter, has it evoked wide appreciation in the literature.

We start by recognizing that the hydrophobic domain of a surfactant aggregate contains the surfactant tails. If the density in this domain is equal to that in similar hydrocarbon liquids, the surfactant tails must entirely fill the space in this domain. This implies that, irrespective of the shape of the aggregate, no point within the aggregate can be farther than the distance ℓ_S from the aggregate–water interface, where ℓ_S is the extended length of the surfactant tail. Therefore, at least one dimension of the surfactant aggregate should be smaller than or at most equal to $2\ell_S$ [1–3,17,18]. The volume of the hydrophobic domain is determined from the number of surfactant molecules g in the aggregate and the volume v_S of the surfactant tail. The molecular packing parameter is defined as $v_S/a\ell_S$, where v_S and ℓ_S are the volume and the length of the surfactant tail and a is the surface area of the hydrophobic core of the aggregate expressed per surfactant molecule constituting the aggregate (hereafter referred to as the area per molecule). As we will see below, the concept of the molecular packing parameter allows a simple and intuitive insight into the self-assembly phenomenon.

B. Geometrical Relations for Aggregates

For aggregates of various shapes containing g surfactant molecules, the volume of the hydrophobic domain of the aggregate, V_g , the surface area of contact between the aggregate and water, A_g, and the surface area at a distance δ from the aggregate–water interface, $A_{g\delta}$, are listed in Table 1. Also given in the table is a packing factor P, defined in terms of the geometrical variables characterizing the aggregate. Note that P is slightly different from the packing parameter $v_S/a\ell_S$ introduced above. The area $A_{g\delta}$ is employed in the computation of the free energy of electrostatic interactions between surfactant headgroups, while the packing factor P is used in the computation of the free energy of tail deformation, both discussed later in this chapter.

From the geometrical relations provided in Table 1, it can be seen that, given any surfactant molecule, the geometrical properties of spherical or

globular micelles depend only on the aggregation number g. In the case of rodlike micelles, the geometrical properties are dependent on two variables—the radius of the cylindrical part and the radius of the spherical endcaps. For spherical bilayer vesicles, any three variables, such as the aggregation number g and the thicknesses t_i and t_o of the inner and outer layers of the bilayer, determine the geometrical properties.

C. Packing Parameter and Predicting Aggregate Shapes

If we consider a spherical micelle with a core radius R_S, made up of g molecules, then the volume of the core $V_g = gv_S = 4\pi R_S^3/3$ and the surface area of the core $A_g = ga = 4\pi R_S^2$; and from these simple geometrical relations we get $R_S = 3v_S/a$. If the micelle core is packed with surfactant tails without any empty space, then the radius R_S cannot exceed the extended length ℓ_S of the tail. Introducing this constraint in the expression for R_S, one obtains, $0 \leq v_S/a\ell_s \leq 1/3$, for spherical micelles.

Similarly for cylindrical or bilayer aggregates made up of g surfactant molecules, the geometrical relations for the volume V_g and the surface area A_g are given in Table 1. These geometrical relations, together with the constraint that at least one dimension of the aggregate (the radius of the sphere or the cylinder, or the half-bilayer thickness) cannot exceed ℓ_s, lead to the following well-known [18] connection between the molecular packing parameter and the aggregate shape: $0 \leq v_S/a\ell_s \leq 1/3$ for sphere; $1/3 \leq v_S/a\ell_s \leq 1/2$ for cylinder; and $1/2 \leq v_S/a\ell_S \leq 1$ for bilayer. Therefore, if we know the molecular packing parameter, the shape and size of the equilibrium aggregate can be readily identified as shown above. This is the predictive sense in which the molecular packing parameter of Israelachvili et al. [18] has found significant use in the literature.

For common surfactants, the ratio v_S/ℓ_S is a constant independent of tail length, equal to 21Å^2 for single tail and 42Å^2 for double tail (1). Consequently, in the packing parameter $v_S/a\ell_S$, only the area a reflects the specificity of the surfactant. The area per molecule a is a *thermodynamic quantity obtained from equilibrium considerations of minimum free energy* and is *not a simple variable connected to the geometrical shape and size of the surfactant headgroup*. To estimate a, Israelachvili et al. [18] invoked the model for the standard free energy change on aggregation pioneered by Tanford [1]. In the framework of Tanford's free energy model, the area a is influenced directly by the surfactant headgroup interactions. Hence, the accepted notion in the surfactant literature is, given a headgroup, a is fixed—which then, determines the packing parameter $v_S/a\ell_S$—thus, the headgroup controls the equilibrium aggregate structure.

TABLE 1 Geometrical Properties of Surfactant Aggregates

Spherical micelles (radius $R_S \leq \ell_S$):

$$V_g = \frac{4\pi R_S^3}{3} = g v_S$$

$$A_g = 4\pi R_S^2 = ga$$

$$A_{g\delta} = 4\pi(R_S + \delta)^2 = g a_\delta$$

$$P = \frac{V_g}{A_g R_S} = \frac{v_S}{a R_S} = \frac{1}{3}$$

Globular micelles (semiminor axis $R_S = \ell_s$, semimajor axis $b \leq 3\ell_S$, eccentricity E):

$$V_g = \frac{4\pi R_S^2 b}{3} = g v_S$$

$$A_g = 2\pi R_S^2 \left[1 + \frac{\sin^{-1} E}{E(1 - E^2)^{1/2}} \right] = ga, \qquad E = \left[1 - \left(\frac{R_S}{b} \right)^2 \right]^{1/2}$$

$$A_{g\delta} = 2\pi(R_S + \delta)^2 \left[1 + \frac{\sin^{-1} E_\delta}{E_\delta(1 - E_\delta^2)^{1/2}} \right] = g_{a_\delta}, \qquad E_\delta = \left[1 - \left(\frac{R_S + \delta}{b + \delta} \right)^2 \right]^{1/2}$$

$$P = \frac{V_g}{A_g R_S} = \frac{v_S}{a R_S}, \qquad \frac{1}{3} \leq P \leq 0.406, \qquad R_{eq} = \left(\frac{3V_g}{4\pi} \right)^{1/3}$$

Cylindrical part of rodlike micelles (radius $R_C \leq \ell_s$, length L_C):

$$V_g = \pi R_C^2 L_C = g v_S$$

$$A_g = 2\pi R_C L_C = ga, \qquad A_{g\delta} = 2\pi(R_C + \delta) L_C = g a_\delta$$

$$P = \frac{V_g}{A_g R_C} = \frac{v_S}{a R_C} = \frac{1}{2}$$

Endcaps of rodlike micelles (endcap radius $R_S \leq \ell_S$, cylinder radius $R_C \leq \ell_S$):

$$H = R_S[1 - \{1 - (R_C/R_S)^2\}^{1/2}]$$

$$V_g = \left[\frac{8\pi R_S^3}{3} - \frac{2\pi}{3} H^2(3R_S - H) \right] = g v_S$$

$$A_g = [8\pi R_S^2 - 4\pi R_S H] = ga$$

$$A_{g\delta} = [8\pi(R_S + \delta)^2 - 4\pi(R_S + \delta)(H + \delta)] = g a_\delta$$

$$P = \frac{V_g}{A_g R_S} = \frac{v_S}{a R_S}$$

TABLE 1 Continued

Spherical vesicles (inner/outer radii R_i, R_o; inner/outer layer thickness t_i, $t_o \leq \ell_s$);

$$V_g = \frac{4\pi[R_o^3 - R_i^3]}{3} = g v_S, \qquad g = g_o + g_i$$

$$V_{go} = \frac{4\pi[R_o^3 - (R_o - t_o)^3]}{3} = g_o v_S$$

$$V_{gi} = \frac{4\pi[(R_i + t_i)^3 - R_i^3)}{3} = g_i v_S$$

$$A_{go} = 4\pi R_o^2, \qquad A_{gi} = 4\pi R_i^2$$

$$A_{g\delta o} = 4\pi(R_o + \delta)^2 = g_o a_{\delta o}$$

$$A_{g\delta i} = 4\pi(R_i - \delta)^2 = g_i a_{\delta i}$$

D. Estimating Equilibrium Area from Tanford's Free Energy Model

In his phenomenological model Tanford suggests that the standard free energy change associated with the transfer of a surfactant molecule from its infinitely dilute state in water to an aggregate of size g (aggregation number) has three contributions:

$$\left(\Delta\mu_g^0\right) = \left(\Delta\mu_g^0\right)_{\text{Transfer}} + \left(\Delta\mu_g^0\right)_{\text{Interface}} + \left(\Delta\mu_g^0\right)_{\text{Head}} \tag{18}$$

The first term, $(\Delta\mu_g^0)_{\text{Transfer}}$, is a negative free energy contribution arising from the transfer of the tail from its unfavorable contact with water to the hydrocarbonlike environment of the aggregate core. The transfer free energy contribution depends on the surfactant tail but not on the aggregate shape or size. The second term, $(\Delta\mu_g^0)_{\text{Interface}}$, provides a positive contribution to account for the fact that the entire surface area of the tail is not removed from water but there is still residual contact with water at the surface of the aggregate core. This is represented as the product of a contact free energy per unit area σ (or an interfacial free energy) and the surface area per molecule of the aggregate core, a. The third term, $(\Delta\mu_g^0)_{\text{Head}}$, provides another positive contribution representing the repulsive interactions between the headgroups that crowd at the aggregate surface. Because the repulsion would increase if the headgroups came close to one another, Tanford proposed an expression with an inverse dependence on a. Thus,

the standard free energy change per molecule on aggregation proposed by Tanford has the form

$$\left(\Delta\mu_g^0\right) = \left(\Delta\mu_g^0\right)_{\text{Transfer}} + \sigma a + \alpha/a \tag{19}$$

where α is the headgroup repulsion parameter.

Starting from the free energy model of Tanford, the equilibrium aggregation behavior can be examined either by treating the surfactant solution as consisting of aggregates with a distribution of sizes or by treating the aggregate as constituting a pseudophase [1–3,15]. If the aggregate is viewed as a pseudophase, in the sense of small systems thermodynamics, the equilibrium condition corresponds to a minimum in the standard free energy change $(\Delta\mu_g^0)$. The minimization can be done with respect to either the aggregation number g or the area per molecule a, since they are dependent on one another through the geometrical relations given in Table 1. In this manner one obtains the equilibrium area per molecule of the aggregate:

$$\frac{\partial}{\partial a}\left(\Delta\mu_g^0\right) = 0 \Rightarrow \sigma - \frac{\alpha}{a^2} = 0 \Rightarrow a = \left(\frac{\alpha}{\sigma}\right)^{1/2} \tag{20}$$

The critical micelle concentration (CMC, denoted as X_{CMC} in mole fraction units) in the pseudophase approximation is obtained from the relation

$$\ln X_{\text{CMC}} = \left(\frac{\Delta\mu_g^0}{kT}\right) = \left(\frac{\Delta\mu_g^0}{kT}\right)_{\text{Transfer}} + \left(\frac{\sigma}{kT}\right)a + \left(\frac{\alpha}{kT}\right)\frac{1}{a} \tag{21}$$

where the area a now stands for the equilibrium estimate given by Eq. (20).

In Tanford's free energy expression [Eq. (19)], the first contribution, the tail transfer free energy, is negative. Hence, this contribution is responsible for the aggregation to occur. It affects only the CMC [as shown by Eq. (21)] but not the equilibrium area a [as shown by Eq. (20)]. Hence it does not affect the size and shape of the aggregate. The second contribution, the free energy of residual contact between the aggregate core and water, is positive and decreases in magnitude as the area a decreases. A decrease in the area a corresponds to an increase in the aggregation number g, for all aggregate shapes, as shown by the geometrical relations in Table 1. Hence, this contribution promotes the growth of the aggregate. The third contribution, the free energy due to headgroup repulsions, is also positive and increases in magnitude if the area a decreases or the aggregation number g increases. Hence, this contribution is responsible for limiting the growth of aggregates to a finite size. Thus, Tanford's model clearly identifies why aggregates form, why they grow, and why they do not keep growing but remain finite in size.

E. Predictive Power of Molecular Packing Model

The packing parameter $v_S/a\ell_S$ can be estimated using the equilibrium area a obtained from Eq. (20). One can observe that a will be small and the packing parameter will be large if the headgroup interaction parameter α is small. The area a will increase and the packing parameter will decrease if the interfacial free energy per unit area σ decreases. These simple considerations allow one to predict many features of surfactant self-assembly as summarized below.

1. For nonionic surfactants with ethylene oxide units as the headgroup, the headgroup parameter α can be expected to increase in magnitude if the number of ethylene oxide units in the headgroup increases. Therefore, when the number of ethylene oxide units is small, α is small, a is small, $v_S/a\ell_S$ is large, and bilayer aggregates (lamellae) are favored. For larger number of ethylene oxide units, α increases, a increases, $v_S/a\ell_S$ decreases, and cylindrical micelles become possible. When the number of ethylene oxide units is further increased, a becomes very large, $v_S/a\ell_S$ becomes small enough so that spherical micelles will form with their aggregation number g decreasing with increasing ethylene oxide chain length.

2. Comparing nonionic and ionic surfactants, the headgroup interaction parameter α will be smaller for nonionics than for ionics, because one has to also consider ionic repulsions in the latter case. Therefore, a will be smaller and $v_S/a\ell_S$ will be larger for the nonionics compared to the ionics. As a result, nonionic surfactants would form aggregates of larger aggregation number compared to ionic surfactants of the same tail length.

3. For a given surfactant molecule, the headgroup repulsion can be decreased by modifying the solution conditions. For example, adding salt to an ionic surfactant solution decreases ionic repulsions; increasing the temperature for a nonionic surfactant molecule with an ethylene oxide headgroup decreases steric repulsions. Because α decreases, a will decrease and $v_S/a\ell_S$ will increase. Thus, one can achieve a transition from spherical micelles to rodlike micelles, and possibly to bilayer aggregates, by modifying solution conditions that control headgroup repulsions.

4. If single-tail and double-tail surfactant molecules are compared, for the same equilibrium area a, the double-tail molecule will have a packing parameter $v_S/a\ell_S$ twice as large as that of the single-tail molecule. Therefore, the double-tail molecule can self-assemble to form bilayer vesicles while the corresponding single-tail molecule aggregates into only spherical or globular micelles.

5. If the solvent is changed from water to a mixed aqueous-organic solvent, then the interfacial tension parameter σ decreases. For a given surfactant, this would lead to an increase in the equilibrium area per mole-

cule a and, hence, a decrease in $v_S/a\ell_S$. Therefore, on the addition of a polar organic solvent to an aqueous surfactant solution, bilayers will transform into micelles, rodlike micelles into spherical micelles, and spherical micelles into those of smaller aggregation numbers including only small molecular clusters.

All the above predictions are in agreement with numerous experiments and are by now well established in the literature. One can thus see the evidence for the predictive power of the molecular packing parameter model and its dramatic simplicity.

F. Neglected Role of the Surfactant Tail

From the previous discussion, it is obvious that the equilibrium area a has become closely identified with the headgroup of the surfactant because of its dependence on the headgroup interaction parameter α. Indeed, a is often referred to as the ''head-group area'' in the literature. This has even led to the erroneous identification of a as a simple geometrical area based on the chemical structure of the headgroup in many papers, in contrast to the actuality that a is an equilibrium parameter derived from thermodynamic considerations. For the same surfactant molecule, the area a can assume widely different values depending on the solution conditions like temperature, salt concentration, additives present, etc.; hence, it is meaningless to associate one specific area with a given surfactant.

While the role of the surfactant headgroup in controlling self-assembly is appreciated in the literature, in marked contrast, the role of the surfactant tail has been virtually neglected. This is because the ratio v_S/ℓ_S appearing in the molecular packing parameter is independent of the chain length for common surfactants and the area a depends only on the headgroup interaction parameter α [Eq. (20)] in the framework of Tanford's free energy model. However, as discussed below, it is necessary to consider an extension to Tanford's free energy expression to account for the packing entropy of the surfactant tail in the aggregates. When this is done, the area a becomes dependent on the tail length of the surfactant and also on the aggregate shape.

In formulating and evaluating his free energy expression, Tanford had already noted [1] that the transfer free energy of the tail has a magnitude different from the free energy for transferring the corresponding hydrocarbon chain from aqueous solution to a pure hydrocarbon phase. He had correctly surmised that the difference arises from the packing constraints inside the aggregates that are absent in the case of a bulk hydrocarbon liquid phase. He took account of this factor empirically, as a correction to the transfer free energy, independent of the aggregate size and shape. Such an

empirical expression for the tail packing free energy, independent of the aggregate size and shape, was employed in our early treatments of micelle and vesicle formation [11–13].

Subsequently, detailed chain packing models to estimate this free energy contribution were developed following different approaches, by Gruen [28–30], Dill et al. [31–35], Ben-Shaul et al. [36–38], Puvvada and Blankschtein [39–41], and Nagarajan and Ruckenstein (16). The inclusion of this free energy contribution obviously leads to the surfactant tail directly influencing a, and hence the packing parameter, size, and shape of the equilibrium aggregate. This is discussed in detail in Ref. [42].

The molecular theory of micellization outlined in the next section is strongly influenced by Tanford's work. Various contributions to the free energy of aggregation are identified phenomenologically. Explicit expressions to estimate these free energy contributions are then developed in molecular terms, involving only molecular constants that are readily estimated from knowledge of surfactant molecular structure and solution conditions. This allows a truly predictive approach to the phenomenon of surfactant self-assembly.

IV. THEORY OF MICELLIZATION OF SURFACTANTS

A. Free Energy of Micellization

1. Contributions to the Free Energy of Micellization

From our previous discussion, it is evident that at the heart of the theory of micellization is the formulation of an expression for the standard free energy difference $\Delta\mu_g^0$ between a surfactant molecule in an aggregate of size g and one in the singly dispersed state. Once such an expression is available, all solution and aggregation properties can be a priori calculated. Tanford's phenomenological model [1] has already suggested the essential components of this free energy change. One can decompose $\Delta\mu_g^0$ into a number of contributions on the basis of phenomenological and molecular considerations [11,13,16]. First, the hydrophobic tail of the surfactant is removed from contact with water and transferred to the aggregate core, which is like a hydrocarbon liquid. Second, the surfactant tail inside the aggregate core is subjected to packing constraints because of the requirements that the polar headgroup should remain at the aggregate–water interface and the micelle core should have a hydrocarbon liquidlike density. Third, the formation of the aggregate is associated with the creation of an interface between its hydrophobic domain and water. Fourth, the surfactant headgroups are brought to the aggregate surface, giving rise to steric repulsions between them. Finally, if the headgroups are ionic or zwitterionic, then electrostatic

repulsions between the headgroups at the aggregate surface also arise. Explicit analytical expressions developed in our earlier studies [11,13,16] are presented in this section for each of these free energy contributions in terms of the molecular characteristics of the surfactant.

2. Transfer of the Surfactant Tail

On aggregation, the surfactant tail is transferred from its contact with water to the hydrophobic core of the aggregate. The contribution to the free energy from this transfer process is estimated by considering the aggregate core to be like a liquid hydrocarbon. The fact that the aggregate core differs from a liquid hydrocarbon gives rise to an additional free energy contribution that is evaluated immediately below. The transfer free energy of the surfactant tail is estimated from independent experimental data on the solubility of hydrocarbons in water [43,44]. On this basis, the transfer free energy for the methylene and methyl groups in an aliphatic tail as a function of temperature T (in °K) is given by [16]

$$\begin{aligned} \frac{(\Delta\mu_g^0)_{\text{tr}}}{kT} &= 5.85\ln T + \frac{896}{T} - 36.15 - 0.0056T \quad (\text{for } CH_2) \\ \frac{(\Delta\mu_g^0)_{\text{tr}}}{kT} &= 3.38\ln T + \frac{4064}{T} - 44.13 + 0.02595T \quad (\text{for } CH_3) \end{aligned} \tag{22}$$

For surfactant tails made up of two hydrocarbon chains, the contribution to the transfer free energy would be smaller than that calculated based on two independent single chains, because of intramolecular interactions. Tanford [1] has estimated that the second chain of a dialkyl molecule contributes a transfer free energy that is only about 60% of an equivalent single chain molecule, and this estimate is used for calculations involving double chain molecules. For fluorocarbons, using the work of Mukerjee and Handa [45], we estimate the transfer free energy to be $-6.2kT$ for the CF_3 group and $-2.25kT$ for the CF_2 group, at 25°C. The temperature dependencies of the transfer free energies for fluorocarbons are presently not available.

3. Packing and Deformation of the Surfactant Tail

Within the aggregates, one end of the surfactant tail, which is attached to the polar headgroup, is constrained to remain at the aggregate–water interface. The other end (the terminal methyl group) is free to occupy any position inside the aggregate as long as a uniform density is maintained in the aggregate core. Obviously, the tail must deform locally, that is, stretch and compress nonuniformly along the tail length, in order to satisfy both the packing and the uniform density constraints. The positive free energy contribution resulting from this conformational constraint on the surfactant tail is referred to as the *tail deformation free energy*. Different methods for

estimating this contribution have appeared in the literature [28–41] that involve either complex expressions or extensive numerical calculations. In constructing our theory, we have followed the method suggested for block copolymer microdomains by Semenov [46], and have developed a simple analytical expression by integrating the local tail deformation energy over the volume of the aggregate. In this manner, we obtain [16] the following expression for spherical micelles:

$$\frac{(\Delta\mu_g^0)_{\text{def}}}{kT} = \left(\frac{9P\pi^2}{80}\right)\left(\frac{R_S^2}{NL^2}\right) \tag{23}$$

where P is the packing factor defined in Table 1, R_S is the core radius, L is the characteristic segment length for the tail, and N is the number of segments in the tail ($N = \ell_S/L$, where ℓ_S is the extended length of the tail). As suggested by Dill and Flory [31,32], a segment is assumed to consist of 3.6 methylene groups (hence, $L = 0.46\,\text{nm}$). L also represents the spacing between alkane molecules in the liquid state, namely, $L^2(= 0.21\,\text{nm}^2)$ is the cross-sectional area of the polymethylene chain. Equation (23) is employed also for nonspherical globular micelles and the spherical endcaps of rodlike micelles. For infinite cylindrical rods, Eq. (23) is still applicable, but with the changes that the coefficient 9 is replaced by 10, the radius R_S is replaced by the radius R_C of the cylinder, and the packing factor $P = 1/2$. For spherical bilayer vesicles, the molecular packing differences between the outer and the inner layers must be accounted for. Consequently, when Eq. (23) is applied to spherical bilayer vesicles, the radius R_S is replaced by the half-bilayer thickness t_o for the molecules in the outer layer, and t_i for the molecules in the inner layer, and the coefficient 9 is replaced by 10 and the packing factor $P = 1$, as for lamellar aggregates. For surfactant tails with two chains, the tail deformation free energy calculated for a single chain should be multiplied by a factor of 2. The segment size L mentioned above for hydrocarbon tails is employed, also for fluorocarbon tails because most calculations involving fluorocarbons have been done for hydrocarbon–fluorocarbon mixed surfactants, and lattice models that allow for two different sizes for sites on the same lattice become mathematically complicated. For pure fluorocarbon surfactants, one can perform predictive calculations taking $L = 0.55\,\text{nm}$ consistent with the cross-sectional area of about $0.30\,\text{nm}^2$ of a fluorocarbon chain.

4. Formation of Aggregate Core–Water Interface

The formation of an aggregate generates an interface between the hydrophobic domain consisting of surfactant tails and the surrounding water medium. The free energy of formation of this interface is calculated as the

product of the surface area in contact with water and the macroscopic interfacial tension σ_{agg} characteristic of the interface [11,13,16]:

$$\frac{(\Delta \mu_g^0)_{int}}{kT} = \left(\frac{\sigma_{agg}}{kT}\right)(a - a_o) \tag{24}$$

Here, a is the surface area of the hydrophobic core per surfactant molecule, and a_o is the surface area per molecule shielded from contact with water by the polar headgroup of the surfactant. For spherical bilayer vesicles, the area per molecule differs between the outer and inner layers and the area a in Eq. (24) is replaced with $(A_{go} + A_{gi})/g$. Expressions for the surface area per molecule corresponding to different aggregate shapes and sizes are provided in Table 1.

The area a_o depends on the extent to which the polar headgroup shields the cross-sectional area L^2 of the surfactant tail ($2L^2$ for a double chain tail). If the headgroup cross-sectional area a_p is larger than the tail cross-sectional area, the latter is shielded completely from contact with water and $a_o = L^2$ (or $2L^2$ for double chains) in this case. If a_p is smaller than the cross-sectional area of the tail, then the headgroup shields only a part of the cross-sectional area of the tail from contact with water, and $a_o = a_p$. Thus, a_o is equal to the smaller of a_p or L^2 ($2L^2$ for a double chain).

The aggregate core–water interfacial tension σ_{agg} is taken equal to the interfacial tension σ_{SW} between water (W) and the aliphatic hydrocarbon of the same molecular weight as the surfactant tail (S). The interfacial tension σ_{SW} can be calculated in terms of the surface tensions σ_S of the aliphatic surfactant tail and σ_W of water via the relation

$$\sigma_{sw} = \sigma_s + \sigma_w - 2.0\psi(\sigma_s\,\sigma_w)^{1/2} \tag{25}$$

where ψ is a constant with a value of about 0.55 [47,48]. The surface tension σ_S can be estimated to within 2% accuracy [16] using the relation

$$\sigma_s = 35.0 - 325M^{-2/3} - 0.098(T - 298) \tag{26}$$

where M is the molecular weight of the surfactant tail, T is in °K, and σ_S is expressed in mN/m. The surface tension of water [49] can be calculated using the expression [16]

$$\sigma_w = 72.0 - 0.16(T - 298) \tag{27}$$

where the surface tension is expressed in mN/m and the temperature in °K.

For fluorocarbon surfactants, σ_{agg} is taken equal to the experimentally determined interfacial tension of 56.45 mN/m at 25°C between water and perfluorohexane [45]. The temperature dependency of this interfacial tension can be approximated by a constant coefficient of 0.1 mN/m/°K, in the absence of available experimental data.

5. Headgroup Steric Interactions

On aggregation, the polar headgroups of surfactant molecules are brought to the surface of the aggregate, where they are crowded when compared to the infinitely dilute state of the singly dispersed molecules. This generates steric repulsions among the headgroups. If the headgroups are compact, the steric interactions between them can be estimated as hard-particle interactions, using any of the models available in the literature. The simplest is the van der Waals approach, on the basis of which the contribution from steric repulsion at the micelle surface is calculated as [11,13,16]

$$\frac{(\Delta\mu_g^0)_{\text{steric}}}{kT} = -ln\left(1 - \frac{a_p}{a}\right) \tag{28}$$

where a_p is the cross-sectional area of the polar headgroup near the micellar surface. This equation is used for spherical and globular micelles as well as for the cylindrical middle and the spherical endcaps of rodlike micelles. For spherical bilayer vesicles, the steric repulsions at both the outer and the inner surfaces must be considered, taking into account that the area per molecule is different for the two surfaces. Noting that g_o and g_i surfactant molecules are present in the outer and the inner layers, respectively, one can write

$$\frac{(\Delta\mu_g^0)_{\text{steric}}}{kT} = -\frac{g_o}{g}\ln\left(1 - \frac{a_p}{A_{go}/g_o}\right) - \frac{g_i}{g}\ln\left(1 - \frac{a_p}{A_{gi}/g_i}\right) \tag{29}$$

The above approach to calculating the headgroup interactions using Eqs.(28) or (29) is inadequate when the polar headgroups are not compact, as in the case of nonionic surfactants having polyoxyethylene chains as headgroups. An alternate treatment for headgroup interactions in such systems is presented later in this section.

6. Headgroup Dipole Interactions

If the headgroup has a permanent dipole moment as in the case of zwitterionic surfactants, the crowding of the aggregate surface by the headgroups also leads to dipole–dipole interactions. The dipoles at the surface of the micelle are oriented normal to the interface and stacked such that the poles of the dipoles are located on parallel surfaces. The dipole–dipole interaction for such an orientation provides a repulsive contribution to the free energy of aggregation. The interaction free energy is estimated by considering that the poles of the dipoles generate an electrical capacitor and the distance between the planes of the capacitor is equal to the distance of charge separation d (or the dipole length) in the zwitterionic headgroup. Consequently, for spherical micelles one gets [11,13,16] the expression

$$\frac{(\Delta \mu_g^0)_{\text{dipole}}}{kT} = \frac{2\pi e^2 R_S}{\varepsilon a_\delta kT}\left[\frac{d}{R_S + \delta + d}\right] \tag{30}$$

where e is the electronic charge, ε the dielectric constant of the solvent, R_S the radius of the spherical core, and δ the distance from the core surface to the place where the dipole is located. This equation is also employed for globular micelles and the endcaps of rodlike micelles. For the cylindrical part of the rodlike micelles, the capacitor model yields

$$\frac{(\Delta \mu_g^0)_{\text{dipole}}}{kT} = \frac{2\pi e^2 R_C}{\varepsilon a_\delta kT} \ln\left[1 + \frac{d}{R_C + d + \delta}\right] \tag{31}$$

where R_C is the radius of the cylindrical core of the micelle. For vesicles, considering the outer and inner surfaces, one can write [12,13]

$$\frac{(\Delta \mu_g^0)_{\text{dipole}}}{kT} = \frac{g_o}{g}\frac{2\pi e^2 R_o}{\varepsilon a_{\delta o} kT}\left[\frac{d}{R_o + \delta + d}\right] + \frac{g_i}{g}\frac{2\pi e^2 R_i}{\varepsilon a_{\delta i} kT}\left[\frac{d}{R_i - \delta - d}\right] \tag{32}$$

where the areas $a_{\delta o}$ and $a_{\delta i}$ are defined in Table 1. The dielectric constant ε is taken to be that of pure water [49] and is calculated using the expression [16]

$$\varepsilon = 87.74 \exp(-0.0046(T - 273)) \tag{33}$$

where the temperature T is in °K.

7. Headgroup Ionic Interactions

If the surfactant has an anionic or cationic headgroup, then ionic interactions arise at the micellar surface. The theoretical computation of these interactions is complicated by a number of factors such as the size, shape, and orientation of the charged groups, the dielectric constant in the region where the headgroups are located, the occurrence of Stern layers, discrete charge effects, etc. [1,4,50,51]. The Debye–Hückel solution to the Poisson–Boltzmann equation is found to overestimate the interaction energy approximately by a factor of 2 [1,15]. An approximate analytical solution to the Poisson–Boltzmann equation derived [52] for spherical and cylindrical micelles is used in the present calculations. This free energy expression has the form

$$\begin{aligned}\frac{(\Delta\mu_g^0)_{\text{ionic}}}{kT} = {} & 2\ln\left\{\frac{S}{2} + \left(1 + \frac{S^2}{4}\right)^{1/2}\right\} - \frac{4}{S}\left\{\left(1 + \frac{S^2}{4}\right)^{1/2} - 1\right\} \\ & - \frac{4C}{\kappa S}\ln\left\{\frac{1}{2} + \frac{1}{2}\left(1 + \frac{S^2}{4}\right)^{1/2}\right\}\end{aligned} \tag{34}$$

where

$$S = \frac{4\pi e^2}{\varepsilon\kappa a_\delta kT} \tag{35}$$

and κ is the reciprocal Debye length. The area per molecule a_δ is evaluated at a distance δ from the hydrophobic core surface (see Table 1), where the center of the counterion is located.

The first two terms on the right-hand side of Eq. (34) constitute the exact solution to the Poisson–Boltzmann equation for a planar geometry, and the last term provides the curvature correction. The curvature-dependent factor C is given by [16]

$$C = \frac{2}{R_S + \delta}, \qquad \frac{2}{R_{eq} + \delta}, \qquad \frac{1}{R_C + \delta} \tag{36}$$

for spheres/spherical endcaps of spherocylinders, globular aggregates (with an equivalent radius R_{eq} defined in Table 1), and cylindrical middle part of spherocylinders, respectively. For spherical bilayer vesicles, the electrostatic interactions at both the outer and inner surfaces are taken into account [12,13]. For the molecules in the outer layer, the free energy contribution is calculated with a_δ replaced by $a_{\delta o}$ and $C = 2/(R_o + \delta)$. For the molecules in the inner layer, a_δ is replaced by $a_{\delta i}$ and $C = -2/(R_i - \delta)$.

The reciprocal Debye length κ is related to the ionic strength of the solution via

$$\kappa = \left(\frac{8\pi n_0 e^2}{\varepsilon kT}\right)^{1/2}, \qquad n_0 = \frac{(C_1 + C_{add}) N_{Av}}{1000} \tag{37}$$

In the above equation, n_0 is the number of counterions in solution per cm^3, C_1 is the molar concentration of the singly dispersed surfactant molecules, C_{add} is the molar concentration of the salt added to the surfactant solution, and N_{Av} is Avogadro's number. The temperature dependence of the reciprocal Debye length κ arises from both the variables T and ε present in Eq. (37).

8. Headgroup Interactions for Oligomeric Headgroups

For nonionic surfactants with polyoxyethylene chains as headgroups, the calculation of the headgroup interactions using Eq. (28) and (29) for the steric interaction energy becomes less satisfactory since it is difficult to define an area a_p characteristic of the oligomeric headgroups (13,16) without ambiguity. For sufficiently large polyoxyethylene chain lengths, it is more appropriate to treat the headgroup as a polymeric chain when estimating the free energy of headgroup interactions. The treatment developed in our earlier work (16) is based on the following conceptual approach. In a singly dispersed surfactant molecule, the polyoxyethylene chain is viewed as an iso-

lated free polymer coil swollen in water. In micelles, the polyoxyethylene chains present in the region surrounding the hydrophobic core (referred to as shell or corona) can be viewed as forming a solution denser in polymer segments compared to the isolated polymer coil. The difference in the two states of polyoxyethylene provides a contribution to the free energy of aggregation, which is computed as the sum of the free energy of mixing of the polymer segments with water and the free energy of polymer chain deformation. As the polyoxyethylene chain length decreases, the use of polymer statistics becomes less satisfactory.

Two limiting models of micellar corona are considered. One assumes that the corona has a uniform concentration of polymer segments. The maintenance of such a uniform concentration in the corona is possible for curved aggregates, only if the chains deform nonuniformly along the radial coordinate. This model may be appropriate when the number of ethylene oxide units in the headgroup is small. The second model assumes a radial concentration gradient of chain segments in the corona consistent with the uniform deformation of the chain. This model may be more appropriate for headgroups with large number of ethylene oxide units.

For either of the above models, in order to calculate the mixing free energies, one has to choose some polymer solution theory. Because of its simplicity, the mean-field approach of Flory [53], which requires only the polyoxyethylene–water interaction parameter χ_{WE} for calculating the free energies, is used here. Usually, it is necessary to consider the composition and temperature dependencies of the interaction parameter χ_{WE} in order to accurately describe the thermodynamic properties of polymer solutions [54–56]. Even with such dependencies incorporated, it has not been possible to satisfactorily describe the properties of a polyethylene oxide–water system, indicating the inadequacy of the polymer solution theory to quantitatively represent the aqueous polymer solution. Nevertheless, we have carried out calculations based on the Flory model and taking χ_{WE} to be a constant, with the justification that the model provides at least an approximate accounting of the mixing free energy needed for our purposes and no better model with comparable simplicity is available. For both uniform concentration and nonuniform concentration models, the free energy of the steric interactions is calculated using Eq. (28) or (29), but taking a_p equal to L^2 to describe the steric repulsions between neighboring surfactant tails at the sharp interface separating the core from the corona.

9. Headgroup Mixing in Corona Region

For a polyoxyethylene chain containing E_X oxyethylene units, the number of segments N_E is given by $N_E = E_X v_E / L^3$, where v_E is the volume of an oxyethylene unit and the characteristic segment volume is retained to be L^3.

Based on available density data [57] at 25°C, $v_E = 0.063\,nm^3$. The volume V_S of the micellar corona, having a thickness D, is calculated from the geometrical relations given in Table 2. In the uniform concentration model, the volume fraction of the polymer segments in the corona is

$$\phi_{Eg} = \frac{g\,E_x\,v_E}{V_S} = \frac{g\,N_E\,L^3}{V_S} \tag{38}$$

In the nonuniform concentration model, the polymer concentration in the corona is determined from the requirement that the polymer chains be uniformly deformed over the thickness D. The radial variation of polymer concentration in the corona is thus found to be (16)

$$\phi(r) = \left(\frac{N_E\,L^3}{D}\right)\frac{g}{4\pi r^2} \tag{39}$$

for spherical aggregates and

$$\phi(r) = \left(\frac{N_E\,L^3}{D}\right)\frac{g}{2\pi r\,L_C} \tag{40}$$

TABLE 2 Corona Volume of Micelles with Polyoxytheylene Headgroups

Spherical micelles:

$$\frac{V_S}{g} = \frac{V_g}{g}\left[\left(1+\frac{D}{R_S}\right)^3 - 1\right]$$

Globluar micelles:

$$\frac{V_S}{g} = \frac{V_g}{g}\left[\left(1+\frac{D}{R_S}\right)^2\left(1+\frac{D}{b}\right) - 1\right]$$

Cylindrical part of rodlike micelles:

$$\frac{V_S}{g} = \frac{V_g}{g}\left[\left(1+\frac{D}{R_C}\right)^2 - 1\right]$$

Spherical endcaps of rodlike micelles:

$$\frac{V_S}{g} = \frac{V_g}{g}\left[\frac{8\pi(R_S+D)^3}{3gv_S} - \frac{2\pi(H+D)^2}{3gv_S}\{3(R_S+D)-(H+D)\} - 1\right]$$

for a cylinder of length L_C containing g molecules. The polymer concentration φ_R at the micellar core–water interface (at $r = R$) reduces for both spheres and cylinders to

$$\phi_R = \left(\frac{N_E L^3}{Da}\right) \tag{41}$$

where a is the surface area of the micellar core per surfactant molecule.

In the corona each polyoxyethylene chain experiences a potential $U(r)$ because of the interactions between the segments of a single molecule and the segments of all the other molecules. This potential is taken in the mean-field approach to be proportional to the total segment density arising from all the molecules of the micelle. The influence of the solvent is also incorporated in this mean potential via the excluded-volume factor [53,58]. The potential is written [16] as

$$U(r) = kT\phi(r)(\tfrac{1}{2} - \chi_{wE}) \tag{42}$$

where $\varphi(r)$ is the segment density of polyoxyethylene in the corona at the radial position r. For the uniform concentration model, $\varphi(r)$ is a constant equal to φ_{Eg}. Therefore, the mixing free energy of the headgroup in the corona with respect to that in an isolated, free polymer coil is given by [16] the expression

$$\frac{(\Delta \mu_g^0)_{mix,E}}{kT} = \frac{1}{g}\frac{1}{L^3}\int_R^{R+D} \phi(r)\frac{U(r)}{kT} 4\pi r^2 \, dr = N_E \phi_{Eg}\left(\frac{1}{2} - \chi_{wE}\right) \tag{43}$$

Here, $R = R_S$ for the spherical micelles. This equation is used to calculate the headgroup mixing free energy for globular aggregates and endcaps of rodlike aggregates, as well. For the cylindrical part of the rodlike micelles, with $R = R_C$, one gets [16]

$$\frac{(\Delta \mu_g^0)_{mix,E}}{kT} = \frac{1}{g}\frac{1}{L^3}\int_R^{R+D} \phi(r)\frac{U(r)}{kT} 2\pi r L_C \, dr = N_E \phi_{Eg}\left(\frac{1}{2} - \chi_{wE}\right) \tag{44}$$

For the nonuniform concentration model, using the radial concentration profile given by Eqs. (39)–(41), the headgroup mixing free energy in spherical micelles is obtained to be [16]

$$\frac{(\Delta \mu_g^0)_{mix,E}}{kT} = \frac{1}{g}\frac{1}{L^3}\int_R^{R+D} \phi(r)\frac{U(r)}{kT} 4\pi r^2 \, dr = N_E \phi_R\left(\frac{1}{2} - \chi_{wE}\right)\frac{1}{(1 + D/R)} \tag{45}$$

This equation is also used for the globular aggregates and the endcaps of spherocylinders, with R denoting the radius of the globular aggregate or of

the spherical endcaps. For the cylindrical part of the spherocylinders, with $R = R_C$, one gets [16]

$$\frac{(\Delta \mu_g^0)_{\text{mix,E}}}{kT} = \frac{1}{g}\frac{1}{L^3}\int_R^{R+D} \phi(r)\frac{U(r)}{kT} 2\pi r\, L_C\, dr$$
$$= N_E\, \phi_R \left(\frac{1}{2} - \chi_{\text{wE}}\right)\frac{R}{D}\ln(1 + D/R) \tag{46}$$

10. Headgroup Deformation in Corona Region

For the uniform concentration model, the elastic deformation of the segments is nonuniform along the length of the polymer molecule. An expression for this nonuniform deformation free energy of the polyoxyethylene chains in the corona region of the micelle is obtained by employing the approach of Semenov [46] mentioned earlier. One can calculate the free energy contribution arising from the headgroup deformation in the corona from the expression [16]

$$\frac{(\Delta \mu_g^0)_{\text{def,E}}}{kT} = \frac{3}{2}\frac{L\, R_S}{a\, \phi_{\text{Eg}}}\frac{D}{R_S + D} \tag{47}$$

for spherical and globular micelles and the endcaps of rodlike micelle and from

$$\frac{(\Delta \mu_g^0)_{\text{def,E}}}{kT} = \frac{3}{2}\frac{L\, R_C}{a\, \phi_{\text{Eg}}}\ln\left[1 + \frac{D}{R_C}\right] \tag{48}$$

for the cylindrical part of the rodlike micelle.

In the nonuniform concentration model, the polymer chain has been assumed to deform uniformly along the chain length. Using Flory's [53] rubber elasticity theory to estimate the deformation free energy of a chain, one obtains

$$\frac{(\Delta \mu_g^0)_{\text{def,E}}}{kT} = \frac{1}{2}\left[\frac{D^2}{N_E\, L^2} + \frac{2\, N_E^{1/2}\, L}{D} - 3\right] \tag{49}$$

which can be employed for all aggregate shapes.

11. Formation of Core–Corona Interface

The interfacial free energy contribution $(\Delta \mu_g^0)_{\text{int}}$ is calculated using Eq. (24) but recognizing that σ_{agg} is now different from σ_{SW} since the interface in these aggregates is that between a domain of surfactant tails and a solution of polyoxyethylene segments in water. σ_{agg} is calculated using the Prigogine theory [59,60] for the surface tensions of solutions. This involves determining the surface phase composition φ^S for a given bulk solution composition

by equating the chemical potentials of the surface and bulk phases. The surface phase composition, in turn, determines the interfacial tension. σ_{agg} is thus dependent on the concentration of the polyoxyethylene segments in the micellar corona and the surfactant tail–polyoxyethylene interfacial tension σ_{SE} in addition to the surfactant tail–water interfacial tension σ_{SW}.

In the uniform concentration model, the micellar corona has a bulk concentration φ_{Eg}. Correspondingly, the concentration φ^S of polymer segments at the interface is determined [16] by solving the implicit equation

$$\ln\left[\frac{(\phi^S/\phi_{Eg})^{1/N_E}}{(1-\phi^S)/(1-\phi_{Eg})}\right] = \frac{(\sigma_{SW}-\sigma_{SE})}{kT}\, v_S^{2/3} + \frac{3}{4}\chi_{WE}[(1-\phi_{Eg})-\phi_{Eg}] - \frac{1}{2}\chi_{WE}[(1-\phi^S)-\phi^S] \tag{50}$$

Once φ^S is determined, the interfacial tension σ_{agg} is calculated [16] from the explicit equation

$$\left(\frac{\sigma_{agg}-\sigma_{SW}}{kT}\right)v_S^{2/3} = \ln\left(\frac{1-\phi^S}{1-\phi_{Eg}}\right) + \left(\frac{N_E-1}{N_E}\right)(\phi^S-\phi_{Eg}) + \chi_{WE}\left[\frac{1}{2}(\phi^S)^2 - \frac{3}{4}(\phi_{Eg})^2\right] \tag{51}$$

The interfacial tension σ_{SE} between polyoxyethylene and surfactant tails is calculated in terms of the surface tension σ_S of the surfactant tails and the surface tension σ_E of polyoxyethylene using the relation

$$\sigma_{SE} = \sigma_S + \sigma_E - 2.0\psi(\sigma_S\,\sigma_E)^{1/2} \tag{52}$$

The constant ψ is taken to be $\psi = 0.55$ as for the surfactant tail–water system in Eq. (25) because of the polar nature of the polyoxyethylene group [47,48]. The surface tension σ_S is calculated using Eq. (26). The surface tension of polyoxyethylene with E_X oxyethylene units is estimated (in mN/m) on the basis of the information given in Ref. [61] using the equation

$$\sigma_E = 42.5 - 19E_X^{-2/3} - 0.098(T-298) \tag{53}$$

where T is in °K.

For the nonuniform concentration model also, the free energy of formation of the core–corona interface is calculated using Eqs. (50) and (51), but with the concentration φ_R replacing φ_{Eg} in both equations.

B. Computational Approach

The equation for the size distribution of aggregates, in conjunction with the geometrical characteristics of the aggregates and the expressions for the different contributions to the free energy of micellization, allow one to calculate the various solution properties of the surfactant system. In Eq. (4) for the aggregate size distribution, $(\Delta\mu_g^0)$ is the sum of various contributions:

$$(\Delta\mu_g^0) = (\Delta\mu_g^0)_{\text{tr}} + (\Delta\mu_g^0)_{\text{def}} + (\Delta\mu_g^0)_{\text{int}} + (\Delta\mu_g^0)_{\text{steric}} + (\Delta\mu_g^0)_{\text{dipole}} + (\Delta\mu_g^0)_{\text{ionic}} \tag{54}$$

where the contribution $(\Delta\mu_g^0)_{\text{dipole}}$ is included if the surfactant is zwitterionic, the contribution $(\Delta\mu_g^0)_{\text{ionic}}$ is included if the surfactant is ionic, and neither of the two contributions is relevant when the surfactant is nonionic. For surfactants with polyoxyethylene headgroups, one has to include the contributions $(\Delta\mu_g^0)_{\text{mix,E}}$ and $(\Delta\mu_g^0)_{\text{def,E}}$ associated with the mixing and deformation of the headgroups in the corona of the aggregate. Explicit equations for calculating each of these contributions have been discussed above. Using them, the various surfactant solution properties are calculated as follows.

1. Calculations Using Complete Size Distribution

An obvious and direct approach to calculating the aggregation behavior of surfactants is based on calculating the entire size distribution of aggregates as a function of the independent variables and then performing the necessary summations to obtain the CMC, average aggregate size, and the variance of the size distribution as described in Section II.C. In contrast to a typical experiment where the total surfactant concentration is fixed and the aggregation behavior is determined, in doing the predictive calculations, it is convenient to calculate the size distribution at a specified value of the singly dispersed surfactant concentration X_1 and then obtain the total surfactant concentration by the summation, as $X_{\text{tot}} = X_1 + \sum gX_{\text{g}}$.

2. Calculations Using the Maximum-Term Method

The approach based on the calculation of the aggregate size distribution is not complicated but is time-consuming. Instead, a simpler approach based on the maximum-term method [62] is employed in our calculations as described below. The simpler approach is built on the recognition that for spherical or globular micelles and spherical bilayer vesicles, the size dispersion is usually narrow. The concentrations of aggregates other than that corresponding to the maximum in the size distribution are relatively small. Because the average properties of the solution are strongly influenced by the

species present in the largest amount, the number average aggregation number g_n can be taken as the value of g for which the number concentration X_g of the aggregates is a maximum ($= X_{g\mathrm{M}}$) , and the weight average aggregation number g_w can be taken as the value of g for which the weight concentration gX_g of the aggregates is a maximum [$= (gX_g)_{\mathrm{M}}$]. These average aggregation numbers are very close to one another and are practically the same as those obtained by calculating the size distribution of aggregates [62]. As mentioned before, only the aggregation number g is the independent variable in the case of spherical or globular micelles; the aggregation number g as well as the inner and outer layer thicknesses t_i and t_o are independent variables in the case of spherical vesicles. Further, for polyoxyethylene surfactants, one has to include the corona thickness D as an additional independent variable.

One can obtain quantitative estimates of the variance of the size distribution, also by the maximum-term method. Approximating the derivatives in Eq. (9) by differences, we can write

$$\left(\frac{\sigma(w)}{g_w}\right)^2 = \frac{\partial \ln g_w}{\partial \sum gX_g} = \frac{\Delta \ln g_w}{\Delta \ln (gX_g)_{\mathrm{M}}}$$
$$\left(\frac{\sigma(n)}{g_n}\right)^2 = \frac{\partial \ln g_n}{\partial \ln \sum gX_g} = \frac{\Delta \ln g_n}{\Delta \ln (g_n X_{g\mathrm{M}})} \tag{55}$$

In the above equation, the average aggregation numbers g_n and g_w are taken as those corresponding to the maximum in X_g or (gX_g), the sum $\sum gX_g$ is approximated by the maximum term $g_n X_{g\mathrm{M}}$ or $(gX_g)_{\mathrm{M}}$, and the derivatives have been replaced by the difference terms denoted by the symbol Δ. One can determine the maximum in X_g (or in $g\mathrm{X_g}$) for two slightly different values of X_1 and the two sets of values for g_n and $X_{g\mathrm{M}}$ or g_w and $(gX_g)_{\mathrm{M}}$ can be introduced in Eq. (55) to calculate the variance in the size distribution.

The CMC is estimated by plotting any one of the variables [X_1, $X_{g\mathrm{M}}$, $(gX_g)_{\mathrm{M}}$, $g_{n,\mathrm{app}}$, $g_{w,\mathrm{app}}$] as a function of the total surfactant concentration X_{tot} and determining the surfactant concentration at which the plotted variable displays a sharp transition in values. It can also be calculated as the value of X_1 for which the amount of surfactant in the micellized form is equal to that in the singly dispersed form, namely $X_{\mathrm{CMC}} = X_1 = \sum gX_g = g_n X_{g\mathrm{M}} = (gX_g)_{\mathrm{M}}$. The predicted average aggregation numbers reported in this chapter correspond to those at the CMC, unless otherwise stated.

3. Calculations for Rodlike Micelles

In the case of rodlike micelles, the size distribution X_g [Eq. (12)] is monotonic and does not have a maximum. In this case, by minimizing $(\Delta\mu^0_{\mathrm{cyl}})$ for

an infinitely long cylinder, the equilibrium radius R_C of the cylindrical part of the micelle is determined. Given the radius of the cylindrical part, the number of molecules g_{cap} in the spherical endcaps is found to be that value which minimizes $(\Delta\mu^0_{cap})$. Given g_{cap}, $(\Delta\mu^0_{cyl})$, and $(\Delta\mu^0_{cap})$, the sphere-to-rod transition parameter K is calculated from Eq. (12), the average aggregation numbers at any total surfactant concentration from Eq. (16), and the CMC from Eq. (17). For polyoxyethylene surfactants, one has to include the corona thickness D as an additional independent variable, and the equilibrium value of D is determined for the cylindrical middle part and the spherical endcaps via the minimizations of $(\Delta\mu^0_{cyl})$ and $(\Delta\mu^0_{cap})$, respectively.

The search for the parameter values that maximize the aggregate concentration X_g (or gX_g) or minimize the standard free energy differences $(\Delta\mu^0_{cyl})$ and $(\Delta\mu^0_{cap})$ was carried out using the IMSL (International Mathematical and Statistical Library) subroutine ZXMWD. This subroutine is designed to search for the global extremum of a function of many independent variables subject to any specified constraints on the variables. This subroutine has been used for all the calculations described in this chapter.

C. Estimation of Molecular Constants

For illustrative purposes, calculations have been carried out for a number of nonionic, zwitterionic, and ionic surfactants. Examples of molecules employed in these calculations are shown in Fig. 2. The molecular constants associated with the surfactant tail are the volume v_S and the extended length ℓ_S of the tail. For the headgroup, one needs the cross-sectional area a_p for all types of headgroups, the distance δ from the core surface where the counterion is located in the case of ionic headgroups, the dipole length d, and the distance δ from the core surface at which the dipole is located, in the case of a zwitterionic headgroup. All these molecular constants can be estimated from the chemical structure of the surfactant molecule. There are no free parameters, and the calculations are therefore completely predictive in nature. Some examples of how the molecular constants are estimated are given below. The molecular constants characterizing the headgroups of surfactants considered in this chapter are listed in Table 3.

1. Estimation of Tail Volume v_S

The molecular volume v_S of the surfactant tail containing n_C carbon atoms is calculated from the group contributions of $(n_C - 1)$ methylene groups and the terminal methyl group

$$v_S = v(CH_3) + (n_C - 1)v(CH_2) \tag{56}$$

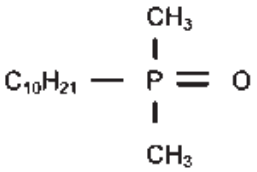

Decyl Dimethyl Phosphene Oxide
($C_{10}PO$)

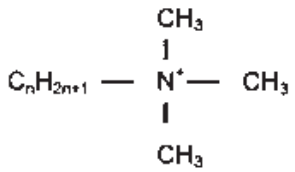

Alkyl Trimethyl Ammonium Bromide
n=10 (DeTAB), n=12 (DTAB)

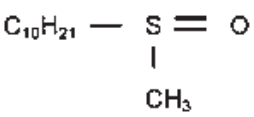

Decyl Methyl Sulfoxide
($C_{10}SO$)

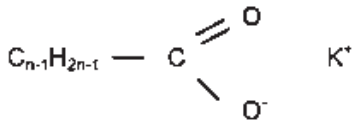

Potassium Alkanoate
n=8 (KC_8), n=10 (KC_{10}),
n=14 (KC_{14})

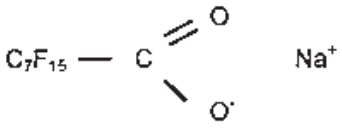

Sodium Perfluoro Octanoate
(SPFO)

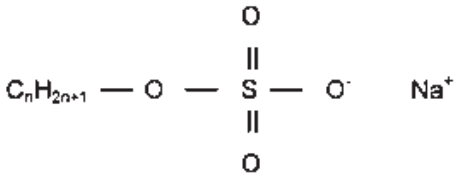

Sodium Alkyl Sulfate
n=10 (SDes), n=12 (SDS)

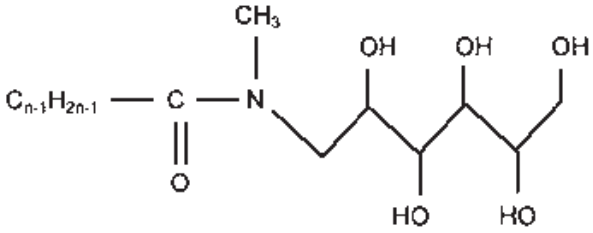

Alkyl N-Methyl Glucamine (MEGA-n)

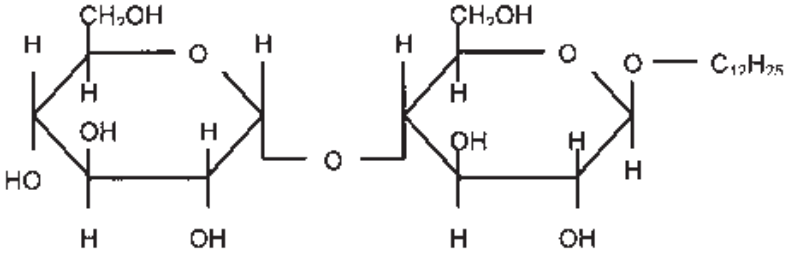

β-D-Dodecyl Maltoside (DM)

FIG. 2 Chemical structure of surfactant molecules considered in this chapter and the symbols used to refer to them in the text.

TABLE 3 Molecular Constants for Surfactant Headgroups

Surfactant headgroup	a_p (nm^2)	a_o (nm^2)	δ (nm)	d (nm)
β-Glucoside	0.40	0.21	—	—
Methyl sulfoxide	0.39	0.21	—	—
Dimethyl phosphene oxide	0.48	0.21	—	—
β-Maltoside	0.43	0.21	—	—
N-methyl glucamine	0.34	0.21	—	—
Sodium sulfate	0.17	0.17	0.545	—
Sodium sulfonate	0.17	0.17	0.385	—
Potassium carboxylate	0.11	0.11	0.60	—
Sodium carboxylate	0.11	0.11	0.555	—
Pyridinium bromide	0.34	0.21	0.22	—
Trimethyl ammonium bromide	0.54	0.21	0.345	—
N-betaine	0.30	0.21	0.07	0.5
Lecithin	0.45	0.42	0.65	0.62

These group molecular volumes, estimated from the density versus temperature data available for aliphatic hydrocarbons, are given [16] by the expressions

$$\begin{aligned} v(CH_3) &= 0.0546 + 1.24 \times 10^{-4}(T - 298)\,\text{nm}^3 \\ v(CH_2) &= 0.0269 + 1.46 \times 10^{-5}(T - 298)\,\text{nm}^3 \end{aligned} \tag{57}$$

where T is in °K. For double-tailed surfactants, v_S is calculated by accounting for both the tails. For the fluorocarbon tails, using the data available [63–65] for 25°C, we estimate that $v(CF_3) = 1.67v(CH_3)$ and $v(CF_2) = 1.44v(CH_2)$. Extensive volumetric data are not yet available to estimate the temperature dependence of the molecular volumes of CF_3 and CF_2 groups. As an approximate estimation, the ratio between the volumes of the fluorocarbon and the hydrocarbon groups is assumed to be the same at all temperatures.

2. Estimation of Extended Tail Length ℓ_S

The extended length of the surfactant tail ℓ_S at 298°K is calculated using a group contribution of 0.1265 nm for the methylene group and 0.2765 nm for the methyl group [1]. Given the small volumetric expansion of the surfactant tail over the range of temperatures of interest, the extended tail length ℓ_S is considered as temperature-independent. Therefore, the small volumetric expansion of the surfactant tail is accounted for by small increases in the cross-sectional area of the surfactant tail. The extended length of the fluorocarbon chain is estimated using the same group contributions as for hydro-

carbon tails, namely, 0.1265 nm for the CF_2 group and 0.2765 nm for the CF_3 group.

3. Estimation of Headgroup Area a_p

The headgroup area a_p is calculated as the cross-sectional area of the headgroup near the hydrophobic core-water interface. The glucoside headgroup in β-glucosides has a compact ring structure [5] with an approximate diameter of 0.7 nm, and hence, the effective cross-sectional area of the polar headgroup a_p is estimated as 0.40 nm^2. For sodium alkyl sulfates, the cross-sectional area of the polar group a_p has been estimated to be 0.17 nm^2. For the zwitterionic N-betaine headgroup, a_p has been estimated to be 0.30 nm^2. The area per molecule a_0 of the micellar core that is shielded by the headgroup from having contact with water, is the smaller of a_p or L^2, as discussed earlier.

4. Estimation of δ and d

For ionic surfactants, the molecular constant δ depends on the size of the ionic headgroup, the size of the hydrated counterion, and also the proximity of the counterion to the charge on the surfactant ion. Visualizing that the sodium counterion is placed on top of the sulfate anion, we estimate $\delta = 0.545$ nm for sodium alkyl sulfates and 0.385 nm for sodium alkyl sulfonates. For alkyl pyridinium bromide the surfactant cation can approach very near the hydrophobic core, and we estimate $\delta = 0.22$ nm. For zwitterionic surfactants we need the molecular constant d, which is the distance of separation of the charges on the dipole (or the dipole length), and also the constant δ, which is the distance from the hydrophobic core surface at which the dipole is located. The computations in this chapter are based on an estimate of $d = 0.5$ nm and $\delta = 0.07$ nm, for N-alkyl betaines, and $d = 0.62$ nm and $\delta = 0.65$ nm, for the lecithin headgroup.

5. Estimation of χ_{WE}

For nonionic surfactants with a polyoxyethylene headgroup, we need the polyoxyethylene–water interaction parameter χ_{WE}. This can, in principle, be estimated using the thermodynamic properties of polyoxyethylene–water solutions (such as the activity data or the phase behavior data). The activity data [54] represented in the framework of the Flory–Huggins theory indicate that χ_{WE} is dependent on the composition of the polymer solution (55). The phase behavior exhibits both a lower critical solution temperature and an upper critical solution temperature [54–56] indicating that χ_{WE} first increases and then decreases with increasing temperature. Further, the headgroup of the surfactant contains a functional group (such as a hydroxyl) that terminates the polymer chain; the presence of this terminal group may also affect the value of χ_{WE} when compared to the estimate based on high-

molecular-weight polyoxyethylenes. The dependence of χ_{WE} on polymer concentration, temperature, polymer molecular weight, and the terminating functional group is, however, not known. Because water is a good solvent for polyoxyethylene, values for χ_{WE} smaller than 0.5, namely $\chi_{WE} = 0.1$ and 0.3, have been chosen for the illustrative calculations.

D. Illustrative Predictions for Surfactants

1. Influence of Free Energy Contributions on Aggregation Behavior

Figure 3 presents the calculated free energy contributions ($\Delta\mu_g^0$) expressed per molecule of surfactant, for cetyl pyridinium bromide in water, as a function of the aggregation number g. Whereas the magnitude of ($\Delta\mu_g^0$)

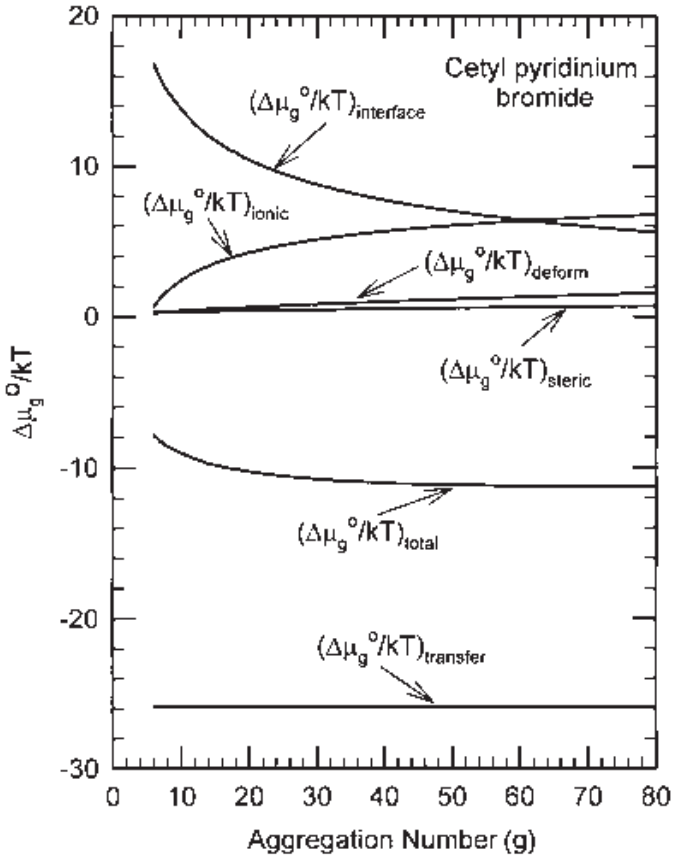

FIG. 3 Contributions to the standard free energy difference between a surfactant molecule in the micellized state and one in the singly dispersed state calculated as a function of the aggregation number g of the micelle for cetyl pyridinium bromide in water at 25°C. Subscripts refer to the following: total (total of all contributions), transfer (transfer free energy of tails), deform (deformation free energy of tails), interface (interfacial free energy), steric (headgroup steric interactions), and ionic (headgroup ionic interactions). Refer to text for detailed discussion.

influences the CMC, the functional dependence of $(\Delta\mu_g^0)$ on g determines the shape and size of the equilibrium aggregates. Of all the contributions to $(\Delta\mu_g^0)$, only the transfer free energy of the surfactant tail is negative. Therefore, it is responsible for the aggregated state of the surfactant being favored over the singly dispersed state. The transfer free energy contribution is a constant independent of the micellar size and hence has no influence on the structural characteristics of the equilibrium aggregate. All the remaining free energy contributions to $(\Delta\mu_g^0)$ are positive and depend on the aggregate size. It is clear from the geometrical relations for aggregates (see Table 1) that as the aggregation number g increases, the area per molecule a decreases. Consequently, the free energy of formation of the aggregate core–water interface decreases with increasing aggregation number. This free energy is thus responsible for the growth of aggregates to large sizes and is said to provide the positive cooperativity of aggregation. All remaining free energy contributions (namely, the surfactant tail deformation energy, the steric repulsions between the headgroups, the dipole–dipole interactions between zwitterionic headgroups, and the ionic interactions between ionic headgroups) increase with increasing aggregation number. These free energy contributions thus provide the negative cooperativity of aggregation and are responsible for limiting the aggregate growth to finite sizes. All the free energy contributions affect, however, the magnitude of the CMC.

The calculated size distributions for cetyl pyridinium bromide are presented in Fig. 4 for two values of the molar concentration $C_1(= 55.55X_1)$ of the singly dispersed surfactant. As expected, near the CMC, a small variation in C_1 gives rise to a large variation in the total aggregate concentration, C_{tot}. The average aggregation number is, however, practically the same at these two concentrations. This implies [see Eq. (9)] that the size dispersion of the aggregates is narrow, which can be seen also from the figure. Various size-dependent solution properties calculated using the model are plotted in Fig. 5 as a function of the total concentration of cetyl pyridinium bromide in water. The concentration at which any one of these properties shows a sharp change in behavior can be taken as the CMC. All four properties plotted in the figure yield CMC values that are very close to one another.

2. Influence of Tail Groups and Headgroups on Aggregation Behavior

The CMC values predicted at 25°C, for nonionic alkyl β-glucosides, zwitterionic N-alkyl betaines, and ionic alkyl sodium sulfates are presented in Fig. 6 as a function of the length of the surfactant tail. The CMC decreases with an increase in the chain length of the surfactant, as a consequence of the increase in the magnitude of the tail transfer free energy. The incremental variation in CMC is roughly constant for a given homologous family of surfactants. The

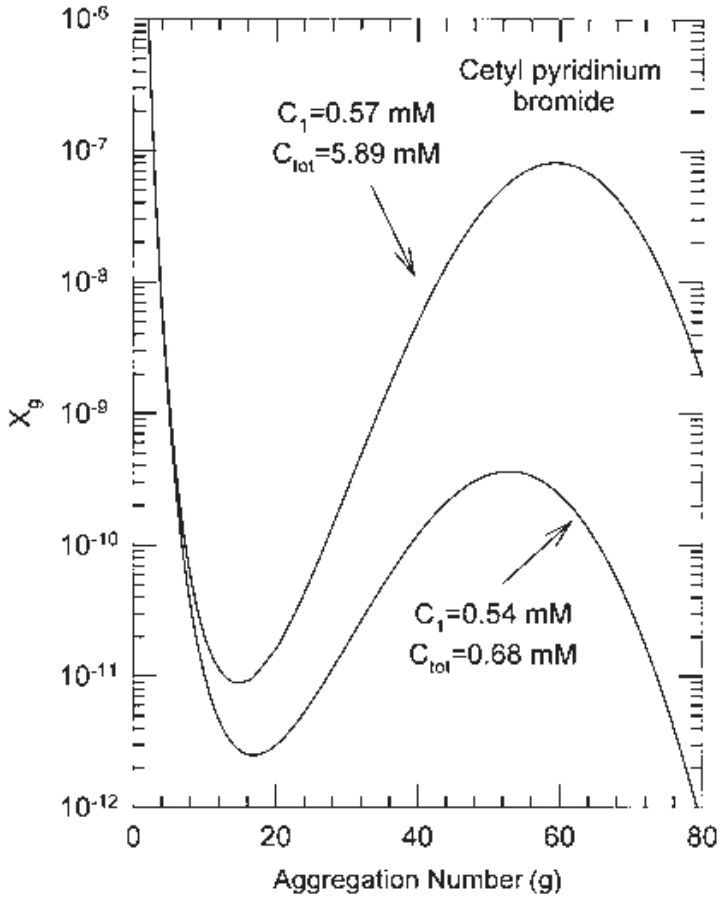

FIG. 4 Calculated size distribution of cetyl pyridinium bromide aggregates in water at 25°C at two values of the total surfactant concentration C_{tot} and the singly dispersed surfactant concentration C_1. (a) $C_1 = 0.54\,\text{mM}$ and $C_{tot} = 0.68\,\text{mM}$; (b) $C_1 = 0.57\,\text{mM}$ and $C_{tot} = 5.89\,\text{mM}$.

experimentally measured CMCs [66–71] are in reasonable agreement with the predicted values. For a given surfactant tail length, the CMC is smaller for a nonionic surfactant than for an anionic surfactant. This is a consequence of the strong repulsive interaction between ionic headgroups compared to the weaker steric interactions between nonionic headgroups.

The predicted average aggregation numbers at the CMC are plotted as a function of the tail length in Fig. 7 for some zwitterionic and anionic surfactants. For the cases considered, the micelles are spherical or globular and are narrowly dispersed in size. For the zwitterionic alkyl N-betaines, the predicted aggregation numbers are in reasonable agreement with the measured values [70,71]. The aggregation number increases with an increase in the chain length of the surfactant tail. The equilibrium area per molecule of the aggregate changes with a change in the tail length, but the range of values assumed by a is small. Consequently, given an equilibrium area per molecule,

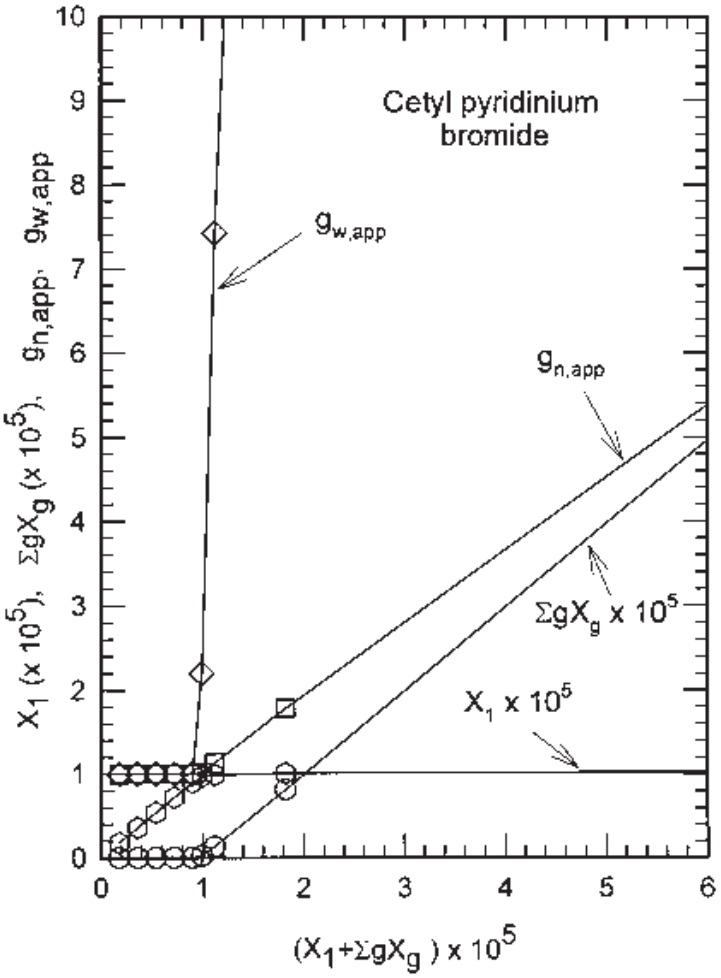

FIG. 5 Calculated size-dependent solution properties of cetyl pyridinium bromide in water as a function of the total surfactant concentration (expressed as mole fraction). $g_{w,app}$ is the apparent weight average aggregation number, $g_{n,app}$ is the apparent number average aggregation number, X_1 denotes the monomer concentration, and $\sum gX_g$ is the total concentration of the surfactant in the form of aggregates. All concentrations are expressed in mole fraction units.

the aggregation number of a spherical or globular micelle must increase with increasing tail length, as dictated by the geometrical relations. For anionic sodium alkyl sulfates with chain lengths smaller than dodecyl, a large number of experimental data have been reported in the literature [72–75], from which we select for plotting in Fig. 7 those that show the largest deviation from the predicted values. For tetradecyl and hexadecyl chains, aggregation numbers mentioned in Ref. [76] have been plotted, although in the work of Tartar [72], which is cited as the source of these experimental data, no report of these experimental aggregation numbers is found; therefore, the reported aggregation numbers for these two surfactants should be discounted. For alkyl sulfates the predicted aggregation numbers do not show a significant increase

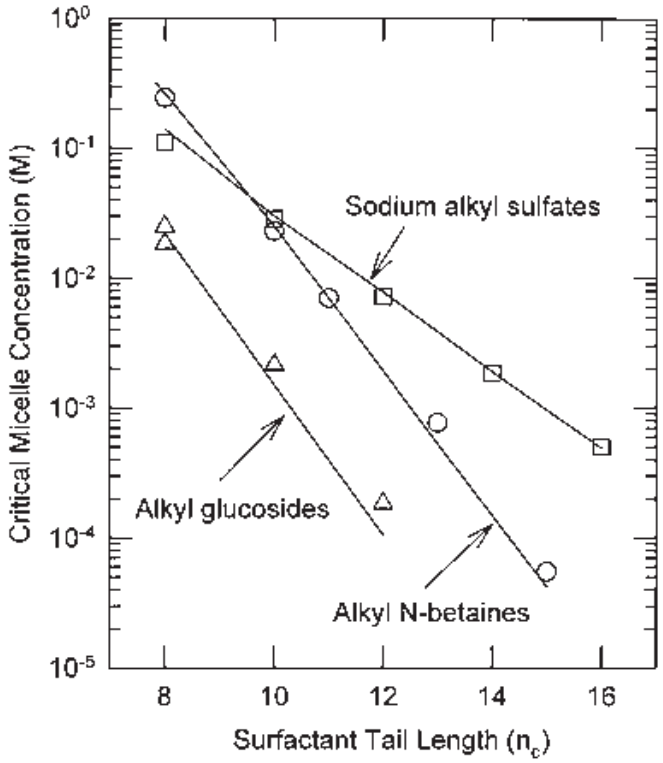

FIG. 6 Dependence of the critical micelle concentration on the number of carbon atoms in the surfactant tail for nonionic alkyl β-glucosides (triangles), zwitterionic N-alkyl betaines (circles), and anionic sodium alkyl sulfates (squares). The lines represent the theoretical predictions while the points are experimental data. (From Refs. 66–71.)

with increasing length of the surfactant tail and remain practically constant for the longer tail lengths. These results can be understood by noting that the CMC for the surfactant with the smaller tail length is large, and for this reason the ionic strength is larger. This decreases the headgroup ionic repulsion, thus leading to a smaller equilibrium area per molecule in the aggregate. In contrast, for surfactants with longer tail lengths, the CMCs are low, the ionic strengths smaller, and hence, the equilibrium area per molecule in the aggregate larger. This increase in the equilibrium area per molecule with increasing tail length is responsible for the relatively small changes in the aggregation number with increasing tail length, in contrast to the behavior exhibited by the zwitterionic surfactant.

3. Influence of Ionic Strength on Aggregation Behavior

The headgroup ionic interactions at the micelle surface are weakened by the addition of salt to the surfactant solution. Figures 8 and 9 present the predicted dependence of the CMC (Figure 8) and the average aggregation number (Figure 9) of sodium dodecyl sulfate, on the amount of added NaCl

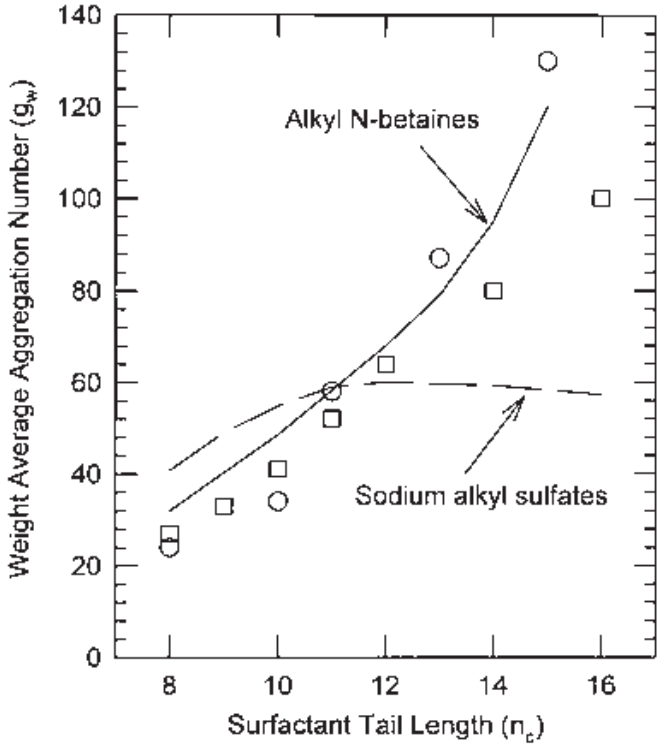

FIG. 7 Dependence of the weight average aggregation number of micelles at the CMC, on the chain length of the surfactant tail for sodium alkyl sulfates (squares) and N-alkyl betaines (circles). The points are experimental data. (From Refs. 70–76.) The dotted line shows predicted values for sodium alkyl sulfates while the continuous line describes the predictions for N-alkyl betaines. See text for comments about the reported experimental aggregation numbers for sodium alkyl sulfates with C_{14} and C_{16} surfactant tails.

electrolyte. For the range of ionic strengths considered, only narrowly dispersed spherical or globular micelles are formed. With decreasing ionic repulsion between the headgroups, the predicted CMC decreases and the average aggregation number of the micelle increases, in satisfactory agreement with experimental measurements (74,75).

4. Influence of Temperature on Aggregation Behavior

The temperature dependence of the CMC and the average aggregation number of the micelle have been calculated for a number of surfactants. Figure 10 compares the predicted CMC values with the experimental data [70,71] for the zwitterionic surfactants N-alkyl betaines for three different alkyl chain lengths. In Fig. 11, the predicted CMCs of the anionic sodium dodecyl sulfate have been plotted for two different concentrations of added NaCl electrolyte and compared with experimental data [77]. Calculated and experimental [78] CMCs are presented in Fig. 12 for the homologous family of sodium alkyl sulfonates. In all cases, the predictions show reasonable

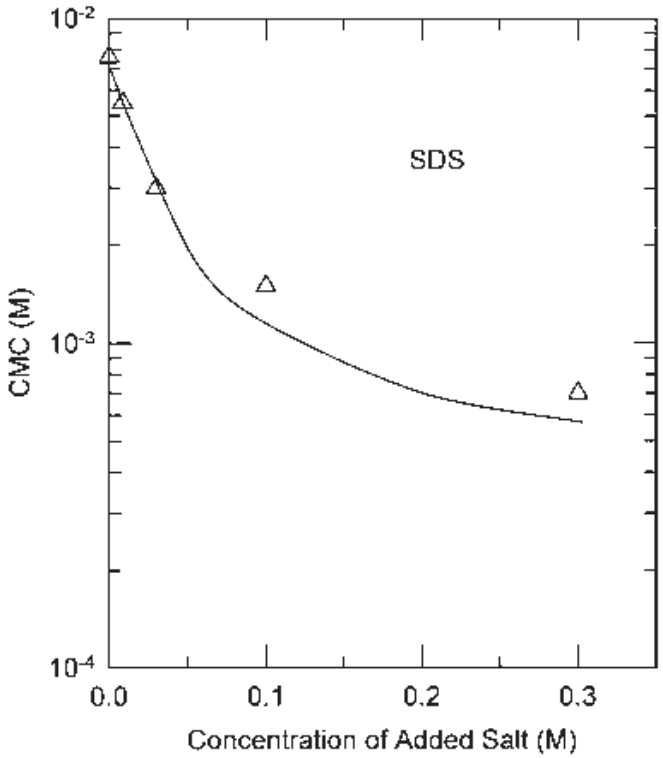

FIG. 8 Influence of added NaCl concentration on the CMC of sodium dodecyl sulfate micelles. The lines denote the predicted values while the points are the experimental measurements at 25°C. (From Refs. 74 and 75.)

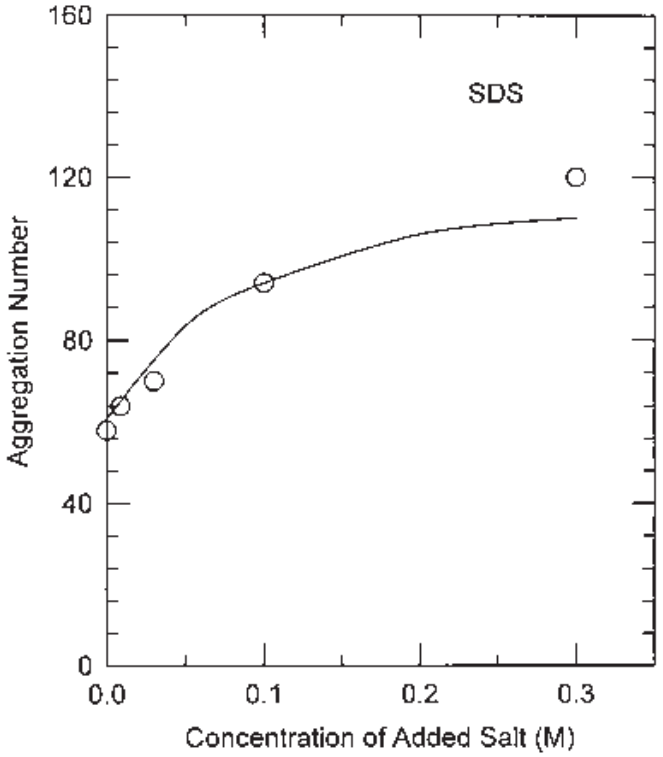

FIG. 9 Influence of added NaCl concentration on the average aggregation number of sodium dodecyl sulfate micelles. The lines denote the predicted values while the points are the experimental measurements at 25°C. (From Refs. 74 and 75.)

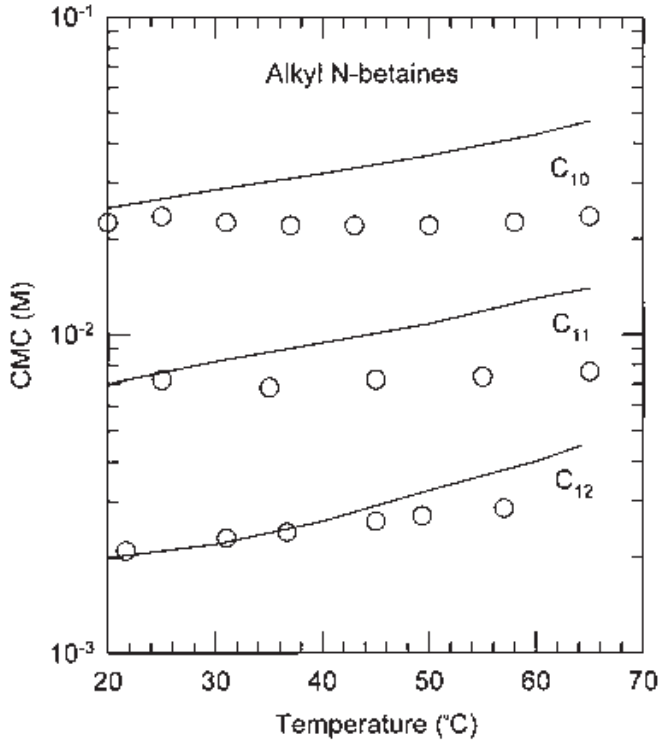

FIG. 10 The dependence of CMC on temperature for N-alkyl betaines having C_{10}, C_{11} and C_{12} chains as surfactant tails. The lines are predictions of the present theory while the points are experimental data. (From Refs. 70 and 71.)

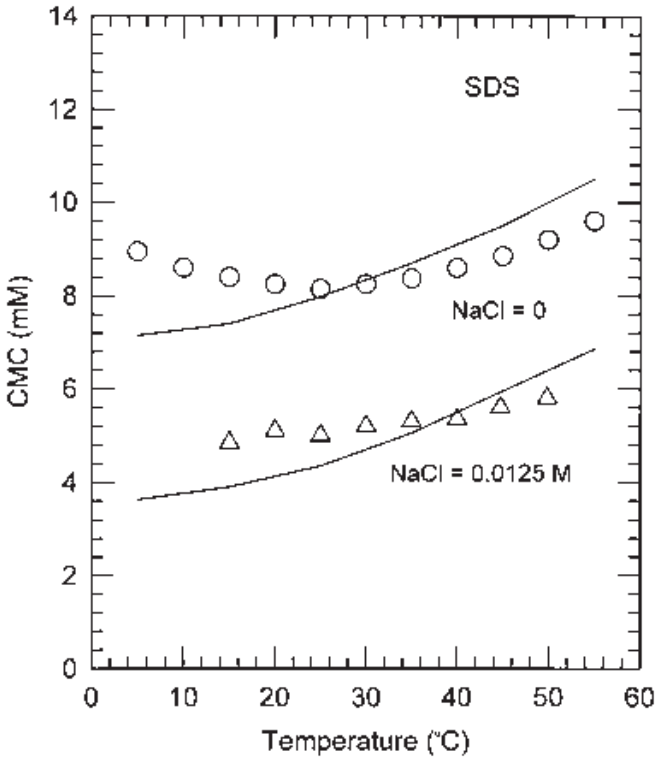

FIG. 11 The dependence of CMC on temperature for sodium dodecyl sulfate in water and in a 0.0125M solution of NaCl. The lines are predictions of the present theory while the points are experimental data. (From Ref. 77.)

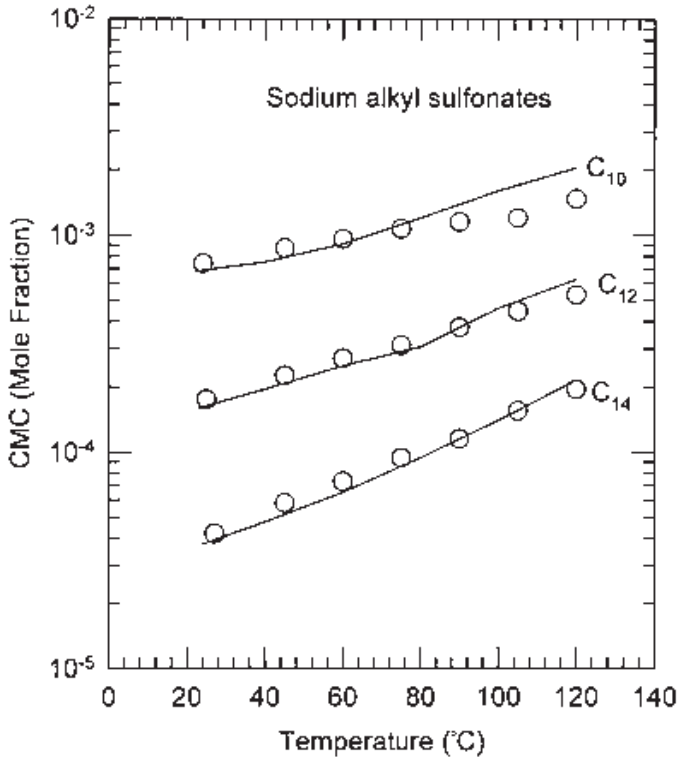

FIG. 12 The dependence of CMC on temperature for sodium alkyl sulfonates having C_{10}, C_{12}, and C_{14} chains as surfactant tails. The lines are predictions of the present theory while the points are experimental data. (From Ref. 78.)

agreement with experiment. One may note that the experiment indicates some increase in the CMC as the temperature is decreased below about 25°C, while the predicted values show a monotonic decrease of the CMC with decreasing temperature. It has been suggested [5] that the hydration state of the ionic headgroup in the micelles may be different from that in the singly dispersed state as the temperature is lowered below 25°C. A free energy contribution accounting for such an effect is not included in the theory since it cannot be calculated with any precision at the present time.

5. Transition from Spherical to Rodlike Micelles

The predicted results for nonionic alkyl β-glucosides indicate that large, polydispersed rodlike micelles form. For octyl glucoside the aggregation numbers are still not very large, but for longer chain lengths very large rods form. The predicted weight average aggregation number is used to compute the hydrodynamic radius of the micelles using the expression

$$R_{\mathrm{H}} = \left(\frac{3\, g_{\mathrm{w}}\, v_{\mathrm{S}}}{4\pi}\right)^{1/3} + \ell_{\mathrm{p}} \tag{58}$$

where ℓ_p is the length of the polar headgroup. For the ring structure of the β-glucoside, ℓ_p has been estimated [5] to be 0.7 nm. The computed hydrodynamic radius as a function of surfactant concentration is presented in Fig.13.

The two predicted lines correspond to two marginally different values of the parameter a_p describing the headgroup of the surfactant. One may note from Eq. (12) that the sphere-to-rod transition parameter K [which determines g_w as per Eq. (16)] can be dramatically altered by small changes in the free energy difference $(\Delta\mu^0_{\text{cap}}) - (\Delta\mu^0_{\text{cyl}})$, since g_{cap}, which appears in the definition of K, is quite large. For example, assuming a typical value of 90 for g_{cap}, a small change of 0.05 kT in the free energy difference $(\Delta\mu^0_{\text{cap}}) - (\Delta\mu^0_{\text{cyl}})$ will cause a change in K of $e^{4.5} = 90$, which, in turn, can change the predicted value for g_w by a factor of about 10. Therefore, the predicted average aggregation numbers are very sensitive even to small changes in

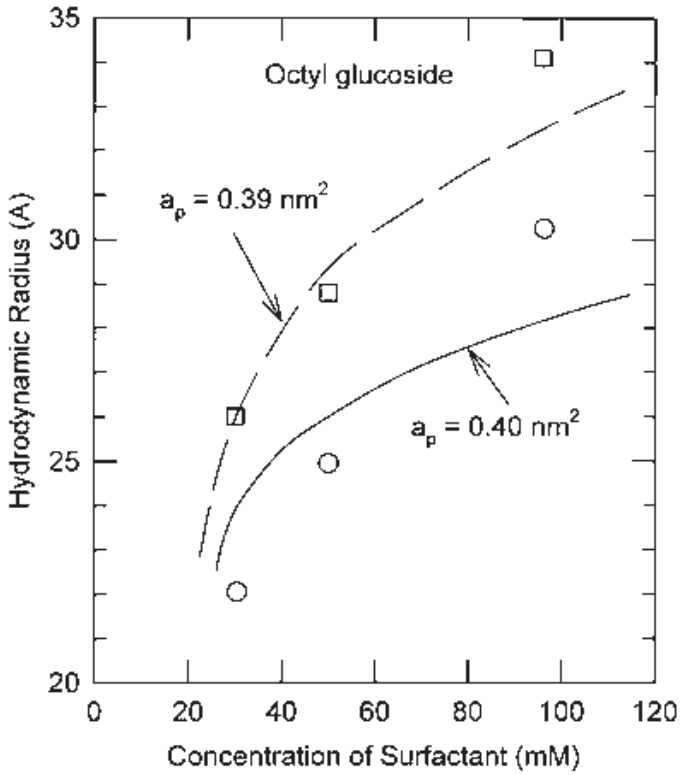

FIG. 13 The dependence of the micellar size (expressed as the hydrodynamic radius) on the concentration of the surfactant for octyl glucoside. Both lines correspond to predicted values but for marginally different values of the molecular constant a_p. The continuous line corresponds to $a_p = 40\text{Å}^2$ while the dotted line corresponds to $a_p = 39\text{Å}^2$. The squares denote the reported experimental data. (From Ref. 68.) The circles correspond to modified experimental data if the reported hydrodynamic radius had included one layer of water. See text for discussion.

the free energy estimates when rodlike micelles form. This is illustrated by the calculations carried out for two slightly different values of the parameter a_p, which affects the magnitude of the headgroup steric interaction energy. The predictions are compared with the data provided by dynamic light scattering measurements [68]. It is not clear whether the reported hydrodynamic radii correspond to the dry or hydrated aggregates. Therefore, both the reported hydrodynamic radii and the radii obtained by subtracting the diameter of a water molecule are plotted in Fig. 13. Given the sensitivity of K to the free energy estimates, the agreement between the measured and predicted aggregate sizes is satisfactory.

For anionic sodium alkyl sulfates with NaCl as the added electrolyte, an increase in ionic strength beyond that in Fig. 9 is expected to contribute to a transition from globular micelles to large spherocylindrical micelles. As already noted, the ability to predict ln K with deviations of about 4.5 or less from the measurements can be considered satisfactory. The predicted values for the sphere-to-rod transition parameter K for sodium dodecyl sulfate are plotted in Fig. 14 against the added concentration of NaCl as the electrolyte

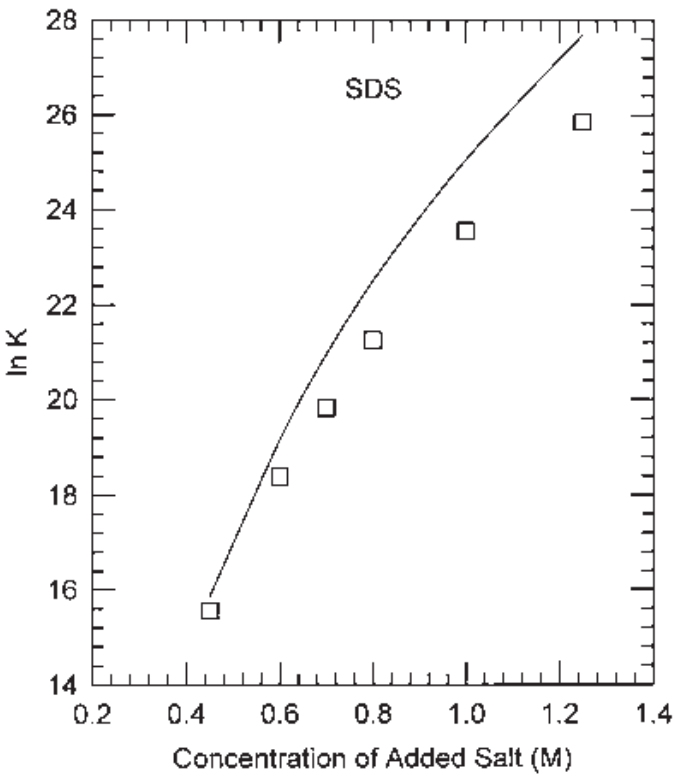

FIG. 14 The dependence of the sphere-to-rod transition parameter K for sodium dodecyl sulfate on the concentration of added electrolyte NaCl. The points are from light scattering measurements (from Ref. 50) and the line represents the predictions, both at 25°C.

and are compared with light scattering measurements [79]. The largest deviation between predicted and experimental value of ℓnK is about 2, at the highest ionic strength. The predicted radius of the cylindrical part of the aggregate is smaller than the fully extended length of the surfactant tail. It increases from 1.45 nm to 1.49 nm as the electrolyte concentration is increased from 0.45 M to 1.25 M at 25°C. For this range of ionic strengths, the radius of the endcaps remains unaltered and is equal to the extended length of the surfactant tail. The predicted CMC, as defined by Eq. (17), decreases from 0.38 mM to 0.204 mM over this range of added salt concentration.

The temperature dependence of the parameter K has been calculated for sodium dodecyl sulfate for two concentrations of the added NaCl electrolyte. The predicted values of K are plotted in Fig. 15 along with the experimental estimates based on dynamic light scattering measurements [79]. The largest deviation in ℓnK is about 4.5, and the theory predicts a somewhat stronger dependence on the temperature than that observed experimentally. Figure 16 presents the predicted values of K as a function of the added electrolyte concentration for the homologous family of sodium alkyl sulfates

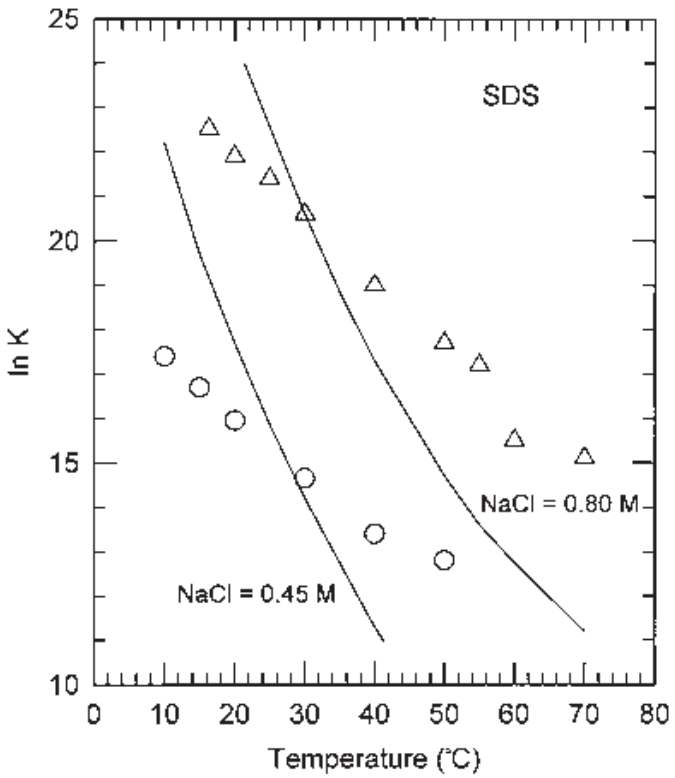

FIG. 15 Influence of temperature on the sphere-to-rod transition parameter K of sodium dodecyl sulfate in solutions containing 0.45M and 0.80M added NaCl electrolyte. The lines denote the predicted values while the points are experimental data. (From Ref. 79.)

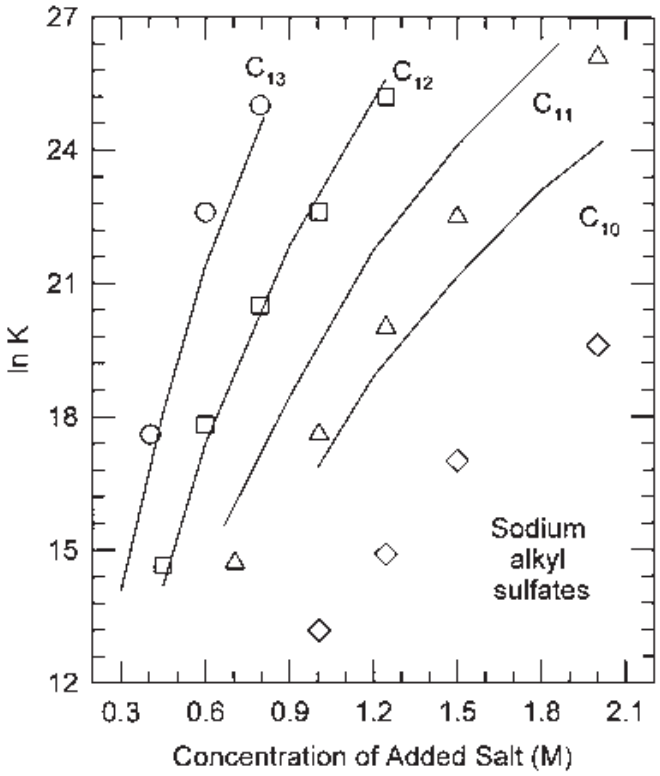

FIG. 16 The dependence of the sphere-to-rod transition parameter K on the surfactant tail length and on the concentration of added electrolyte NaCl for sodium alkyl sulfates. The lines are predictions obtained from the present theory while the points denote the experimental data (from Ref. 79), both at 30°C. The predicted lines are labeled with the surfactant tail lengths, and the corresponding experimental data are indicated by circles, squares, triangles, and diamonds, respectively.

with 10 to 13 carbon atoms in their hydrophobic tails. The figure shows that even the largest deviation in $\ln K$ between the predicted and the experimental values [79] is smaller than 2 for C_{11}, C_{12}, and C_{13} sodium sulfates and is about 4 for the C_{10} sodium sulfate.

Given the sensitivity of the parameter K to the free energy estimates, the ability of the theory to predict K accurately as a function of the ionic strength, temperature, and tail length for sodium alkyl sulfates is remarkable. However, when the calculations are repeated for alkyl sulfates with other counterions such as Li, K, etc., the predicted K values significantly deviate from the measurements [79]. As mentioned before, this is not surprising given the sensitivity of K. In contrast, the prediction of the CMC and micelle size is quite satisfactory in the presence of various counterions, when only spherical or globular micelles form. Therefore, improved accounting of the counterion effects beyond what is considered in the approximate analytical solution to the Poisson–Boltzmann equation is necessary for predicting accurate values of K. Such treatment of counterion effects remains to be developed.

6. Formation of Bilayer Vesicles

The aggregation behavior of the anionic dialkyl sodium sulfate at an ionic strength of 0.01 M has been calculated. Because of the presence of two tails, these surfactants can form spherical vesicular structures provided the length of the surfactant tail is large enough and the ionic strength is not too small. The predicted aggregation number, the inner and the outer radii, the thicknesses of the inner and the outer layer, the numbers of molecules of surfactant present in the two layers, and the CMC are all listed in Table 4. The inner and the outer layers differ somewhat in thicknesses, with the inner layer more compressed than the outer. The thicknesses are much smaller than the extended lengths of the tails and are also smaller than the radii of spherical and cylindrical micelles formed of single-tailed sodium alkyl sulfates, discussed before. The equilibrium areas per surfactant molecule are substantially different from one another for the molecules in the two layers. The vesicles are not too large and the aggregation number increases with increasing chain length of the surfactant. As one may anticipate, the CMC is small because of the larger magnitude of the tail transfer free energy in case of the dialkyl tail.

Calculated results for dialkyl lecithins with phosphotidylcholine headgroup are also presented in Table 4 for alkyl chain lengths varying from 12 to 18. The vesicles formed of lecithins also have inner and outer layers of differing thicknesses. However, the radii of the lecithin vesicles and, hence,

TABLE 4 Predicted Structural Properties of Vesicles

n_C	R_i (nm)	R_o (nm)	t_i (nm)	t_o (nm)	a_i (nm^2)	a_o (nm)	g_i	g_o	X_{cmc}
di-$C_n SO_4Na$ + 0.01M NaCl									
12	4.63	6.68	0.98	1.07	0.5825	0.771	462	727	7.67×10^{-8}
14	5.30	7.57	1.09	1.08	0.6065	0.805	580	893	1.07×10^{-9}
16	5.83	8.31	1.20	1.28	0.627	0.836	684	1041	1.46×10^{-11}
18	6.36	9.04	1.30	1.38	0.646	0.865	787	1185	1.92×10^{-13}
di-C_n-lecithin									
12	20.90	22.67	0.846	0.92	0.796	0.794	6929	8163	1.58×10^{-9}
14	20.11	22.09	0.95	1.03	0.813	0.82	6260	7490	2.01×10^{-11}
16	19.61	21.80	1.05	1.14	0.828	0.845	5855	7086	2.49×10^{-13}
18	19.30	21.70	1.15	1.25	0.842	0.869	5577	6822	3.04×10^{-15}

Note: i refers to the inner layer of the bilayer and o to the outer layer, R is the radius at the hydrophobic domain–water interface, t is the layer thickness, a is the area per surfactant molecule, and g is the number of surfactant molecules.

the aggregation numbers are much larger than those formed of dialkyl sodium sulfates. Consequently, the areas per molecule in the inner and outer layers are closer to one another. The vesicle radius deceases slightly with an increase in the chain length of the surfactant. The differences between the two types of molecules can be traced to the decrease in the headgroup repulsions in the case of the zwitterionic lecithin headgroups compared to that in the case of anionic sodium sulfate headgroups. In all cases listed in Table 4, the aggregates are narrowly dispersed.

7. Influence of Polyoxyethylene Headgroups

The predicted CMC values for a surfactant $C_{12}E_x$ with dodecyl hydrocarbon tail and 6 to 53 oxyethylene units are presented in Fig. 17 for both the uniform concentration model and the nonuniform concentration model

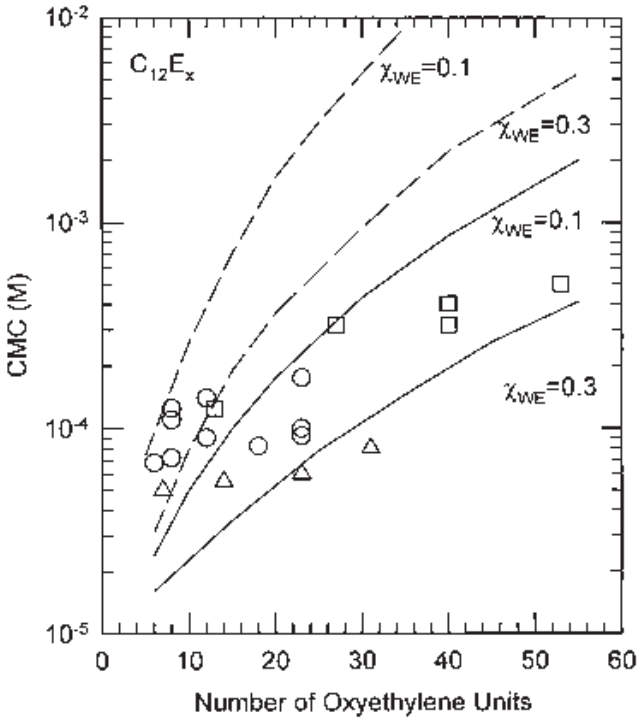

FIG. 17 Dependence of the CMC on the length of the polyoxyethylene headgroup of nonionic surfactants $C_{12}E_x$. The points refer to measured values while the lines denote predictions from the present model, both at 25°C. The continuous lines represent the results from the nonuniform concentration model while the dotted lines denote the predictions based on the uniform concentration model. Calculated results are shown for two different values of the polyoxyethylene–water interaction parameter χ_{WE}. The circles refer to commercial polyoxyethylene glycol ethers (from Refs. 81–84), triangles represent commercial samples where the distribution of oxyethylene chain lengths is reduced by molecular distillation (from Ref. 85), and squares correspond to purified polyoxyethylene methyl ethers (from Ref. 86).

and for $\chi_{WE} = 0.1$ and 0.3. As mentioned before in Section IV.A.8, the uniform concentration model may be appropriate for small values of E_x and the nonuniform concentration model may be more suitable for larger E_x. The experimental data used for comparison are for polyoxyethylene glycol ethers [80–85] and polyoxyethylene methyl ethers [86]. The considerable scatter in the measured CMCs is a consequence of the heterogeneity of some of the surfactant samples that have been used, the samples containing a range of polyoxyethylene chain lengths distributed around the reported mean value. Figure 18 presents the predicted as well as measured CMC data for a surfactant $C_{16}E_x$ with a hexadecyl hydrocarbon tail and 8 to 63 oxyethylene units. The experimental data are for polyoxyethylene glycol ethers [87–90] and polyoxyethylene methyl ethers [86]. The smaller scatter in the experimental data of Fig. 18 compared to that of Fig. 17, is primarily due to the fewer measurements available for the $C_{16}E_x$ surfactants.

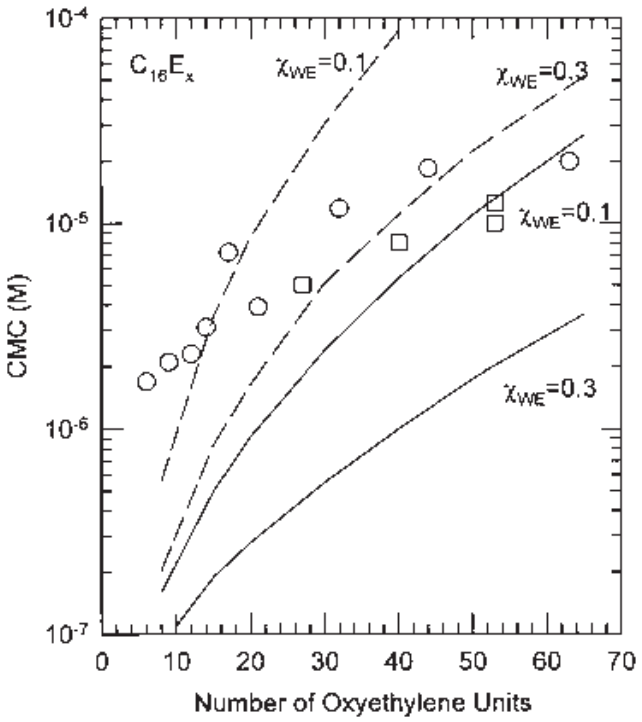

FIG. 18 Dependence of the CMC on the length of the polyoxyethylene headgroup of nonionic surfactants $C_{16}E_x$. The points refer to measured values while the lines denote predictions from the present model, both at 25°C. The continuous lines represent the results from the nonuniform concentration model while the dotted lines denote the predictions based on the uniform concentration model. Calculated results are shown for two different values of the polyoxyethylene-water interaction parameter χ_{WE}. Circles denote polyoxyethylene glycol ethers (from Refs. 87–90) while the squares represent purified polyoxyethylene methyl ethers (from Ref. 86).

The predicted aggregation numbers based on the nonuniform concentration model are plotted in Figs. 19 and 20 for $C_{12}E_x$ and $C_{16}E_x$ surfactants, respectively. Measured aggregation numbers [81,87–90] are also included for comparison. The calculated aggregation numbers are in qualitative agreement with the experimental values. The predicted aggregation numbers are larger when a larger value is taken for χ_{WE}. The agreement between the predicted and measured aggregation numbers is satisfactory even from a quantitative point of view. The predicted thickness D of the micellar corona region is plotted in Figs. 21 and 22, respectively, for the $C_{12}E_x$ and $C_{16}E_x$ surfactants, on the basis of the non-uniform concentration model. The experimental shell thicknesses are those estimated by Tanford et al. [91] from intrinsic viscosity measurements [87–90]. As expected, the shell thickness D calculated assuming a smaller value for χ_{WE} ($= 0.1$, implying a better solvent) is larger than that based on a larger value ($= 0.3$, implying a relatively poorer solvent).

The predicted aggregation numbers based on the uniform concentration model are presented in Figs. 23 and 24 for $C_{12}E_x$ and $C_{16}E_x$ surfactants. The

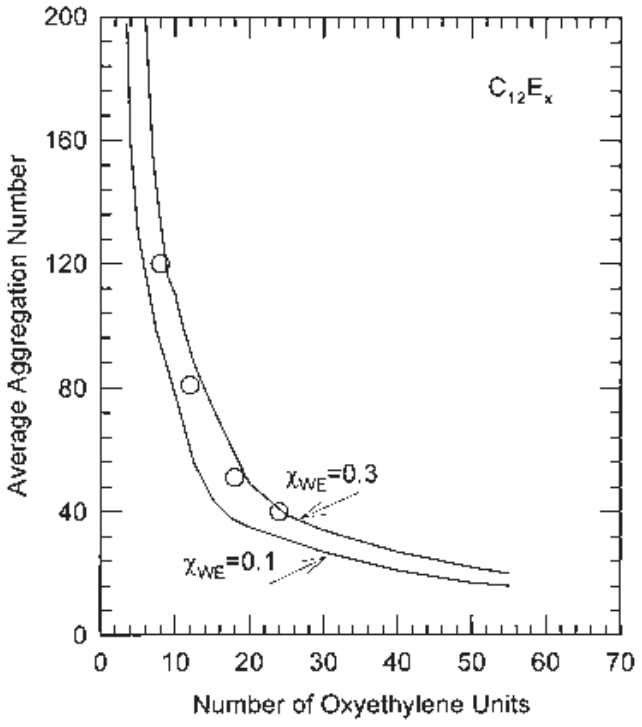

FIG. 19 Influence of the polyoxyethylene headgroup size on the average aggregation number of micelles for surfactants with dodecyl hydrophobic tail. The points are experimental data at 25°C (from Refs. 80 and 87-90) and the lines represent the predictions of the present theory. The calculated results are based on the nonuniform concentration model.

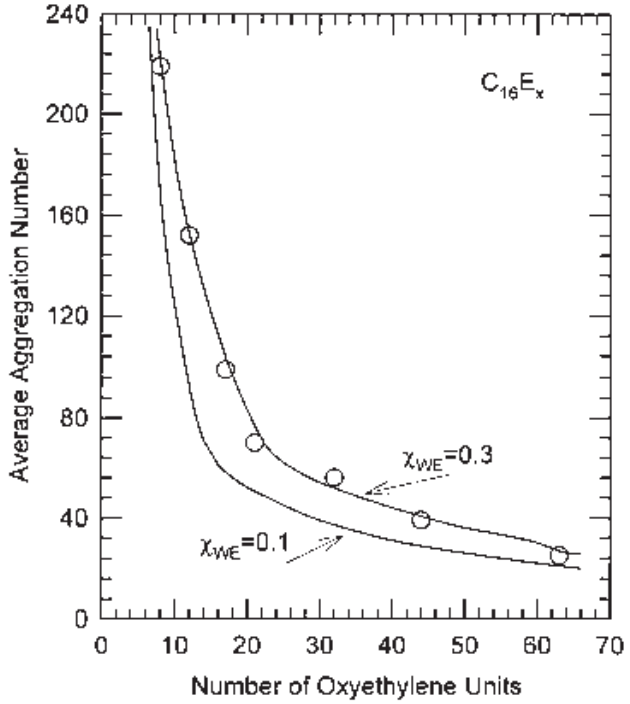

FIG. 20 Influence of the polyoxyethylene headgroup size on the average aggregation number of micelles for surfactants with hexadecyl hydrophobic tail. The points are experimental data at 25°C (from Refs. 80 and 87–90) and the lines represent the predictions of the present theory. The calculated results are based on the nonuniform concentration model.

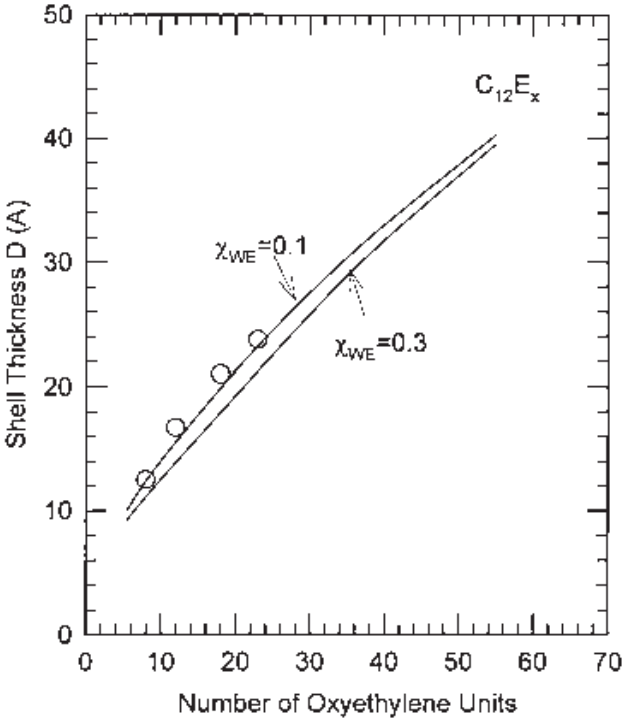

FIG. 21 Influence of the polyoxyethylene headgroup size on the shell thickness of the micelles for the $C_{12}E_x$ surfactants. The points are experimental data at 25°C (from Ref. 91), and the lines represent the predictions of the present theory. The calculated results are based on the nonuniform concentration model.

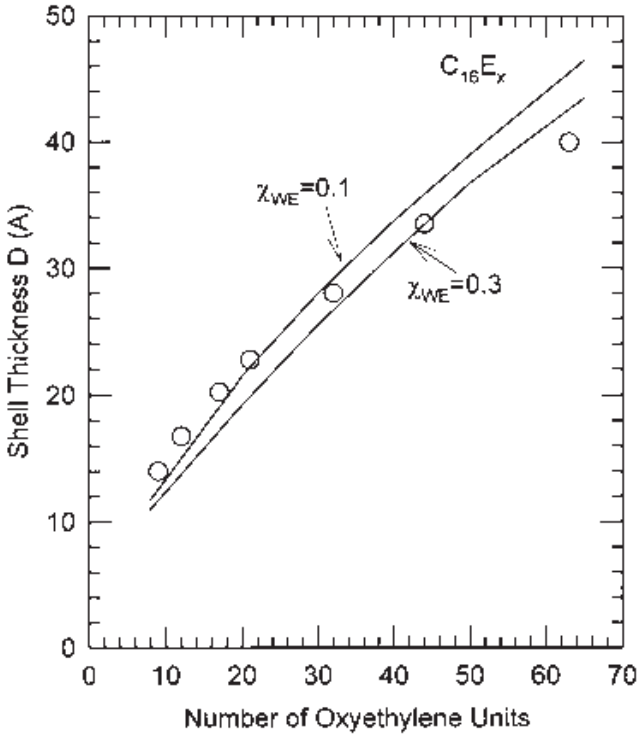

FIG. 22 Influence of the polyoxyethylene headgroup size on the shell thickness of the micelles for the $C_{16}E_x$ surfactants. The points are experimental data at 25°C (from Ref. 91), and the lines represent the predictions of the present theory. The calculated results are based on the nonuniform concentration model.

predicted shell thicknesses based on the uniform concentration model are presented in Figs. 25 and 26 for $C_{12}E_x$ and $C_{16}E_x$ surfactants. The predicted dependence of the micelle aggregation numbers on the polyoxyethylene chain length is in reasonable agreement with the experimental data, but the calculated aggregation numbers are smaller than the experimental values. Figures 25 and 26 show that the model predicts much smaller values for the corona thickness D than that estimated from intrinsic viscosity measurements [91].

The temperature dependence of the aggregation behavior of surfactants with polyoxyethylene headgroups is expected to differ from that of ionic and zwitterionic surfactants because of the way the interactions between polyoxyethylene headgroups depend on temperature. For ionic and zwitterionic surfactants, the various contributions to the free energy of micellization display a temperature dependence that leads to a lowering of the aggregation number with increasing temperature. These temperature-dependent effects are, however, overshadowed by the temperature-dependent χ_{WE}, which governs the interactions between the polyoxyethylene headgroups and water in the micellar shell region. As suggested by the observed phase behavior of the polyoxyethylene–water systems [54–56], the interaction

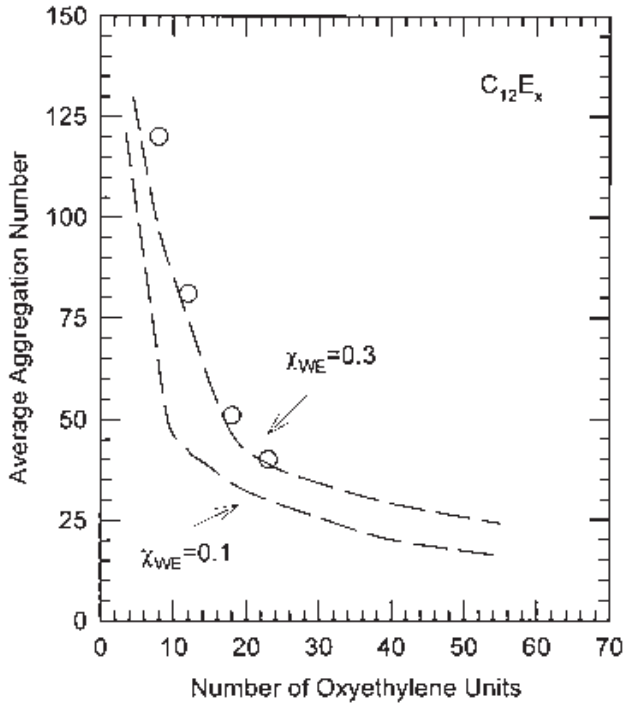

FIG. 23 Influence of the polyoxyethylene headgroup size on the average aggregation number of micelles. The surfactants contain dodecyl hydrophobic tails. The points are experimental data at 25°C (from Refs. 80 and 87–90), and the lines represent the predictions of the present theory. The calculated results are based on the uniform concentration model.

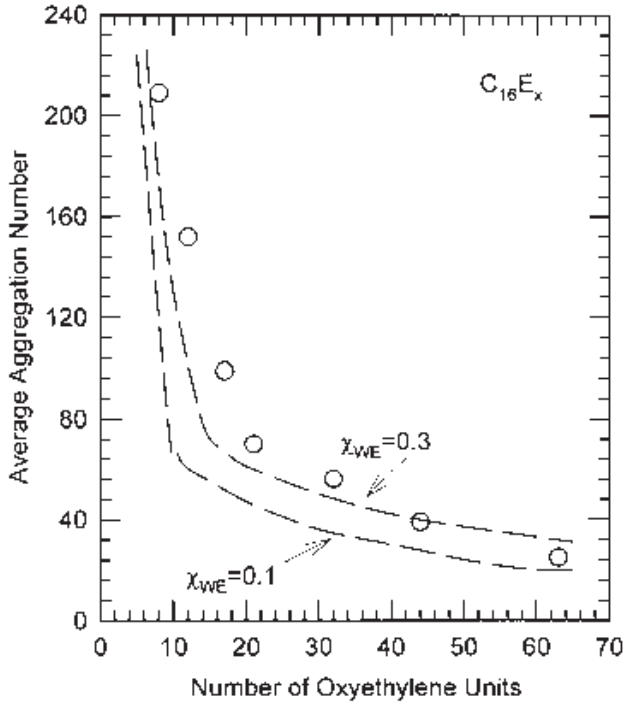

FIG. 24 Influence of the polyoxyethylene headgroup size on the average aggregation number of micelles. The surfactants contain hexadecyl hydrophobic tails. The points are experimental data at 25°C (from Refs. 80 amd 87–90), and the lines represent the predictions of the present theory. The calculated results are based on the uniform concentration model.

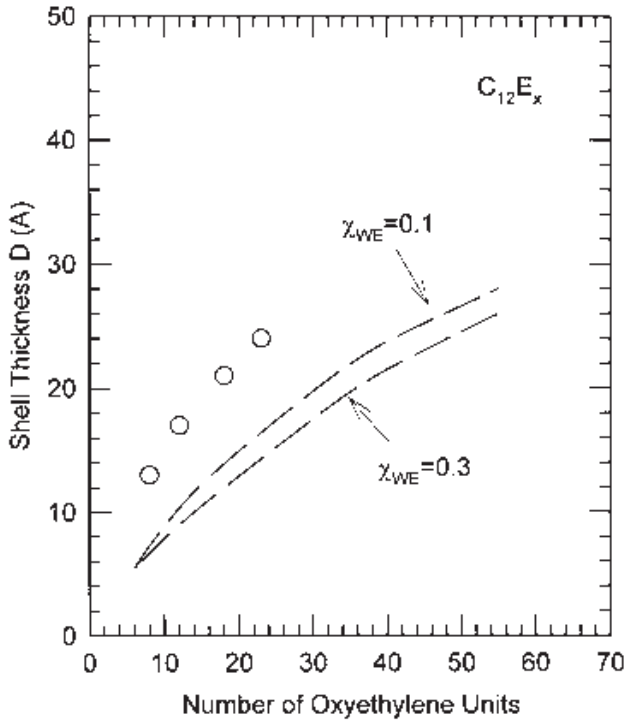

FIG. 25 Influence of the polyoxyethylene headgroup size on the thickness of the micellar shell for the $C_{12}E_x$ surfactants. The points are experimental data at 25°C (91) and the lines represent the predictions of the present theory. The calculated results are based on the uniform concentration model.

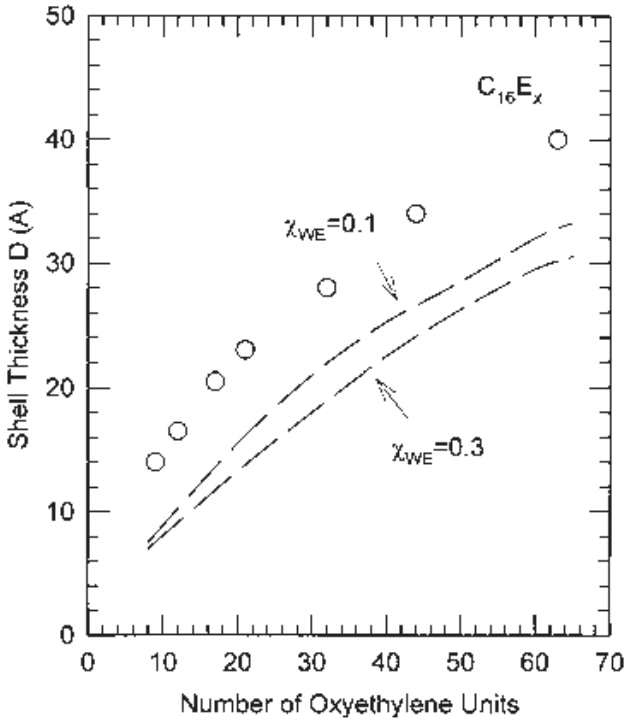

FIG. 26 Influence of the polyoxyethylene headgroup size on the thickness of the micellar shell for the $C_{16}E_x$. surfactants. The points are experimental data at 25°C (from Ref. 91), and the lines represent the predictions of the present theory. The calculated results are based on the uniform concentration model.

parameter χ_{WE} first increases as the temperature is increased (giving rise to the lower critical solution temperature, LCST), passes through a maximum, and then decreases with increasing temperature (giving rise to the upper critical solution temperature, UCST). Thus, for temperatures smaller than the LCST (which is the temperature range for which the aggregation behavior is examined), the interaction parameter χ_{WE} should increase with increasing temperature. The calculations presented above show that the aggregation numbers increase with increasing χ_{WE} if none of the other variables is changed (Figs. 19 and 20 or 23 and 24). Consequently, for polyoxyethylene surfactants, the headgroup interactions with water promote aggregate growth with increasing temperature. The remaining free energy contributions favor a decrease in the aggregation number with increasing temperature. It is interesting to note that an increase in χ_{WE} with increasing temperature promotes both the phase separation of the polymer solution (LCST) and also the growth of the micelles to large aggregation numbers [92,93].

The calculated results show that for nonionic surfactants with polyoxyethylene headgroups, the predictions from the nonuniform concentration model are in somewhat better agreement with experiments than those from the uniform concentration model. However, improved agreement between predicted and experimental micellar properties should await a more satisfactory treatment of polyoxyethylene–water solutions than presently available. Alternately, a modified treatment of headgroup interactions, considering the headgroups to be oligomers rather than polymers, is necessary. It is important that the general validity of any model for nonionic polyoxyethylene surfactants be tested by comparing experimental and predicted results for all the micellar characteristics, namely the CMC, the aggregation number, and the shell thickness over an extended range of polyoxyethylene chain lengths. Although these surfactants are among the most commonly used in practical applications, a comprehensive prediction of their solution properties remain to be developed despite many papers that have appeared in the literature.

V. THEORY OF MICELLIZATION OF SURFACTANT MIXTURES

A. Size and Composition Distribution of Micelles

The thermodynamic treatment and illustrative calculations presented in this section focus on binary mixtures of surfactants for which many experimental results are available. The approach, however, can be readily extended to a mixture of three or more surfactants. A molecular theory of mixed micelles

was first proposed in our earlier work [94], which was later improved by incorporating a better treatment of molecular packing in mixed micelles [95]. This latter model constitutes the basis of this section.

We consider a solution of surfactant molecules A and B and denote by g the aggregation number of the mixed micelle containing g_A molecules of A and g_B molecules of B. At equilibrium, in analogy with Eq. (4), one obtains [94–96] for the aggregate size and composition distribution, the equation

$$X_g = X_{1A}^{g_A} X_{1B}^{g_B} \exp -\left(\frac{g\Delta\mu_g^0}{kT}\right), \qquad \left(\frac{g\Delta\mu_g^0}{kT}\right) = \left(\frac{\mu_g^0 - g_A\,\mu_{1A}^0 - g_B\,\mu_{1B}^0}{kT}\right) \tag{59}$$

Here, μ_g^0 is the standard chemical potential of the mixed micelle, while μ_{1A}^0 and μ_{1B}^0 are the standard chemical potentials of the singly dispersed A and B molecules, respectively; $\Delta\mu_g^0$ is the difference in the standard chemical potentials between g_A/g molecules of surfactant A plus g_B/g molecules of surfactant B present in an aggregate of size g and the same numbers of molecules present in their singly dispersed states in water; X_{1A} and X_{1B} are the mole fractions of the singly dispersed surfactants A and B, while X_g is the mole fraction of aggregates of size g in the solution. The mole fraction X_g is dependent not only on the size g but also on the composition of the micelle.

We define the solvent-free composition of the singly dispersed surfactant mixture, the mixed micelle, and the total surfactant mixture by the relations

$$\begin{aligned}
\alpha_{1A} &= \frac{X_{1A}}{X_{1A} + X_{1B}} = \frac{X_{1A}}{X_1}, & \alpha_{1B} &= \frac{X_{1B}}{X_{1A} + X_{1B}} = \frac{X_{1B}}{X_1} \\
\alpha_{gA} &= \frac{g_A}{g_A + g_B} = \frac{g_A}{g}, & \alpha_{gB} &= \frac{g_B}{g_A + g_B} = \frac{g_B}{g} \\
\alpha_{tA} &= \frac{X_{1A} + \sum g_A X_g}{X_1 + \sum g X_g}, & \alpha_{tB} &= \frac{X_{1B} + \sum g_B X_g}{X_1 + \sum g X_g}
\end{aligned} \tag{60}$$

In the definition for the total surfactant composition, the summation is over two independent variables, namely, the aggregation number $g = 2$ to ∞ and the micelle composition $\alpha_{gA} = 0$ to 1. One may note that for spherical bilayer vesicles, the compositions of the inner and the outer layers need not be the same. Therefore, we define the composition variables α_{gAi} and α_{gBi} for the inner layer and α_{gAo} and α_{gBo} for the outer layer, similar to the definitions given above for the overall composition of the aggregate. From the size and composition distribution one can compute the average sizes of

the aggregates via Eq. (5). The average composition of the mixed micelle can be calculated from

$$\overline{\alpha}_{g\mathrm{A}} = \sum (g_{\mathrm{A}}/g)\, X_g \,/ \sum X_g, \qquad \overline{\alpha}_{g\mathrm{B}} = \sum (g_{\mathrm{B}}/g)\, X_g \,/ \sum X_g \tag{61}$$

The geometrical relations for various micellar shapes have been presented in Table 1. In these relations, the tail volume v_{S} is now given by $v_{\mathrm{S}} = (\alpha_{g\mathrm{A}}\, v_{\mathrm{SA}} + \alpha_{g\mathrm{B}}\, v_{\mathrm{SB}})$, where, v_{SA} and v_{SB} denote the volumes of the hydrophobic tails of surfactants A and B.

B. Free Energy of Formation of Mixed Micelles

Expressions for the standard free energy difference between the surfactant molecules A and B present in a mixed micelle and those present in the singly dispersed state in water are obtained by a simple extension of the equations developed in Section IV for single-component surfactant systems. Only the modifications necessary for the treatment of surfactant mixtures compared to the analysis of pure surfactant behavior are described below.

1. Transfer of the Surfactant Tail

For a mixed micelle having the composition $(\alpha_{g\mathrm{A}}, \alpha_{g\mathrm{B}})$, the transfer free energy per surfactant molecule is given by [94,95]

$$\frac{(\Delta\mu_g^0)_{\mathrm{tr}}}{kT} = \alpha_{g\mathrm{A}} \frac{(\Delta\mu_g^0)_{\mathrm{tr,A}}}{kT} + \alpha_{g\mathrm{B}} \frac{(\Delta\mu_g^0)_{\mathrm{tr,B}}}{kT} \tag{62}$$

The transfer free energy contribution can be estimated as described in Section IV.A.2 using the group contributions. The transfer free energy calculated from Eq. (62) does not include contributions arising from the mixing of the A and the B tails inside the micellar core, which are accounted for separately.

2. Deformation of the Surfactant Tail

When surfactants A and B have different tail lengths, segments of both molecules may not be simultaneously present everywhere in the micellar core. Let us assume that surfactant A has a longer tail than surfactant B, $\ell_{\mathrm{SA}} > \ell_{\mathrm{SB}}$. If the micelle radius R is less than both ℓ_{SA} and ℓ_{SB}, then even the shorter tail can reach everywhere within the core of the micelle. If $\ell_{\mathrm{SA}} > R_{\mathrm{S}} > \ell_{\mathrm{SB}}$, then the inner region of the micellar core, of dimension $(R_{\mathrm{S}} - \ell_{\mathrm{SB}})$, can be reached only by the A tails. Taking into account the different extent to which the A and the B tails are stretched for the two situations described above, one obtains [95] the expression

$$\frac{(\Delta\mu_g^0)_{\text{def}}}{kT} = B_g\left[\alpha_{g\text{A}}\,\frac{R_{\text{S}}^2}{N_{\text{A}}L^2} + \alpha_{g\text{B}}\,\frac{Q_g^2}{N_{\text{B}}L^2}\right], \qquad B_g = \left(\frac{9P\pi^2}{80}\right)$$
$$Q_g = R_{\text{S}} \quad \text{if} \quad R_{\text{S}} < \ell_{\text{SA}}, \ell_{\text{SB}},$$
$$Q_g = \ell_{\text{SB}} = N_{\text{B}}L \quad \text{if} \quad \ell_{\text{SA}} > R_{\text{S}} > \ell_{\text{SB}} \tag{63}$$

This equation is used for spherical and globular micelles and for the spherical endcaps of rodlike micelles. N_{A} and N_{B} stand for the number of segments in the tails of surfactants A and B, respectively, and P is the packing factor defined in Table 1. Because the innermost region of the micelle is not accessible to surfactant B, the micelle must contain a sufficient number of A surfactant molecules to completely fill up the inner region. This packing condition is satisfied if the radius R_{S} is less than the composition averaged tail length, $R_{\text{S}} \leq (\eta_{\text{A}}\ell_{\text{SA}} + \eta_{\text{B}}\ell_{\text{SB}})$, where η_{A} and η_{B} are the volume fractions of surfactant tails in the micellar core. In all the calculations reported here, the upper limit of R_{S} is taken to be this composition averaged tail length [95]. For the cylindrical part of the rodlike micelles, the coefficient 9 in B_{g} is replaced by 10, the radius R_{S} is replaced by the radius R_{C} of the cylindrical core, and the packing factor $P = 1/2$. For spherical bilayer vesicles, the coefficient 9 in B_{g} is replaced with 10, the radius R_{S} is replaced by the layer thickness t_i for the molecules in the inner layer and by the layer thickness t_o for the molecules in the outer layer, and $P = 1$, as for lamellar aggregates. For fluorocarbon chains, as mentioned in Section IV.A, the calculations are performed retaining the definition for the segment length L to be 0.46 nm.

3. Formation of Aggregate Core–Water Interface

The free energy associated with the formation of the hydrophobic core–water interface is given for the case of binary mixtures by the expression [94,95]

$$\frac{(\Delta\,\mu_g^0)_{\text{int}}}{kT} = \frac{\sigma_{\text{agg}}}{kT}\left(a - \alpha_{g_{\text{A}}}\,a_{o\text{A}} - \alpha_{g_{\text{B}}}\,a_{o\text{B}}\right) \tag{64}$$

Here, $a_{o\text{A}}$ and $a_{o\text{B}}$ are the areas per molecule of the core surface shielded from contact with water by the polar headgroups of surfactants A and B. Because the interfacial tension against water of various hydrocarbon and fluorocarbon tails of surfactants are close to one another, the aggregate core–water interfacial tension σ_{agg} is approximated by the micelle composition averaged value:

$$\sigma_{\text{agg}} = \eta_{\text{A}}\,\sigma_{\text{AW}} + \eta_{\text{B}}\,\sigma_{\text{BW}} \tag{65}$$

where σ_{AW} and σ_{BW} are interfacial tensions between water and the tails of A and B surfactants. For spherical bilayer vesicles, the area per molecule differs for the inner and the outer layers, and a in Eq. (64) is replaced by $(A_{go} + A_{gi})/g$.

4. Headgroup Steric Interactions

Extending the expression used for single surfactant systems to binary surfactant mixtures, one can write [94,95] for mixed micellar aggregates

$$\frac{(\Delta\mu_g^0)_{\text{steric}}}{kT} = -ln\left(1 - \frac{\alpha_{g\text{A}}\, a_{p\text{A}} + \alpha_{g\text{B}}\, a_{p\text{B}}}{a}\right) \tag{66}$$

For spherical bilayer vesicles, we take into account the composition variation between the inner and the outer layers. Equation (29) for a single surfactant is now extended to the form

$$\begin{aligned}\frac{(\Delta\mu_g^0)_{\text{steric}}}{kT} = &-\frac{g_o}{g}\ln\left(1 - \frac{\alpha_{g\text{A}o}a_{p\text{A}} + \alpha_{g\text{B}o}a_{p\text{B}}}{A_{go}/g_o}\right)\\ &-\frac{g_i}{g}\ln\left(1 - \frac{\alpha_{g\text{A}i}a_{p\text{A}} + \alpha_{g\text{B}i}a_{p\text{B}}}{A_{gi}/g_i}\right)\end{aligned} \tag{67}$$

5. Headgroup Dipole Interactions

The dipole–dipole interactions for dipoles having a charge separation d and located at a distance δ from the hydrophobic domain surface can be computed for spherical and globular micelles and the spherical endcaps of rodlike micelles from [94,95]

$$\frac{(\Delta\mu_g^0)_{\text{dipole}}}{kT} = \frac{2\pi e^2 R_{\text{S}}}{\varepsilon\, a_{\text{dipole}}\, kT}\left[\frac{d}{R_S + \delta + d}\right]\alpha_{g,\text{dipole}} \tag{68}$$

For the cylindrical part of the rodlike micelles, one can write

$$\frac{(\Delta\mu_g^0)_{\text{dipole}}}{kT} = \frac{2\pi e^2 R_{\text{C}}}{\varepsilon\, a_{\text{dipole}}\, kT}\ln\left[1 + \frac{d}{R_{\text{C}} + d + \delta}\right]\alpha_{g,\text{dipole}} \tag{69}$$

In the above relations, $\alpha_{g,\text{dipole}}$ is the fraction of surfactant molecules in the aggregate having a dipolar headgroup. If both A and B are zwitterionic surfactants with the same headgroup, then

$$\alpha_{g,\text{dipole}} = \alpha_{g\text{A}} + \alpha_{g\text{B}} = 1,\ a_{\text{dipole}} = a_\delta \tag{70}$$

If surfactant A is zwitterionic and surfactant B is nonionic or ionic, then

$$\alpha_{g,\text{dipole}} = \alpha_{g\text{A}}, \qquad a_{\text{dipole}} = \frac{a_\delta}{\alpha_{g,\text{dipole}}} \tag{71}$$

The dipole–dipole interactions may be relevant even when the surfactants do not possess zwitterionic headgroups. Such a situation occurs when the surfactant mixture consists of an anionic and a cationic surfactant. The two oppositely charged surfactants may be visualized as forming ion pairs. Depending on the location of the charges on the two surfactant headgroups, these ion pairs may act as dipoles. The distance of charge separation d in the zwitterionic headgroup, now refers to the distance between the locations of the anionic and the cationic charges, measured normal to the micelle core surface. Thus, for such systems,

$$\begin{aligned} \alpha_{g,\text{dipole}} &= \text{the smaller of } \frac{(\alpha_{g\text{A}}, \alpha_{g\text{B}})}{2} \\ a_{\text{dipole}} &= \frac{a_\delta}{\alpha_{g,\text{dipole}}}, \qquad d = |\delta_{\text{A}} - \delta_{\text{B}}| \end{aligned} \tag{72}$$

The factor 2 in the expression for $\alpha_{g,\text{dipole}}$ accounts for the fact that a dipole is associated with two surfactant molecules, treated as a pair. δ_{A} and δ_{B} represent the distance normal to the hydrophobic core surface at which the charges are located on the A and B surfactants.

For spherical bilayer vesicles, Eq. (32) is extended to binary surfactant mixtures taking into account the composition variation between the two layers. Noting that the numbers of surfactant molecules in the two layers are g_o and g_i and $\alpha_{go,\text{dipole}}$ and $\alpha_{gi,\text{dipole}}$ are the fractions of surfactant molecules in the outer and the inner layers having a dipolar headgroup, one gets

$$\begin{aligned} \frac{(\Delta\mu_g^0)_{\text{dipole}}}{kT} = {} & \frac{g_o}{g}\,\frac{2\pi e^2 R_o}{\varepsilon a_{o,\text{dipole}}\,kT}\left[\frac{d}{R_o + \delta + d}\right]\alpha_{go,\text{dipole}} \\ & + \frac{g_i}{g}\,\frac{2\pi e^2 R_i}{\varepsilon a_{i,\text{dipole}}\,kT}\left[\frac{d}{R_i - \delta - d}\right]\alpha_{gi,\text{dipole}} \end{aligned} \tag{73}$$

The areas per molecule $a_{o,\text{dipole}}$ and $a_{i,\text{dipole}}$ and the fractions of surfactant molecules that are dipolar $\alpha_{go,\text{dipole}}$ and $\alpha_{gi,\text{dipole}}$, are evaluated by applying Eqs. (70) to (72) for both the inner and the outer layers.

6. Headgroup Ionic Interactions

The ionic interactions that arise at the aggregate surface are calculated using Eq. (34), in conjunction with the curvature factor C given by Eq. (36), with the modification that S is now given by

$$S = \frac{4\pi e^2}{\varepsilon\kappa\, a_{\delta,\text{ion}}\, kT} \tag{74}$$

If both A and B are ionic surfactants with the same kind of charged headgroups, then

$$\alpha_{g,\text{ion}} = \alpha_{g\text{A}} + \alpha_{g\text{B}} = 1, \qquad a_{\delta,\text{ion}} = a_\delta, \qquad \delta = \alpha_{g\text{A}}\,\delta_\text{A} + \alpha_{g\text{B}}\,\delta_\text{B} \tag{75}$$

If A is ionic while B is nonionic or zwitterionic, then

$$\alpha_{g,\text{ion}} = \alpha_{g\text{A}}, \qquad a_{\delta,\text{ion}} = \frac{a_\delta}{\alpha_{g,\text{ion}}}, \qquad \delta = \delta_\text{A} \tag{76}$$

If A and B are both ionic but of opposite charge, then

$$\alpha_{g,\text{ion}} = \left|\alpha_{g\text{A}} - \alpha_{g\text{B}}\right|, \qquad a_{\delta,\text{ion}} = \frac{a_\delta}{\alpha_{g,\text{ion}}}, \qquad \delta = \alpha_{g\text{A}}\,\delta_\text{A} + \alpha_{g\text{B}}\,\delta_\text{B} \tag{77}$$

For spherical bilayer vesicles, the electrostatic interactions at both the outer and the inner surfaces are taken into account. For the molecules in the outer layer, a_δ is replaced with $a_{\delta o}$, $\alpha_{g,\text{ion}}$ with $\alpha_{go,\text{ion}}$, and the curvature factor $C = 2/(R_o + \delta)$. For the molecules in the inner layer, a_δ is replaced with $a_{\delta i}$, $\alpha_{g,\text{ion}}$ with $\alpha_{gi,\text{ion}}$, and the curvature factor $C = -2/(R_i - \delta)$. The fraction of charged molecules $\alpha_{go,\text{ion}}$ and $\alpha_{gi,\text{ion}}$ is calculated by applying Eqs. (75) to (77) to both the outer and the inner surfaces of the vesicle.

7. Free Energy of Mixing of Surfactant Tails

This is the only contribution that is not present in the free energy model for single-component surfactant solutions. This contribution accounts for the entropy and the enthalpy of mixing of the surfactant tails of molecules A and B in the hydrophobic core of the micelle, with respect to the reference states of pure A and pure B micelle cores. Any available solution model can be employed to calculate the entropy and the enthalpy of mixing. Consistent with our use of the Flory–Huggins model in various cases considered before (because of its relative simplicity), we retain the same model here as well:

$$\begin{aligned}\frac{(\Delta\mu_g^0)_\text{mix}}{kT} = {} & \alpha_{g\text{A}} \ln \eta_\text{A} + \alpha_{g\text{B}} \ln \eta_\text{B} + [\alpha_{g\text{A}} v_\text{SA} (\delta_\text{A}^\text{H} - \delta_\text{mix}^\text{H})^2 \\ & + \alpha_{g\text{B}} v_\text{SB} (\delta_\text{B}^\text{H} - \delta_\text{mix}^\text{H})^2]/kT\end{aligned} \tag{78}$$

where δ_A^H and δ_B^H are the Hildebrand solubility parameters of the tails of surfactants A and B and $\delta_\text{mix}^\text{H}$ is the volume fraction averaged solubility parameter of all the components within the micelle core, $\delta_\text{mix}^\text{H} = \eta_\text{A}\,\delta_\text{A}^\text{H} + \eta_\text{B}\,\delta_\text{B}^\text{H}$.

8. Free Energy Model and Mixture Nonideality

The free energy change on the formation of a mixed micelle can be written in terms of the free energies of formation of the two pure component micelles, the ideal entropy of mixing of surfactants inside the mixed micelle, and an excess free energy that is responsible for all nonidealities. This implies that if the free energy of formation of the mixed micelles, excluding the ideal entropy of mixing, is a linear function of the micelle composition, then

the excess free energy is zero and the mixed micelles are said to behave ideally. Any nonlinear dependence on the micelle composition is thus a signature for the nonideal behavior of the mixed surfactant system. In the framework of the molecular theory outlined in this section, the transfer free energy is a linear function of the micelle composition. All other contributions have a nonlinear dependence on micelle composition because they are dependent nonlinearly on the micelle core radius or the area per molecule. Further, these structural parameters are themselves dependent nonlinearly on the micelle composition if the tail lengths of the surfactants are different from one another. Depending on the quantitative importance of these nonlinear contributions, the mixed surfactant system displays small or large deviations from ideal behavior, as we will discuss below.

C. Predictions for Surfactant Mixtures

1. Estimation of Molecular Constants and Computational Approach

The molecular constants needed for the surfactants have been discussed before in Section IV.C, and the constants characterizing various surfactant headgroups are listed in Table 3. The only additional molecular constant needed for calculations involving surfactant mixtures is the Hildebrand solubility parameter for the hydrocarbon and fluorocarbon tails of the surfactants. This can be estimated using a group contribution approach based on the properties of pure components [97–99]. For hydrocarbon tails, the solubility parameters can be estimated in units of $MPa^{1/2}$ (1 MPa = 1 J/cm^3) from the relation

$$\delta^{H} = \frac{0.7 + 0.471(n_C - 1)}{v_S} \text{ MPa}^{1/2}), v_S \text{ in nm}^3 \tag{79}$$

The solubility parameter for the fluorocarbon tail of the surfactant sodium perfluoro octanoate (SPFO) estimated using the group contribution approach yields 12.3 $MPa^{1/2}$. Since the solubility parameters estimated in this manner have been found inadequate for the quantitative description of hydrocarbon–fluorocarbon mixture properties, Mukerjee and Handa [45] have estimated group contributions to the solubility parameters by fitting the critical solution temperature of the hydrocarbon–fluorocarbon mixtures. On the basis of these group contributions, one can calculate the solubility parameter of the SPFO tail to be approximately 9.5 $MPa^{1/2}$. Computed results for hydrocarbon–fluorocarbon surfactant mixtures are presented later, utilizing both of these estimates.

The predictive computations have been carried out using the maximum-term method described in Section IV.B.2. For the binary mixtures, the

concentration of the singly dispersed surfactant mixture X_1 ($= X_{1A} + X_{1B}$) and the composition of this mixture α_{1A} are used as inputs and the aggregation number g of the equilibrium aggregate and the composition α_{gA} of the equilibrium aggregate are obtained by finding the maximum in the aggregate size distribution. For spherical bilayer vesicles, one has to determine the thicknesses of the inner and the outer layers and the compositions of each layer as well. The critical micelle concentration is estimated using the results based on the maximum-term method calculations as described earlier in Section IV.B.

2. Nonionic Hydrocarbon–Nonionic Hydrocarbon Mixtures

The calculated aggregation properties of binary mixtures of decyl methyl sulfoxide (designated as $C_{10}SO$) and decyl dimethyl phosphene oxide (designated as $C_{10}PO$) at 24°C are presented in Figs. 27 and 28. In Fig. 27 the CMC is plotted against the composition of the micelles and the composition of the singly dispersed surfactants. One can practically equate the composition of the singly dispersed surfactant to the composition of the total surfactant, when the total surfactant concentration is equal to the CMC since

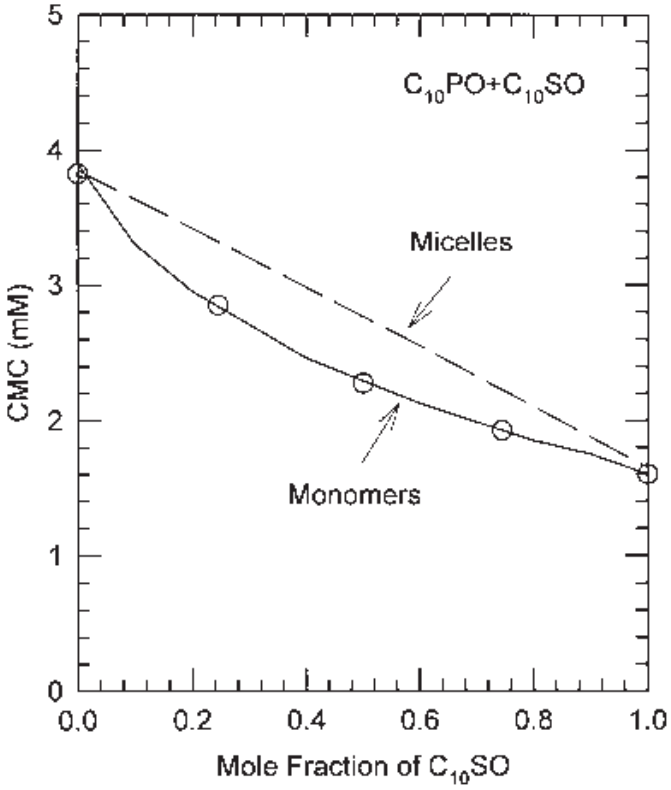

FIG. 27 The CMC of $C_{10}PO + C_{10}SO$ binary mixture as a function of the composition of micelles (dashed line) and that of singly dispersed surfactants (solid line) at 24°C. The points are experimental data from Ref. (100).

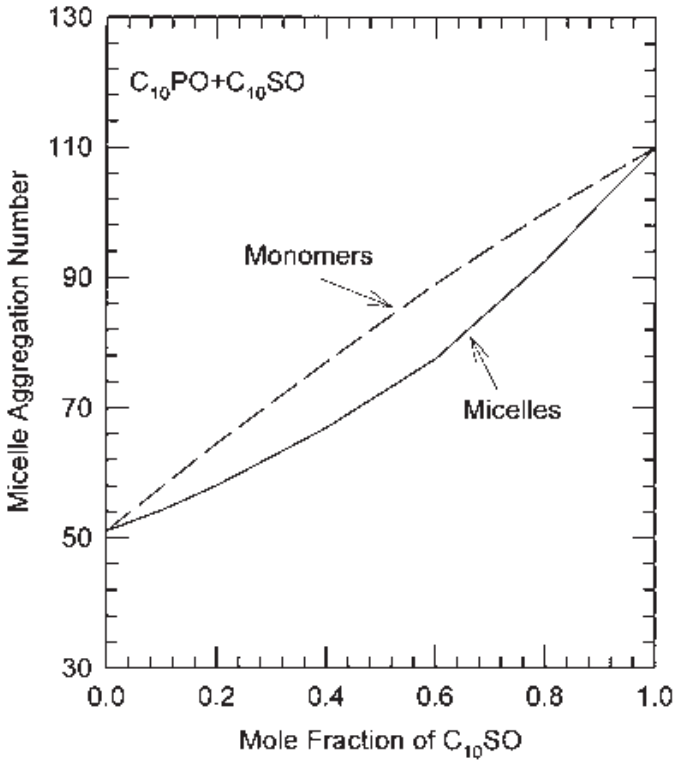

FIG. 28 The average aggregation number of $C_{10}PO + C_{10}SO$ mixed micelles at the CMC as a function of the composition of micelles (solid line) and that of the singly dispersed surfactants (dashed line) at 24°C.

the amount of surfactant present as micelles is small. Figure 27 contains also the experimental data obtained by Holland and Rubingh [100] on the basis of surface tension measurements. Figure 28 presents the average aggregation numbers predicted by the theory as a function of the composition of the mixed micelle and that of the monomers. No experimental data are, however, available for comparison. The size of the mixed micelle varies approximately linear with the composition.

It has been shown that the CMC of this binary surfactant system can be calculated from the CMC values of the individual surfactants by assuming the mixture to be ideal [100]. In the framework of the molecular theory presented here, nonidealities in this binary mixture can arise even when the two surfactants have somewhat different headgroup cross-sectional areas while possessing identical tails [94,95]. Because there are no volume differences between the hydrophobic tails of the two surfactants, for any aggregation number, the area per molecule of the mixed micelle is independent of the micelle composition. However, the steric interaction between headgroups at any aggregation number is a nonlinear function of the micelle composition. This constitutes a source of mixture nonideality. However, because of the small magnitude of the steric repulsion free energy, the devia-

tion from ideal mixing is rather small. For this reason, the ideal mixed micelle model can satisfactorily predict the mixture CMC.

3. Ionic Hydrocarbon–Ionic Hydrocarbon Mixtures

The predicted CMC of mixtures of two anionic surfactants sodium dodecyl sulfate (SDS) and sodium decyl sulfate (SDeS), which differ from one another in their hydrocarbon tail lengths, is plotted against the composition of the singly dispersed surfactant in Fig. 29. The figure also contains the experimental data obtained by Mysels and Otter [101] based on conductivity measurements, and the data of Shedlowsky et al. [102] based on e.m.f. measurements. The predicted mixed micelle composition as a function of the composition of the singly dispersed surfactants is compared in Fig. 30 with the data obtained by Mysels and Otter [101]. In these binary mixtures, one of the sources of nonideality arises from the volume differences between the hydrophobic tails of the two surfactants. Consequently, at any given aggregation number, the area per molecule of the mixed micelle is a nonlinear function of the micelle composition and, hence, nonlinearity is reflected in all the free energy contributions. Another source of nonideality is the change in

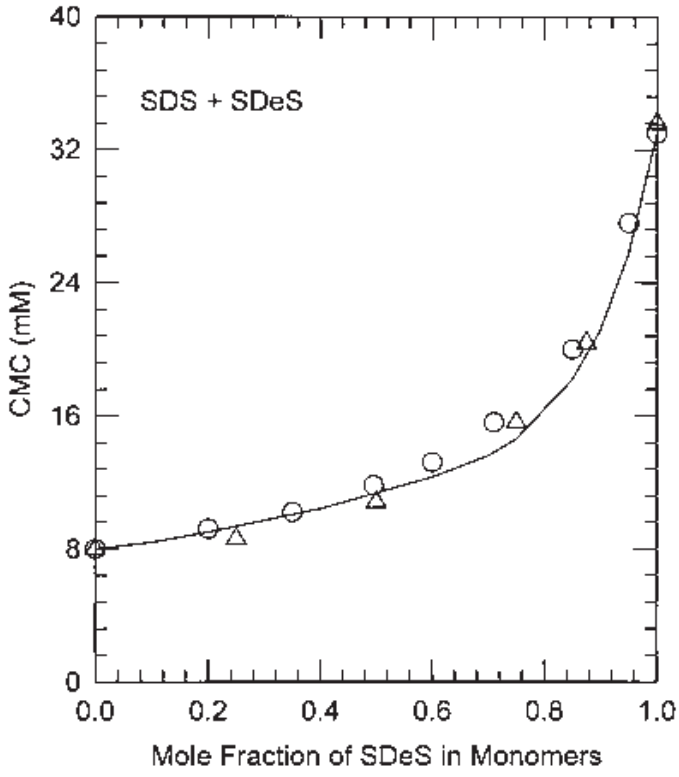

FIG. 29 The CMC of SDS + SDeS mixtures as a function of the composition of singly dispersed surfactants. (The experimental data shown by circles are from Ref. 101 and those shown by triangles are from Ref. 102.)

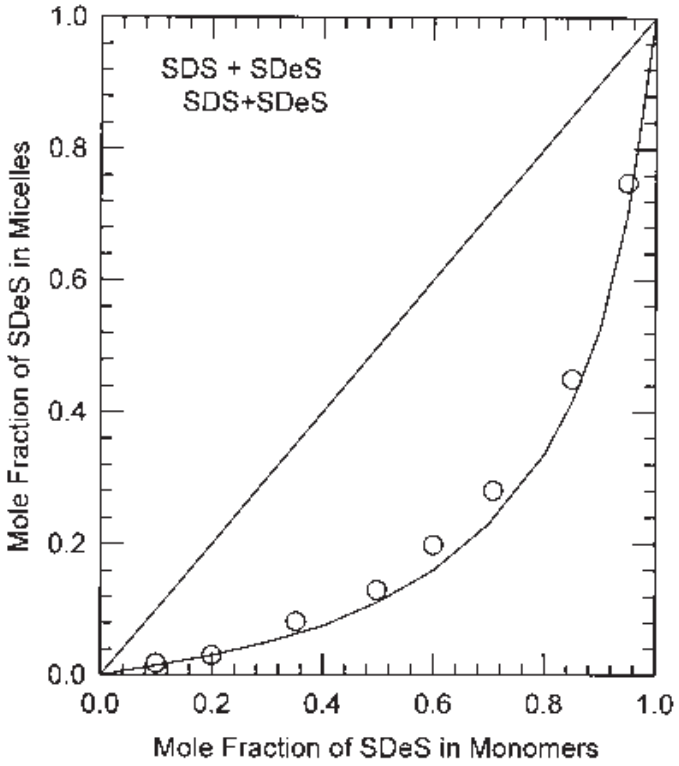

FIG. 30 The composition of SDS + SDeS mixed micelles as a function of the composition of singly dispersed surfactants. (The experimental data shown by circles are from Ref. 101.)

ionic strength of the solution as the composition is modified. In the absence of any added salt, the ionic strength is determined mainly by the concentration of the singly dispersed surfactants. This concentration changes with the composition of the mixed micelle and thus modifies the ionic interactions at the micelle surface nonlinearly as a function of the micelle composition. Given the importance of the ionic interactions to the free energy of micellization, the nonideality is more perceptible in these binary mixtures.

Similar behavior is exhibited by the mixtures of cationic surfactants, dodecyl trimethyl ammonium bromide (DTAB), and decyl trimethyl ammonium bromide (DeTAB). This mixture is similar to the SDS-SDeS mixture as concerns the tail lengths of the two surfactants. However, the trimethyl ammonium bromide headgroup has a larger area a_p compared to that of the anionic sulfate headgroup. The predicted CMC as a function of the micelle and the monomer compositions is presented in Fig. 31, which also contains the experimental CMC data obtained by Garcia-Mateos et al. [103] using electrical conductivity measurements. One can observe large CMC changes for the DTAB-DeTAB mixture as the composition is altered, which also influences the ionic strength of the solution. The predicted aggregation numbers do not show much growth beyond the size of the pure component

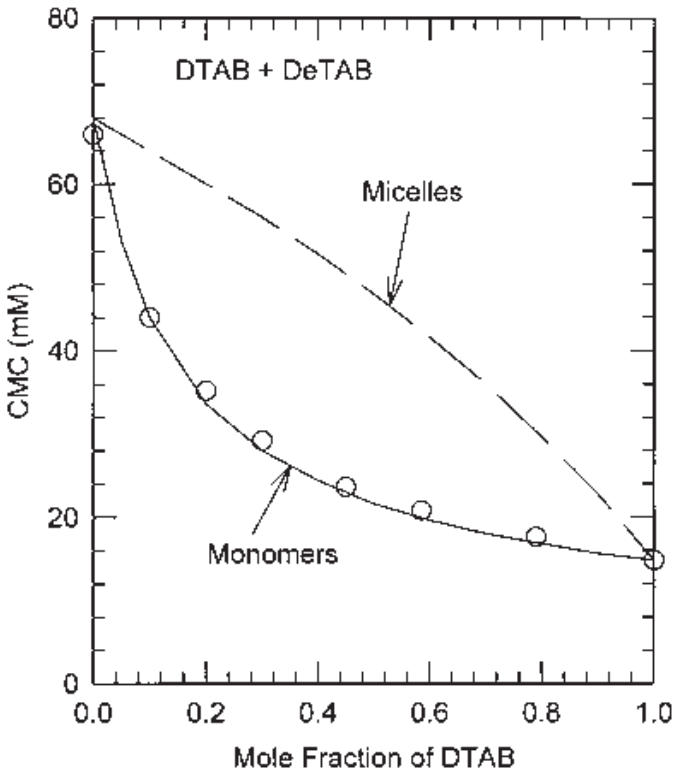

FIG. 31 The CMC of DTAB + DeTAB mixtures as a function of the composition of the micelles (dashed line) and that of singly dispersed surfactants (solid line). (The points are experimental data from Ref. 101.)

micelles. In contrast, for SDS-SDeS mixtures, the mixed micelles are larger than the pure component micelles. This different behavior is a consequence of the larger steric repulsion for these cationic surfactants with a bulky headgroup, when compared to the sulfate headgroups of SDS-SDeS.

To explore the effect of different chain lengths of the hydrophobic tails, we have computed the micellization behavior of mixtures of anionic potassium alkanoates, namely, potassium tetradecanoate (KC_{14})–potassium octanoate (KC_8) and potassium decanoate (KC_{10})–potassium octanoate (KC_8) at 25°C. The calculated CMC and micelle composition are plotted in Figs. 32 and 33 as a function of the composition of the singly dispersed surfactant, together with the experimental CMC data [104] obtained by Shinoda using dye solubilization measurements. One can observe from Fig. 33 that the less hydrophobic KC_8 is almost completely excluded from the micelles in $KC_8 + KC_{14}$ mixtures because of the much stronger hydrophobicity of KC_{14}. The singly dispersed surfactants contain almost exclusively the less hydrophobic KC_8 molecules. Such exclusion of KC_8 from the mixed micelles is reduced in case of the $KC_8 + KC_{10}$ mixtures, where the chain length difference between the surfactants is smaller.

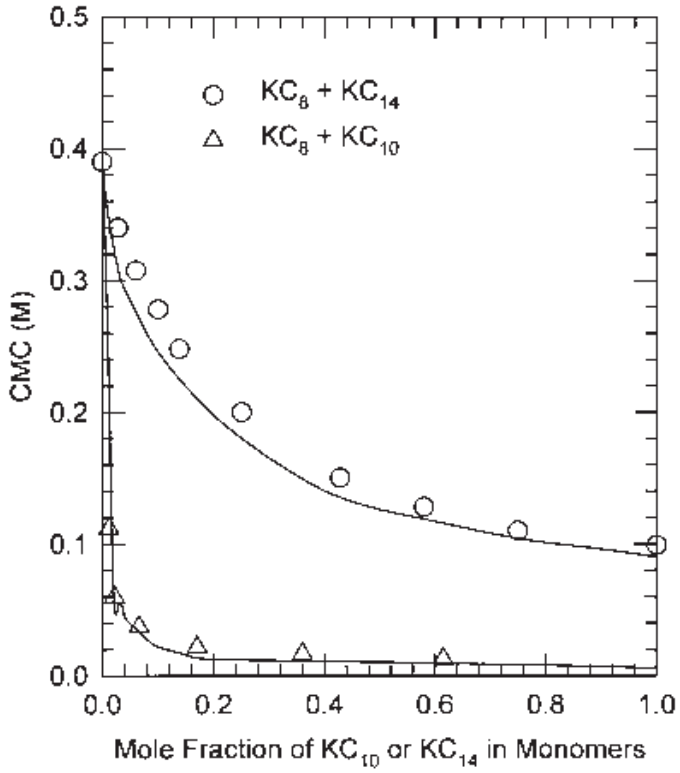

FIG. 32 The CMC of mixtures of potassium alkanoate (KC_n) surfactants, $KC_8 + KC_{10}$ mixtures, and $KC_8 + KC_{14}$ mixtures as a function of the composition of singly dispersed surfactants. (The experimental data [circles and triangles] are from Ref. 104.)

4. Ionic Hydrocarbon–Nonionic Hydrocarbon Mixtures

The mixture of anionic sodium dodecyl sulfate (SDS) and nonionic decyl methyl sulfoxide ($C_{10}SO$) at 24°C, in the presence of 1-mM Na_2CO_3, is taken for illustrative calculations. The calculated CMC is plotted in Fig. 34 as a function of the composition of the singly dispersed molecules. The experimental CMC data based on surface tension measurements [100] are also included in the figure. The results show that this binary mixture exhibits considerable nonideality. The CMC of the mixed system is substantially smaller than that anticipated for the ideal mixed micelle. The two surfactants differ somewhat in their hydrophobic tail lengths and in the sizes of the polar headgroups. Similar differences occurred in the case of nonionic–nonionic mixtures considered before, but they did not give rise to significant nonidealities. However, in the present case, one component is ionic while the other is nonionic. Therefore, the area per charge at the micelle surface and the ionic strength are strongly affected by the composition of the micelle. This results in a large variation in the ionic interaction energy at the micelle

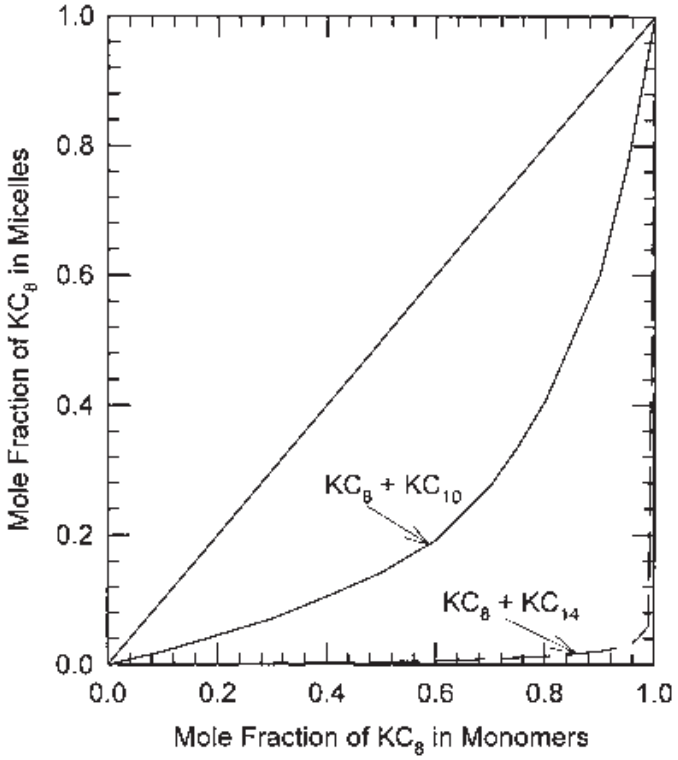

FIG. 33 The composition of $KC_8 + KC_{10}$ mixed micelles and $KC_8 + KC_{14}$ mixed micelles as a function of the composition of singly dispersed surfactants.

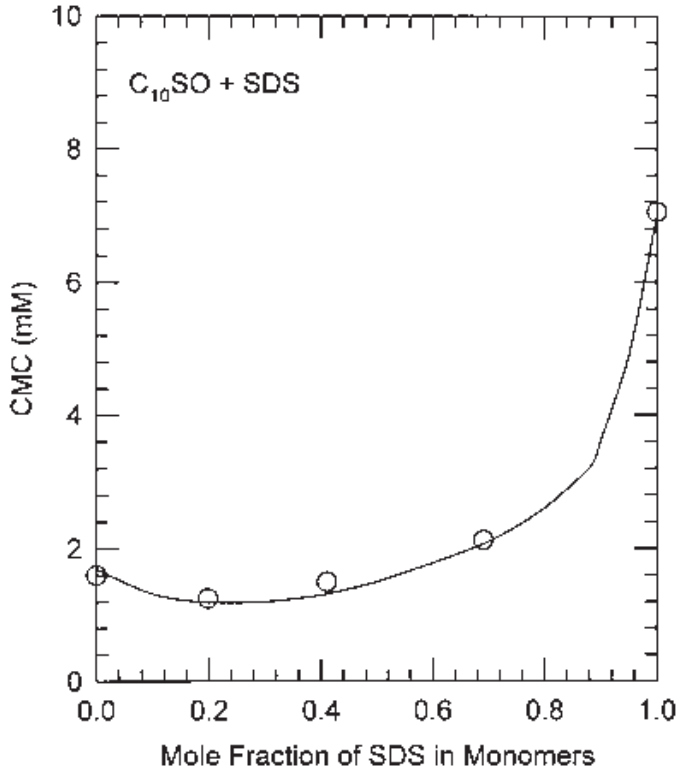

FIG. 34 The CMC of SDS + decyl methyl sulfoxide ($C_{10}SO$) mixtures as a function of the composition of singly dispersed surfactants. (The experimental data [circles] are from Ref. 100.)

surface as the micelle composition is changed. This free energy contribution is mostly responsible for the nonideal behavior exhibited by this system.

The predictions for binary mixtures of the anionic sodium dodecyl sulfate (SDS) and nonionic β-dodecyl maltoside (DM) are now compared with the experimental data obtained by Bucci et al. [105] in Figs. 35 to 37. In this system the two surfactants have identical hydrophobic chains, and hence the nonideality arises from the differences in the size and charge of the two headgroups. The calculated average aggregation numbers and those estimated from neutron scattering measurements [105] are plotted in Fig. 35 with and without added salt. The average aggregation number and the average micelle composition are estimated at a total surfactant concentration of 50 mM and at 25°C. Figures 36 and 37 present the CMC and micelle composition as functions of the composition of the singly dispersed surfactants at two concentrations of added electrolyte, NaCl. They show that the nonionic DM molecules are preferentially incorporated in the micelles over most of the composition range. In the absence of any added electrolyte, this

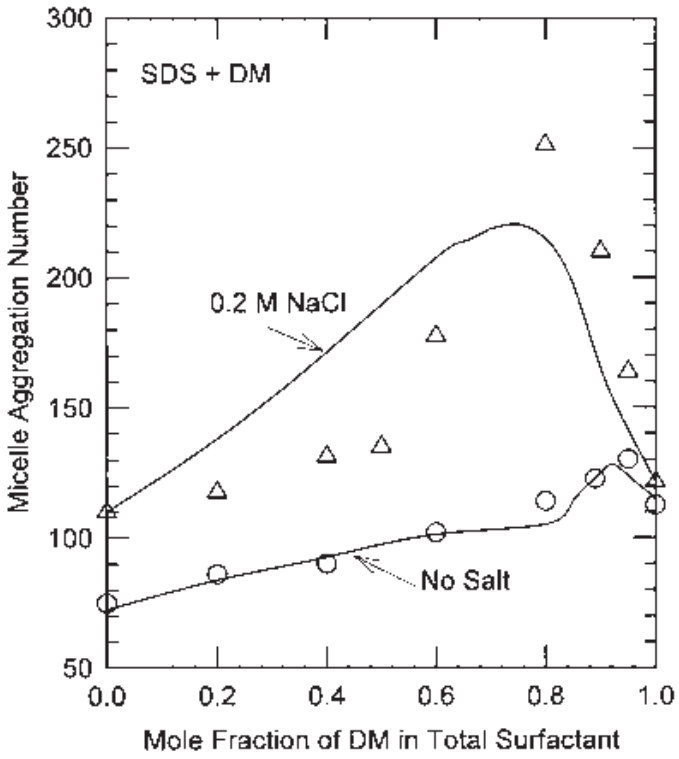

FIG. 35 The average aggregation number of SDS + dodecyl maltoside (DM) mixed micelles as a function of the total surfactant composition at a total surfactant concentration of 50 mM. (The experimental data are from Ref. 105, where the circles refer to micelle sizes in the absence of any added salt while the triangles correspond to a 0.2M concentration of added NaCl.)

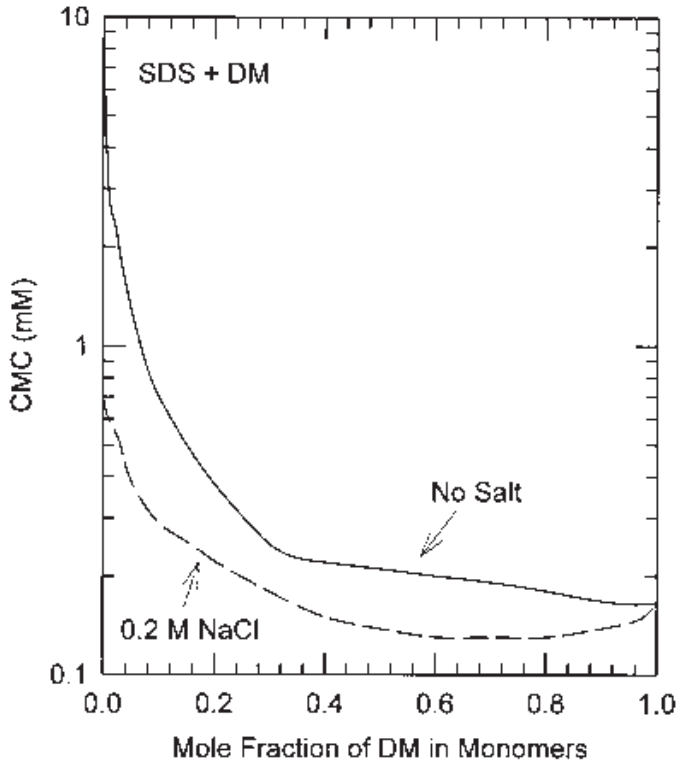

FIG. 36 The CMC of SDS + DM mixtures as a function of the composition of monomers. The conditions correspond to those in Fig. 35.

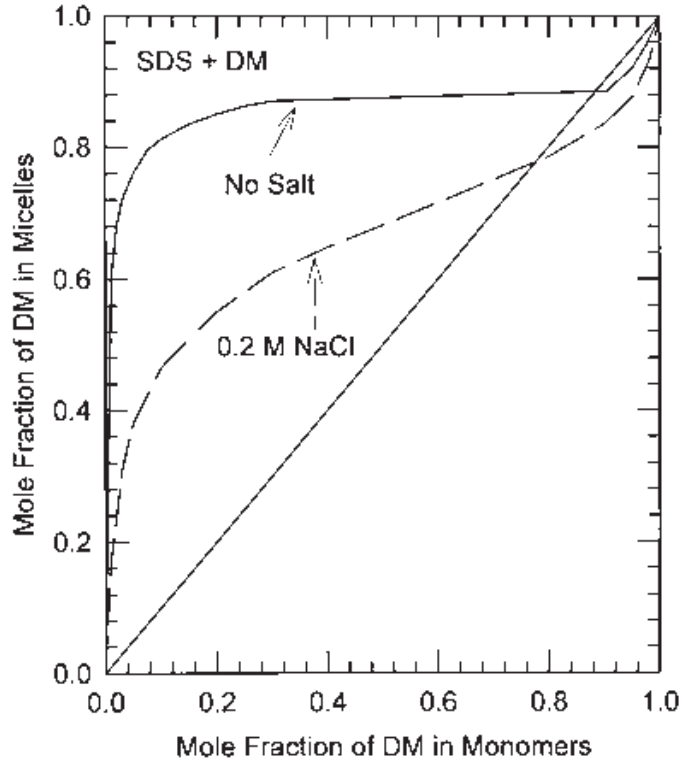

FIG. 37 The composition of mixed micelles of SDS + DM as a function of the composition of monomers. The conditions correspond to those in Fig. 35.

preference is stronger since this decreases the positive free energy contribution due to the presence of the anionic SDS in micelles. Obviously, in the presence of NaCl, the electrostatic repulsions between ionic headgroups are reduced, and hence a larger number of SDS molecules is incorporated into the mixed micelles.

5. Anionic Hydrocarbon–Cationic Hydrocarbon Mixtures

When present together, the anionic and cationic surfactants are expected to form ion pairs with no net charge; this decreases their aqueous solubility and results in precipitation [106,107]. These surfactant mixtures can also generate mixed micelles or mixed spherical bilayer vesicles in certain concentration and composition ranges. As noted earlier, depending on the location of the charges on the anionic and the cationic surfactants, one can associate a dipole moment with each ion pair. Consequently, these surfactant mixtures can behave partly as ionic single chain molecules and partly as zwitterionic paired chain molecules. We have calculated the aggregation characteristics of binary mixtures of decyl trimethyl ammonium bromide (DeTAB) and sodium decyl sulfate (SDeS). The calculated and experimental [100] CMC values are presented in Fig. 38, while information regarding the micelle

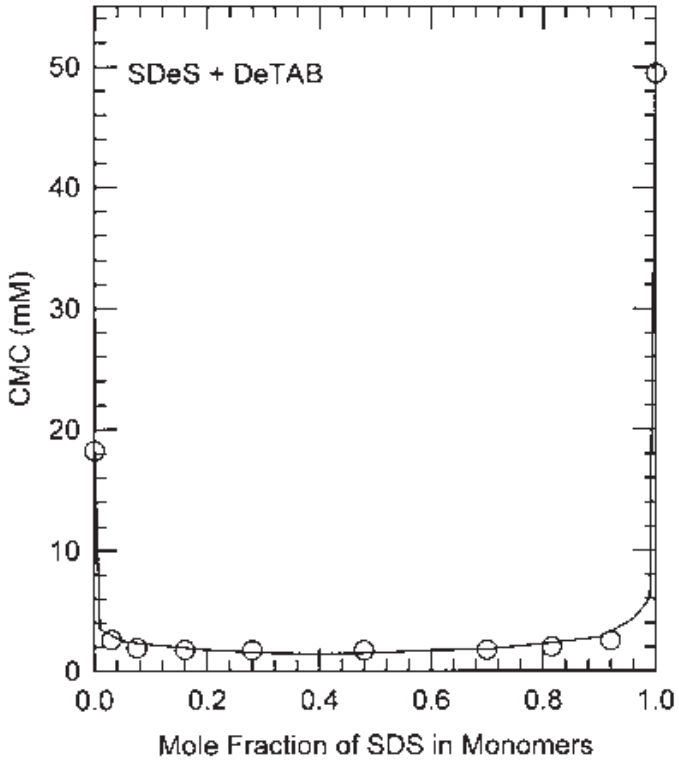

FIG. 38 The CMC of SDeS + DeTAB mixtures as a function of the composition of singly dispersed surfactants. (The points are experimental data from Ref. 100.)

composition is provided by Fig. 39. The calculations show that rodlike mixed micelles are formed over most of the composition range. The micelle composition data show that the mixed micelles contain approximately equal numbers of the two types of surfactants over the entire composition range. The small deviation from the micelle composition value of 0.5 arises because of the different sizes of the polar headgroups.

Some binary mixtures of anionic and cationic surfactants have been observed to give rise to spherical bilayer vesicles in aqueous solutions [108–111]. In these mixtures, the surfactant tails have appreciably differing lengths. Here, we have calculated the solution behavior of binary mixtures of cationic cetyl trimethyl ammonium bromide (CTAB) and anionic sodium dodecyl sulfate (SDS), in the presence of 1-mM NaBr as electrolyte, to explore the formation of micelles versus vesicles in such mixtures. Figure 40 shows the calculated critical aggregate (micelle or vesicle) concentration as a function of the composition of the aggregate. The lower the critical concentration for the formation of a given kind of aggregate, aggregates of that type are favored at equilibrium. In CTAB-poor systems, for CTAB mole fractions in the aggregates $\alpha_{g,\mathrm{CTAB}}$ less than 0.2, only micelles are generated. For CTAB compositions in the region $0.2 < \alpha_{g,\mathrm{CTAB}} < 0.29$,

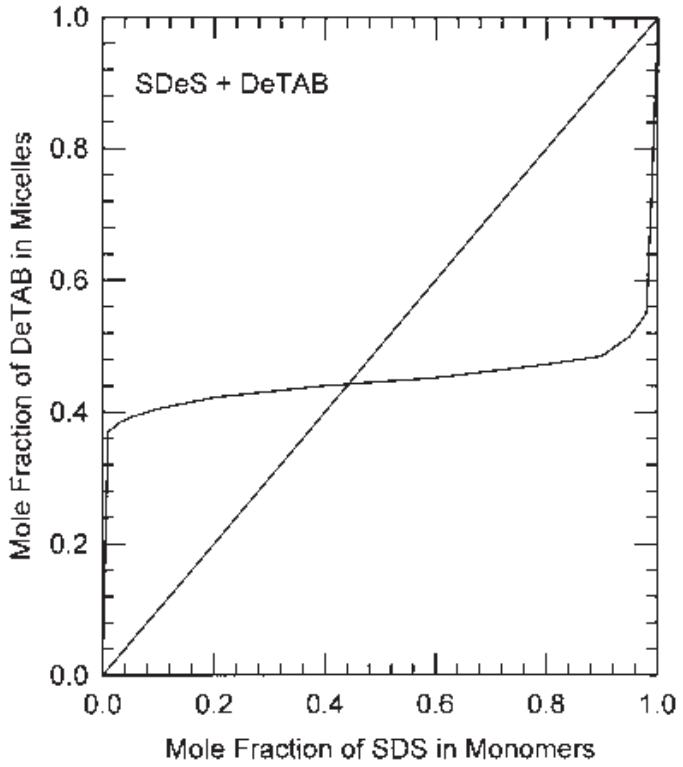

FIG. 39 The average composition of SDeS + DeTAB mixed micelles as a function of the composition of monomers.

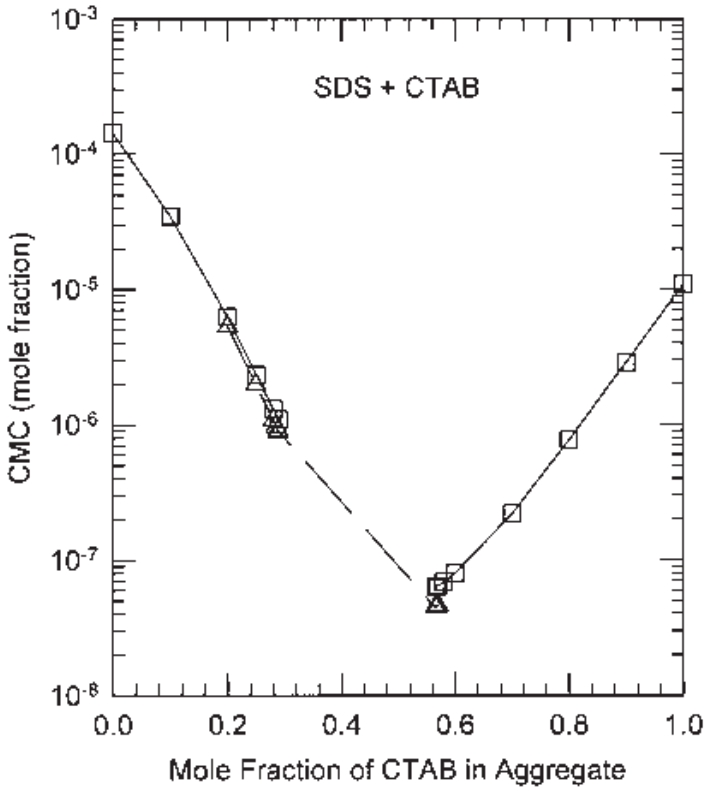

FIG. 40 The critical micelle (or vesicle) concentration of CTAB + SDS mixtures as a function of the composition of the aggregates. Squares denote micelles and triangles refer to spherical bilayer vesicles. The lines simply connect the calculated results. The dashed line near the composition region between 0.29 and 0.57 corresponds to a precipitated surfactant phase of lamellar aggregates.

spherical bilayer vesicles are predicted to form. In CTAB-rich systems, again for $\alpha_{g,\mathrm{CTAB}} > 0.57$, only micelles are present in solution. In the narrow composition region of $0.565 < \alpha_{g,\mathrm{CTAB}} < 0.567$, vesicles are formed in solution. For a wide range of CTAB composition $0.29 < \alpha_{g,\mathrm{CTAB}} < 0.565$, the calculations indicate the formation of lamellar aggregates rather than spherical bilayer vesicles. This may correspond to the formation of a precipitating surfactant phase. Figure 41 presents the calculated average aggregation numbers of the micellar and vesicular aggregates. The micelles correspond to spherical or globular aggregates. The smallest vesicles formed are not very much larger than the larger micellar aggregates. The vesicles (corresponding to the results shown in the figure) have outer radii in the range of 3 to 14 nm. The inner and outer layers of the bilayer vesicles have differing compositions. In CTAB-poor vesicles the inner layer is enriched somewhat with CTAB, while in CTAB-rich vesicles the inner layer is somewhat depleted of CTAB.

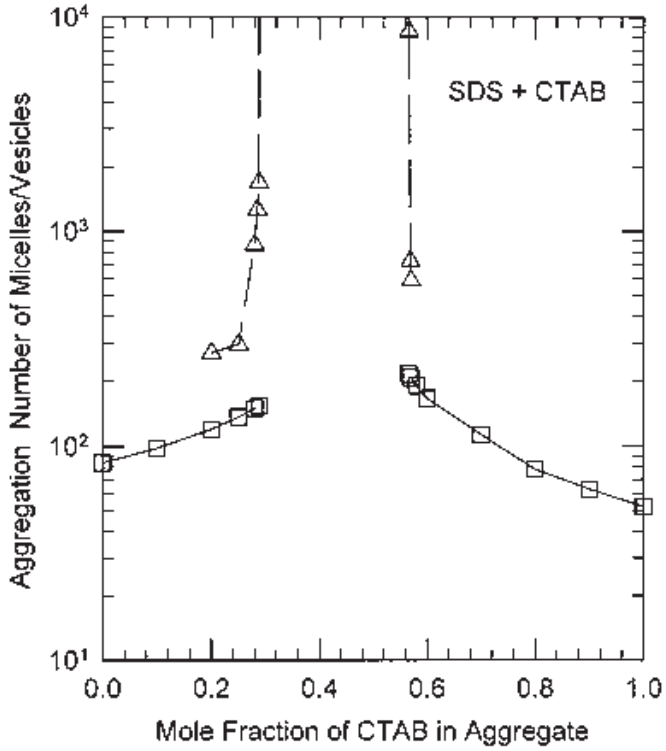

FIG. 41 The aggregation number of mixed micelles and mixed vesicles formed of CTAB + SDS mixtures as a function of the composition of the aggregates. Squares denote micelles and triangles refer to vesicles. The lines simply connect the calculated results. The dashed line near the compositions 0.29 and 0.57, which extend vertically, suggest the formation of infinite lamellar aggregates in that region corresponding to the precipitation of a surfactant phase.

6. Anionic Fluorocarbon–Nonionic Hydrocarbon Mixtures

The aggregation behavior of mixtures of nonionic alkyl-N-methyl glucamines (MEGA-*n*) and anionic sodium perfluoro octanoate (SPFO), studied experimentally by Wada et al. (112) was investigated using the present model. In such mixtures the nonideality associated with the mixing of hydrocarbon and fluorocarbon surfactant tails is superimposed on the nonideality associated with the mixing of anionic and nonionic headgroups. For hydrocarbon surfactants with these polar headgroups, the results presented earlier revealed considerable negative deviations from ideality (i.e., the free energy of mixed micelle formation is lower than the composition averaged sum of the free energies of the pure component micelles) [94,95]. For mixtures of hydrocarbon and fluorocarbon tails one can anticipate strong positive deviations from ideality. Thus, for the mixtures under study, both negative and positive deviations from ideality occur, which partially compensate for one another. As a result, these binary mixtures exhibit reduced nonideality. Figures 42 and 43 present

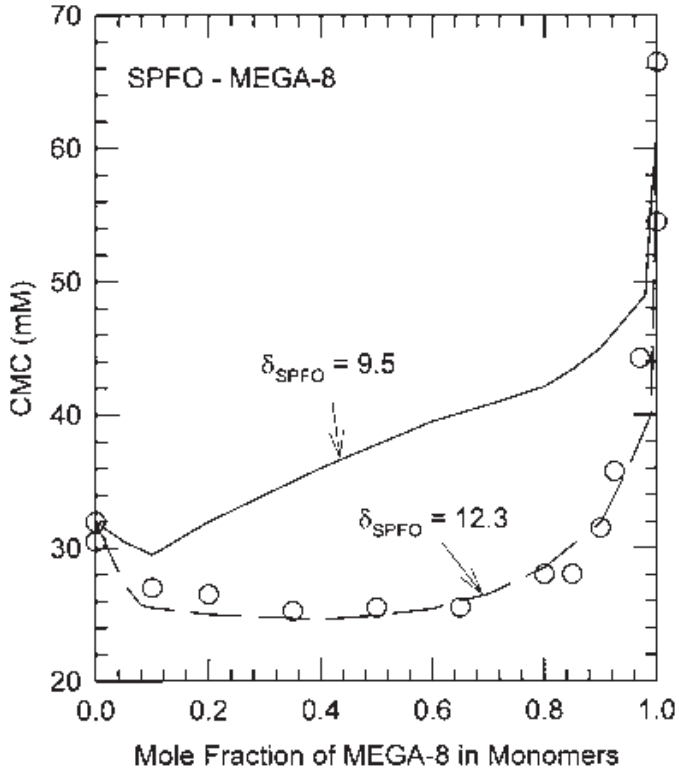

FIG. 42 The CMC of MEGA-8 + SPFO mixtures as a function of the composition of singly dispersed surfactants. The calculated results are presented for two alternate estimates of the solubility parameter of the SPFO tail. (The experimental data [circles] are from Ref. 112.)

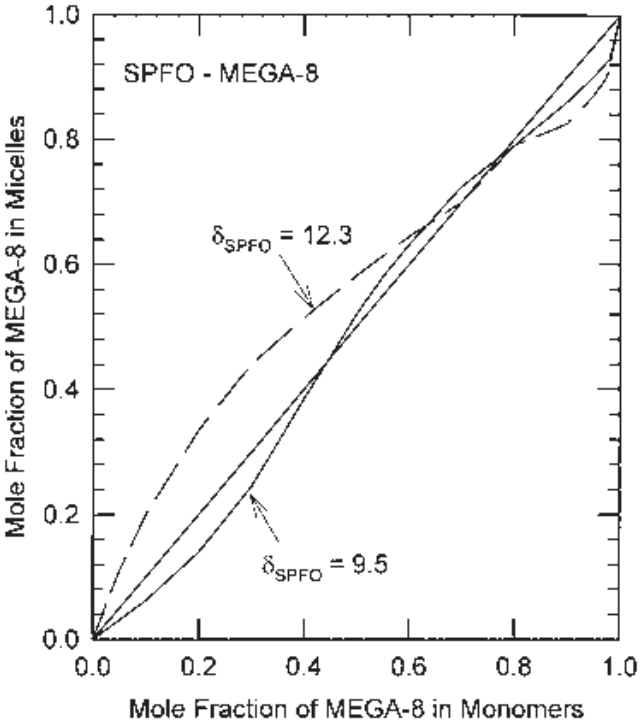

FIG. 43 The average composition of MEGA-8 + SPFO mixed micelles as a function of the composition of monomers. The conditions correspond to those described in Fig. 42.

the calculated CMC and the composition of the mixed micelles as a function of the composition of the singly dispersed surfactant for MEGA-8-SPFO mixtures. Similar results for the MEGA-9-SPFO mixtures are presented in Figs. 44 and 45. The calculations have been performed for two different values of the solubility parameter of SPFO, one determined from the properties of pure fluorocarbons (12.3 $MPa^{1/2}$), and the other determined from the properties of fluorocarbon–hydrocarbon mixtures (9.5 $MPa^{1/2}$). Both MEGA-8-SPFO and MEGA-9-SPFO mixtures display the same qualitative behavior. The miscibility between the two surfactants is promoted by the headgroup interactions, which lead to a single kind of mixed micelles in solution. As shown by the data presented in Figs. 43 and 45, there is no demixing of micelles for the MEGA-8-SPFO and MEGA-9-SPFO mixtures.

7. Anionic Hydrocarbon–Anionic Fluorocarbon Mixtures

The micellization behavior of sodium perfluoro octanoate (SPFO) and sodium decyl sulfate (SDeS) mixtures is plotted in Figs. 46 and 47. The

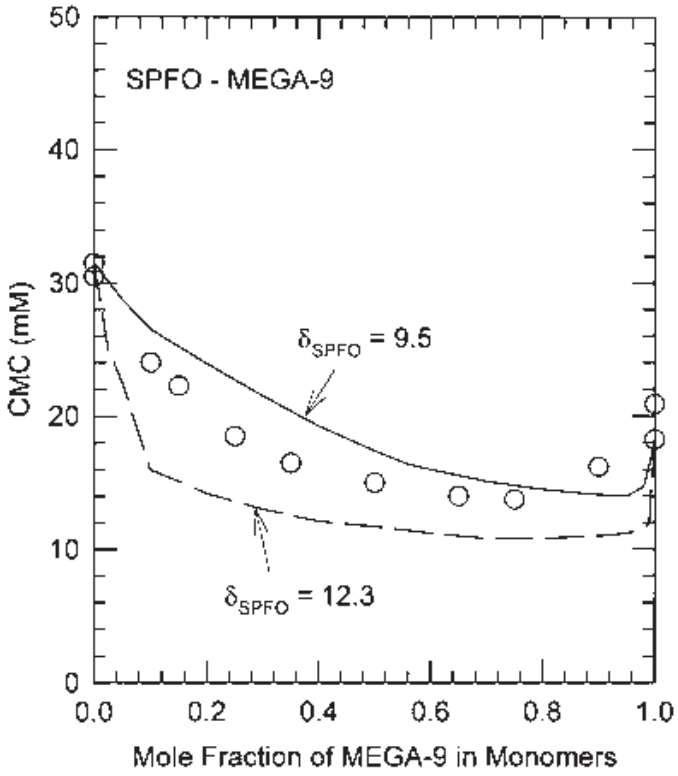

FIG. 44 The CMC of MEGA-9 + SPFO mixtures as a function of the composition of singly dispersed surfactants. The calculated results are presented for two alternate estimates of the solubility parameter of the SPFO tail. (The experimental data [circles] are from Ref. 112.)

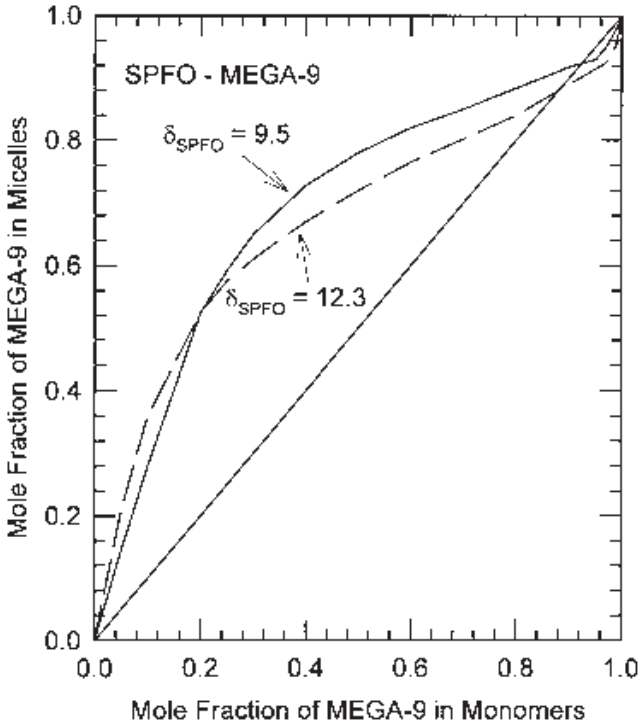

FIG. 45 The average composition of MEGA-9 + SPFO mixed micelles as a function of the composition of monomers. The conditions correspond to those described in Fig. 44.

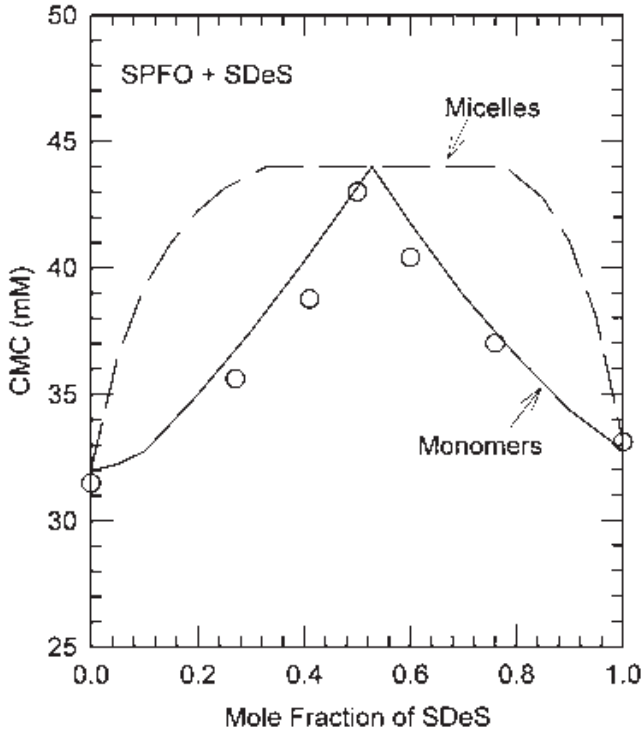

FIG. 46 The CMC of SDeS + SPFO mixtures as a function of the composition of micelles (dashed line) and that of singly dispersed surfactants (solid line). (The experimental data [circles] are from Ref. 112.) The experimental and calculated results indicate the coexistence of two micelle populations.

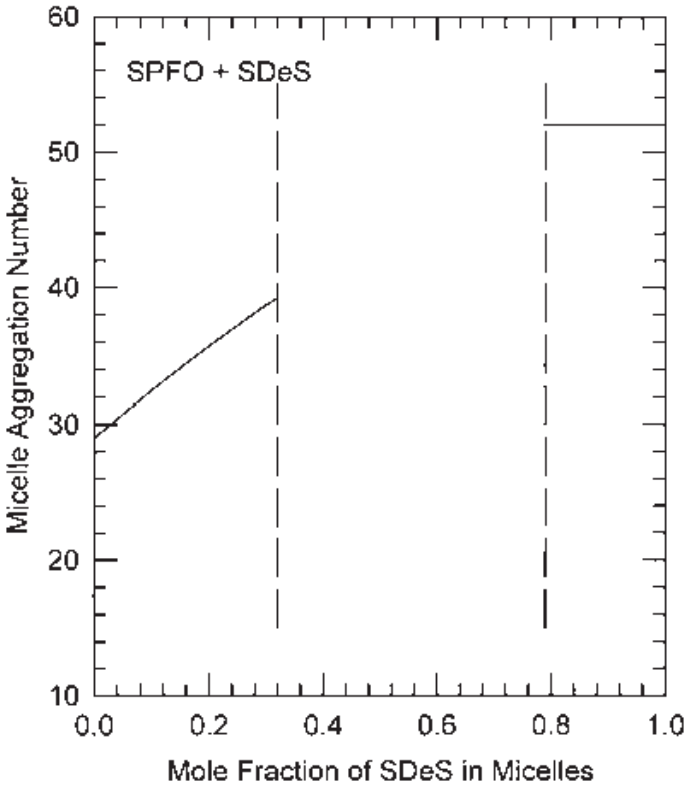

FIG. 47 The average aggregation number of SDeS + SPFO mixed micelles as a function of the composition of micelles. A single type of mixed micelle exists in the SDeS-rich and SPFO-rich mixtures, while for intermediate compositions, two distinct micelle sizes corresponding to the two coexisting micelle populations are indicated.

CMCs are compared with available experimental data [112] in Fig. 46, which also provides the composition of the mixed micelle. There are positive deviations in the CMC in contrast to the negative deviations observed in the binary mixtures examined previously. This positive deviation is a direct consequence of the interactions between the hydrocarbon and fluorocarbon tails. This positive deviation, which was also present in SPFO-MEGA-*n* mixtures, was partially compensated for there by the negative deviations due to headgroup interactions. Such compensating effects are, however, absent in the SPFO-SDeS mixtures since the headgroups of both surfactants are anionic. The calculations show the interesting feature that over a certain composition domain, two types of micelles coexist. One is hydrocarbon-rich and the other one is fluorocarbon-rich, with average compositions $\alpha_{g\mathrm{A}} = 0.32$ and 0.79, respectively. The predicted average aggregation numbers of the mixed micelles are plotted in Fig. 47. The

fluorocarbon- and hydrocarbon-rich micelles that coexist have different aggregation numbers.

VI. MICELLIZATION OF SURFACTANTS IN THE PRESENCE OF POLYMERS

The interactions between surfactant molecules and synthetic polymers in aqueous solutions are of importance to many applications in detergents and personal care products, chemical, pharmaceutical, mineral processing, and petroleum industries. In general, the mutual presence of polymer and surfactant molecules alter the rheological properties of solutions, adsorption characteristics at solid–liquid interfaces, stability of colloidal dispersions, the solubilization capacities in water for sparingly soluble molecules, and liquid–liquid interfacial tensions [113–117]. The ability of the surfactant and the polymer molecules to influence the solution and interfacial characteristics is controlled by the state of their occurrence in aqueous solutions, namely whether they form mixed aggregates in solution and, if so, the nature of their microstructures.

A. Polymer–Surfactant Association Structures

Various morphologies of polymer-surfactant complexes can be visualized [118–121] depending on the molecular structures of the polymer and the surfactant and on the nature of the interaction forces operative between the solvent, the surfactant, and the polymer. A schematic view of these morphologies is presented in Fig. 48. Structure A denotes only the polymer, implying that no polymer–surfactant association occurs. This would be the case when both the polymer and the surfactant carry the same type of ionic charges. This could also occur when the polymer is relatively rigid and for steric reasons does not interact with ionic or nonionic surfactants. It could also be the situation when both the polymer and the surfactant are uncharged and no obvious attractive interactions, promoting association, exist between them. Structure B denotes a system where the polymer and the surfactant carry opposite electrical charges. Their mutual association is promoted by electrostatic attractions. These cause the creation of a complex with reduced charge and, hence, reduced hydrophilicity. Indeed, this eventually leads to the precipitation of these complexes from solution. Structure C also occurs in systems containing surfactant and polymer possessing opposite charges. In this case, the surfactant promotes intramolecular bridging within a polymer molecule by interacting with multiple sites on one molecule or intermolecular bridging by interacting simultaneously with sites on different polymer molecules.

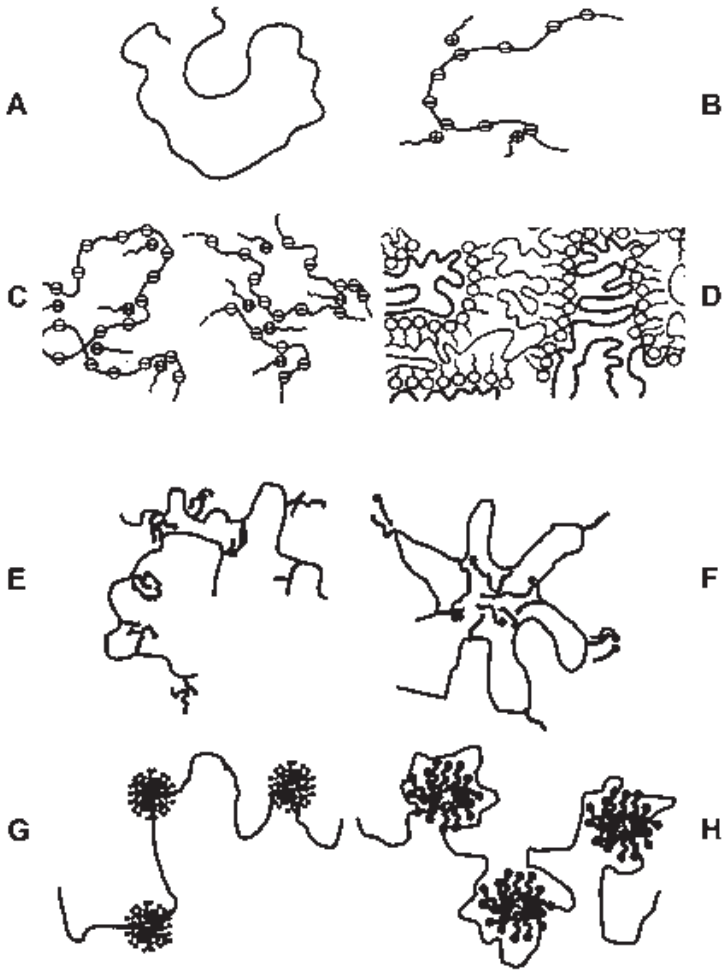

FIG. 48 Schematic representation of association structures involving surfactant and polymer molecules. A. Polymer molecule does not interact with surfactants for electrostatic or steric reasons. No surfactant is bound to the polymer. For example, the surfactant and the polymer are both anionic or both cationic. B. The polymer and the surfactant are oppositely charged. Single-surfactant molecules are bound linearly along the length of the polymer molecules. C. The polymer and the surfactant are oppositely charged. A single-surfactant molecule binds at multiple sites on a single-polymer molecule, giving rise to intramolecular bridging. Alternatively, it binds to more than one polymer molecule, allowing intermolecular bridging. D. The polymer is an uncharged random or multiblock copolymer. The surfactant molecules orient themselves at domain boundaries separating the polymer segments of different polarities. E. Polymer is hydrophobically modified. Individual surfactant molecules associate with one or more of the hydrophobic modifiers on a single-polymer molecule or multiple-polymer molecules. F. Polymer is hydrophobically modified. Clusters of surfactant molecules associate with multiple hydrophobic modifiers on a single-polymer molecule. G. Polymer is hydrophobically modified. Clusters of surfactant molecules associate with each of the hydrophobic modifier on a single-polymer molecule. H. The polymer segments partially penetrate and wrap around the polar headgroup region of the surfactant micelles. A single polymer molecule can associate with one or more surfactant micelles.

Structure D depicts a situation when the polymer is a random copolymer or multiblock copolymer with relatively short blocks. In this case, the polymer molecule assumes a conformation in solution characterized by segregation of dissimilar segments or blocks of varying polarity. Depending on whether the polymer is a random copolymer or a block copolymer, the segregation in the polymer can take different forms, including the formation of polymeric micelles. In either case, one can imagine the surfactant molecules to locate themselves at the interfaces between the segregated regions.

Structures E, F, and G pertain to hydrophobically modified polymers. In this case the size of the hydrophobic modifier, its grafting density along the polymer, and the relative concentrations of the surfactant and the polymer all influence the nature of the association structure. In general, at low surfactant concentrations, structure E may be obtained with single-surfactant molecules or very small surfactant clusters (dimers, trimers, etc.) interacting with one or more hydrophobic modifiers, without causing any conformational changes on the polymer. When the surfactant concentration is increased, somewhat larger surfactant clusters form co-aggregates with multiple hydrophobic modifiers belonging to the same polymer molecule, causing the polymer conformation to change significantly. At larger surfactant concentrations, it is possible to obtain structure *G*, where surfactant aggregates are formed around each of the hydrophobic modifier.

Structure H denotes a complex consisting of the polymer molecule wrapped around surfactant micelles with the polymer segments partially penetrating the polar headgroup region of the micelles and reducing the micelle core–water contact. Such a structure can describe a nonionic polymer interacting with surfactant micelles. Such a structure can also be imagined in the case of an ionic polymer interacting with oppositely charged micelles.

For each type of polymer molecule such as those depicted in Fig. 48, including the nonionic polymer, charged polymer, hydrophobically modified polymer, star polymer, random or block copolymer, some of the unique features of the polymer molecule will have to be invoked in developing quantitative models of polymer–surfactant association. Given the widespread use of nonionic polymers, in this paper we explore the association of surfactants with such polymers. The general ideas of molecular aggregation and the formation of competitive association structures discussed in this paper are applicable to the various types of polymers mentioned above, but the details of the modeling would have to be modified in each case to account for the particularities of the polymer molecule.

B. Modeling Nonionic Polymer–Surfactant Association

The model presented below follows our earlier thermodynamic analysis of polymer-micelle association [121]; a somewhat different approach has been presented by Ruckenstein et al. [122]. We have extended the model also to treat the association of nonionic polymers with rodlike micelles and vesicles [123] and various types of microemulsions [124].

We visualize a polymer–surfactant association complex (Structure H in Fig. 48) as consisting of fully formed surfactant aggregates interacting with the polymer segments. In the polymer-bound aggregates, the polymer segments are assumed to adsorb at the aggregate–water interface, shielding a part of the hydrophobic domain of the aggregate from being in contact with water. The physicochemical properties of the polymer molecule determine the area of mutual contact between the polymer molecule and the hydrophobic surface of the aggregate. A characteristic parameter a_{pol} is defined to represent this area of mutual contact per surfactant molecule in the aggregate. Although it is not very realistic to anticipate that the polymer molecule can provide a uniform shielding of the aggregate surface from water by the amount a_{pol} per surfactant molecule, this area parameter is defined in the mean-field spirit to serve as a quantitative measure of the nature of polymer–aggregate interactions.

C. Free Energy of Micellization in the Presence of Polymer

1. Modification of Free Energy Contributions Due to Polymer

The various contributions to the standard free energy of formation of micelles or vesicles have been summarized in Eq. (54), and detailed expressions to calculate each of these contributions are described in Section IV.A. For an ionic surfactant, the free energy of micellization has the form

$$\frac{(\Delta \mu_g^0)}{kT} = \frac{(\Delta \mu_g^0)_{\text{tr}}}{kT} + \frac{(\Delta \mu_g^0)_{\text{def}}}{kT} + \frac{(\Delta \mu_g^0)_{\text{int}}}{kT} + \frac{(\Delta \mu_g^0)_{\text{steric}}}{kT} + \frac{(\Delta \mu_g^0)_{\text{ionic}}}{kT} \tag{80}$$

where the five terms respectively account for the transfer free energy of the surfactant tail, the deformation free energy of the tail, the free energy of formation of the micelle–water interface, the steric repulsions between the headgroups at the micelle surface, and the electrostatic repulsions between the ionic headgroups. The last term is absent for nonionic surfactants and is replaced by the dipole interaction free energy term for zwitterionic surfactants. The standard free energy of formation of aggregates bound to the nonionic polymer molecule can be written in a similar form, with modifications to account for the presence of polymer segments at the aggregate–

water interface. As mentioned above, we assume that the polymer segments shield the hydrophobic domain from water by an area a_{pol} per surfactant molecule. This gives rise to three competing contributions to the free energy of aggregation. First, a decrease in the hydrophobic surface area of the aggregate exposed to water occurs. This decreases the positive free energy of formation of the aggregate–water interface and thus favors the formation of polymer-bound aggregates. Second, steric repulsions arise between the polymer segments and the surfactant headgroups at the aggregate surface. This increases the positive free energy of headgroup repulsions and thus disfavors the formation of the polymer-bound aggregates. Finally, the contact area a_{pol} of the polymer molecule is removed from water and transferred to the surface of the aggregate, which is concentrated in the surfactant headgroups. This alters the free energy of the polymer and can favor or disfavor the formation of the polymer-bound micelles depending on the type of interactions between the polymer segments and the interfacial region rich in headgroups. Taking these factors into account, one may write

$$\frac{(\Delta\mu_g^0)}{kT} = \frac{(\Delta\mu_g^0)_{\text{tr}}}{kT} + \frac{(\Delta_g^0)_{\text{def}}}{kT} + \frac{\sigma_{\text{agg}}}{kT}(a - a_o - a_{\text{pol}}) - \ln\left(1 - \frac{a_p + a_{\text{pol}}}{a}\right) + \frac{(\Delta\mu_g^0)_{\text{ionic}}}{kT} - \frac{\Delta\sigma_{\text{pol}} a_{\text{pol}}}{kT} \tag{81}$$

The first two terms and the fifth term are identical to those appearing in Eq. (80). The modified third term accounts for the enhanced shielding of the micellar core from water provided by the polymer. The modified fourth term accounts for the increase in the steric repulsions due to the presence of the polymer. The sixth term is new and represents the change in the interaction free energy of the polymer molecule. This interaction free energy is written as the product of an interfacial tension and the area of the polymer that is removed from water and brought into contact with the micellar surface. Here, $\Delta\sigma_{\text{pol}}$ is the difference between the macroscopic polymer-water interfacial tension and the interfacial tension between the polymer and the aggregate headgroup region. The factor $\Delta\sigma_{\text{pol}}$ is obviously affected by both the hydrophobic character of the polymer molecule and its interactions with the surfactant headgroups that are crowded at the interface. One may expect $\Delta\sigma_{\text{pol}}$ to be positive and larger for more hydrophobic polymers and for polymers that may have attractive interactions with surfactant headgroups. Given the above free energy equation, the equilibrium aggregation number, the surface area per surfactant molecule of the bound micelle, and the CMC are calculated as described in Section IV.B.2 by finding the maximum in the aggregate size distribution.

2. Estimation of Molecular Constants

Two new molecular constants, a_{pol} and $\Delta\sigma_{pol}$, that depend on the type of the polymer are necessary for predictive calculations. At present, there are no a priori methods available for estimating a_{pol}, while $\Delta\sigma_{pol}$ can, in principle, be determined from interfacial tension measurements as suggested by Ruckenstein et al. [122]. Consequently, a reasonable and simple way to estimate both these parameters is by fitting the measured CMC and aggregation number of any one surfactant that forms spherical or globular micelles to the model; the fitted parameters can then be used to make a priori predictions for any other surfactant and for systems forming not only globular micelles but those forming rodlike micelles, vesicles, and microemulsions as well. For the illustrative calculations discussed below, we take $a_{pol} = 0.20\,nm^2$ and $\Delta\sigma_{pol} = 15$, 0, or -15 mN/m. The three values for $\Delta\sigma_{pol}$ allow the investigation of the subtle role this contribution plays in governing the formation of polymer-bound aggregates. One may note that $\Delta\sigma_{pol}$ affects only the CMC and not the aggregation number since the polymer interaction free energy contribution is a constant independent of the aggregation number g.

D. Interaction of Polymer with Globular Micelles

The equilibrium aggregation number, the area per molecule of the micelle, and the CMC calculated for the anionic surfactant—sodium dodecyl sulfate (SDS)—and the nonionic surfactant—decyl dimethyl phosphene oxide ($C_{10}PO$)—are given in Table 5. In polymer-free solutions the anionic SDS micelles are small, only marginally larger than the largest spherical micelle possible, and the CMC is approximately 7.85 mM. In the presence of the polymer, the CMC is substantially decreased (2.45 mM, 1.2 mM, and 5.0 mM for $\Delta\sigma_{pol} = 0$, 15, and -15 mN/m, respectively), corresponding to a lower free energy for the formation of polymer-bound micelles. Therefore, polymer-bound globular micelles will be favored over free micelles in this case. The aggregation number of the polymer-bound micelles are smaller than those of the free micelles. Results for the nonionic surfactant $C_{10}PO$ are also given in Table 5. In the absence of the polymer, small ellipsoidal micelles (slightly larger than the largest spheres that are geometrically allowed) are formed and the CMC is approximately 0.386 mM. In the presence of the polymer, the CMC is significantly decreased (0.18 and 0.088 mM) if $\Delta\sigma_{pol} = 0$ or 15 mN/m. Therefore, micelles that are bound to the polymer will be favored over free micelles. The aggregation number of the polymer-bound spherical micelles are substantially smaller compared to that of the free micelles. The CMC of 0.368 mM calculated for $\Delta\sigma_{pol} = -15$ mN/m is closer to but still smaller than that in the polymer-free solution,

TABLE 5 Polymer Association with Surfactant Aggregates at 25°C

Surfactant	CMC (mM)	a (nm^2)	g	K	Shape
$C_{10}PO$	0.386	0.584	52	—	Globular
$C_{10}PO + P$*	0.18	0.789	20	—	Sphere
$C_{12}SO_4Na$	7.85	0.629	56	—	Sphere
$C_{12}SO_4Na + P$	2.45	0.781	29	—	Sphere
$C_{12}PO$	0.243	0.582	—	5.6×10^9	Rod
$C_{12}PO + P$	0.128	0.795	28	4.5×10^2	Sphere
$C_{12}SO_4Na + 0.8M$ NaCl	0.313	0.477	—	6.0×10^4	Rod
$C_{12}SO_4Na + 0.8M$ NaCl + P	0.057	0.561	88	6.1×10^4	Globular
di-$C_{12}SO_4Na + 0.01M$ NaCl	4.26×10^{-3}	0.583	462	—	Vesicle**
		0.771	727		
di-$C_{12}SO_4Na + P + 0.01M$ NaCl	2.61×10^{-3}	1.065	60	—	Globular

*P refers to polymer-bound aggregates, the corresponding CMCs listed are for $\Delta\sigma_{pol} = 0$ mN/m. These CMCs should be multiplied by 0.49 if $\Delta\sigma_{pol} = 15$ or by 2.043 if $\Delta_{pol} = -15$ mN/m.
**The two values listed for both a and g correspond to the inner and the outer layers of vesicle.

suggesting that polymer-bound micelles will be formed in this case as well. But a further decrease in $\Delta\sigma_{pol}$ (say, -16.5 mN/m) will result in the CMC for polymer-bound micelles being larger than the CMC for the polymer-free micelles. Therefore, a preference for free micelles over bound micelles would be predicted. Evidently, subtle free energy differences associated with the hydrophobicity of the polymer and its interactions with the surfactant headgroups can tilt the equilibrium favoring free micelles over bound micelles, or vice versa.

The contrasting behavior of anionic and nonionic surfactants can be interpreted in the framework of the present thermodynamic model. If the polymer associates with the micelle, the presence of the polymer segments increases the equilibrium area per surfactant molecule. For nonionic surfactants, this incremental increase in the equilibrium area a is roughly comparable to the polymer-micelle contact area a_{pol} (see Table 5). Correspondingly, the negative increment in the free energy of shielding of the micellar core from water by the polymer segments is close in magnitude to the positive increment in the free energy of steric repulsions at the aggregate surface. If only these two effects are considered, then the CMC values for the formation of bound and free micelles are always very near one another, with the free micelles generally favored over the bound micelles. The tail deformation free energy decreases for the polymer-bound micelles because of their reduced size, thus favoring the bound micelles over the free micelles. The polymer interaction free energy provides a positive or negative contribution to the formation of the polymer-bound aggregates, depending on the polymer hydrophobicity and the polymer–surfactant headgroup interactions. This factor decreases further the CMC when $\Delta\sigma_{pol} > 0$ and tilts the balance more in favor of bound micelles. On the other hand, when $\Delta\sigma_{pol} < 0$ and has a sufficiently large magnitude, this factor inhibits the occurrence of binding.

The calculated results for the anionic surfactants are different from the above behavior of nonionic surfactants. In the case of anionic surfactants, the increase in the equilibrium area per molecule of the aggregate due to the presence of the polymer is generally smaller than the polymer–aggregate contact area a_{pol}. This is because of the importance of the electrostatic headgroup interaction term in determining the equilibrium area of the aggregate. Therefore, the negative increment in the free energy of shielding of the aggregate core from water by the polymer segments more than offsets the positive increment in the free energy of steric repulsions at the micellar surface. More importantly, there is a negative increment in the free energy of electrostatic interactions at the aggregate surface because the equilibrium area in the presence of the polymer is somewhat larger. These free energy contributions dominate over the polymer interaction free energy with the

result that the polymer-bound anionic micelles are always favored over free micelles. It has been reported that cationic surfactants do not bind with a nonionic polymer such as polyoxyethylene [117–121]. This differing behavior compared to anionic surfactants must thus come because $\Delta\sigma_{pol} < 0$ and has a sufficiently large magnitude than that considered, for example, here. Such a situation can arise because of the weakly cationic nature of the ether oxygens in polyoxyethylene [118–121] and may lead to a larger CMC if polymer-bound aggregates are to form; hence binding does not occur in these cases.

E. Interaction of Polymer with Rodlike Micelles

The general thermodynamic analysis of rodlike micelles was discussed in Section II.D. Given Eqs. (80) and (81) for the free energy of micellization, the sphere-to-rod transition parameter K and the CMC can be calculated as described in Section IV.B. We again note that the radius of the cylindrical middle part of the micelle and that of the spherical endcaps are allowed to differ from one another and are determined by the equilibrium conditions. The calculated results are included in Table 5 for the surfactant solution containing the anionic SDS in the presence of 0.8M NaCl. In the absence of the polymer, large polydispersed rodlike micelles are formed in solution as shown by the large value for K. When the polymer molecules are present, the magnitude of K is dramatically reduced. Consequently, only small globular micelles are formed. The CMC corresponding to the formation of the polymer-bound globular micelles (0.057, 0.028, and 0.116 mM for $\Delta\sigma_{pol} = 0$, 15, and -15 mN/m, respectively) is lower than that for the formation of polymer-free rodlike micelles (0.313 mM). Therefore, the equilibrium favors the formation of the smaller ellipsoidal micelles in the presence of the polymer. Thus, a rod-to-globule transition is induced by the addition of the polymer. In the case of the nonionic surfactant dodecyl dimethyl phosphene oxide (designated as $C_{12}PO$), large rodlike micelles are formed in polymer-free solutions as reflected in the large value for K and at a CMC of 0.243 mM. In the presence of the nonionic polymer, K is dramatically decreased and the allowed aggregate is a small ellipsoid. The calculations show that if $\Delta\sigma_{pol} = 0$ or 15 mN/m, the CMC is 0.128 or 0.063 mM in the presence of the polymer. This implies that equilibrium will favor the formation of small polymer-bound ellipsoidal micelles. In contrast, if $\Delta\sigma_{pol} = -15$ mN/m, the CMC corresponding to the polymer-bound micelles is larger (0.262 mM) than the CMC corresponding to the polymer-free micelles. In such a case, the binding with polymer does not occur and polymer-free rodlike micelles coexist with free polymer molecules in solution. One can also visualize

situations when $\Delta\sigma_{pol}$ assumes values such that the CMCs corresponding to both polymer-free and polymer-bound micelles are comparable. This condition will lead to the coexistence of both large rodlike and small polymer-bound ellipsoidal micelles.

F. Interaction of Polymer with Vesicles

The free energy of aggregation is still given by Eqs. (80) and (81), with the understanding that the headgroup interaction free energies and the free energy of formation of the aggregate–water interface should be written for both inner and outer layers of the bilayer vesicle, the areas per molecule at these two layers can differ from one another, and the layers can have different thicknesses. The polymer molecules are assumed to be present at both inner and outer surfaces of the spherical bilayer vesicle. Calculations have been carried out for didodecyl sodium sulfate (designated as di-C_{12} SO_4Na), and the results are included in Table 5. In the absence of the polymer, calculations show (see also Table 4) that di-C_{12} SO_4Na forms small spherical bilayer vesicles. The inner and the outer radii of the hydrophobic shell are 4.63 nm and 6.68 nm, respectively. The volume of the aqueous core per surfactant molecule is approximately 0.350 nm^3, whereas the volume of the polar headgroup of di-C_{12} SO_4Na is less than 0.100 nm^3. When the polymer molecule is present, the formation of the vesicular structure is not predicted. Calculations to examine the formation of closed aggregates have been carried out for the aggregate geometries described in Table 1. The results show that small globular micelles are favored (see Table 5). Thus, the addition of polymer to the solution containing vesicles can lead to a disruption of the vesicle structure and the generation of smaller closed aggregates.

VII. MICELLIZATION OF BLOCK COPOLYMERS

A. Aggregation of Block Copolymers in Selective Solvents

Block copolymer molecules exhibit self-assembly behavior similar to conventional low molecular-weight surfactants. The different blocks of the AB copolymer can have differing affinities for the solvent: the A block being solvophobic and the B block being solvophilic. The two blocks thus resemble the tail and the head of a conventional low-molecular-weight surfactant. As a result, the block copolymer forms micelles in a variety of solvents that are selective to one block and nonselective to the other block (Fig. 49). In these micelles, the solvophobic blocks constitute the core and the solvophilic blocks constitute the corona or the shell region of the micelle. For BAB triblock copolymers, the A block has to bend back and form a loop so as to

FIG. 49 Schematic representation of a micelle formed of AB diblock copolymers in a solvent selective for the B block. The thick lines denote the solvophobic blocks constituting the core of the micelle while the thin lines denote the solvophilic blocks forming the corona region of the micelle. A significant amount of solvent is present in the corona region

ensure that the two B blocks are in the corona; similarly, in the case of an ABA copolymer, the B block has to form a loop and bend back so that the two A blocks can be inside the core.

The micellization tendency of block copolymers may be viewed as more general compared to that of low-molecular-weight surfactants in the sense that aggregation of block copolymers is achievable in almost any solvent by selecting the appropriate block copolymer, whereas for low-molecular-weight surfactants, water constitutes the best solvent for promoting aggregation [125–127]. Further, in the case of block copolymers, because of the large size of the solvophobic block, the CMC is often too small to be measurable when compared to the CMCs of low-molecular-weight surfactants. The block copolymer aggregates can assume a variety of shapes such as spheres, cylinders, and bilayers including vesicles.

Theoretical treatments of block copolymer micelles have been pioneered by de Gennes [128], Leibler et al. [129], Noolandi and Hong [130], and

Whitmore and Noolandi [131]. de Gennes [128] has analyzed the formation of a diblock copolymer micelle in selective solvents by minimizing the free energy per molecule of an isolated micelle with respect to the aggregation number or core radius. The micelle core was assumed fully segregated and devoid of any solvent. The free energy of formation of the core–corona interface and the elastic free energy of stretching of the core blocks control the micellization behavior. Leibler et al. [129] have treated the problem of micelle formation of a symmetric diblock copolymer in a homopolymer solvent. In their study and in de Gennes' work, the interface is taken to be sharp. Noolandi and Hong [130] and Whitmore and Noolandi [131] have formulated mean-field models taking into account the possibility of a diffuse interface between the core and corona regions.

The ideas of chain deformation and corona mixing effects discussed in these studies have been applied to the treatment of micelles formed of non-ionic surfactants with polyethylene oxide headgroups in Section IV. A. In this section the thermodynamic treatment of aggregation is presented for AB diblock and BAB triblock copolymers, and one can observe the close similarity between the model for low-molecular weight surfactants and that for the high-molecular-weight block copolymers.

B. Aggregate Shapes and Geometrical Relations

Before developing a free energy model, we will first define the geometrical relations connecting aggregate shapes to the molecular size properties of the block copolymer. The shape of the aggregate and the assumption of incompressibility lead to the geometrical relations summarized in Table 6 for different morphologies. We denote the molecular volumes of the A and the B segments and the solvent by v_A, v_B, and v_W, respectively. The characteristic lengths of the A and the B segments are denoted by L_A $(= v_A^{1/3})$ and L_B $(= v_B^{1/3})$. The variables N_A and N_B refer to the number of segments of block A and block B for the AB diblock as well as the BAB triblock

TABLE 6 Geometrical Properties of Spherical, Cylindrical, and Lamellar Block Copolymer Aggregates

Property	Sphere	Cylinder	Lamella
V_c	$4\pi R^3/3$	πR^2	2R
V_s	$V_c[(1 + D/R)^3 - 1]$	$V_c[(1 + D/R)^2 - 1]$	$V_c[(1 + D/R) - 1]$
g	$V_c\varphi_A/(N_A v_A)$	$V_c\varphi_A/(N_A v_A)$	$V_c\varphi_A/(N_A v_A)$
a	$3N_A v_A/(R\varphi_A)$	$2N_A v_A/(R\varphi_A)$	$N_A v_A/(R\varphi_A)$
φ_B	$(N_B v_B/N_A v_A)\varphi_A(V_c/V_s)$	$(N_B v_B/N_A v_A)\varphi_A(V_c/V_s)$	$(N_B v_B/N_A v_A)\varphi_A(V_c/V_s)$

copolymers, implying that the BAB triblock copolymer has two terminal blocks of size $N_B/2$ attached to a middle block of size N_A. We use the variable R to denote the hydrophobic core dimension (radius for sphere or cylinder and half-bilayer thickness for lamella), D for the corona thickness, and a for the surface area of the aggregate core per constituent block copolymer molecule. The number of molecules g, the micelle core volume V_C, and the corona volume V_S all refer to the total quantities in the case of spherical aggregates, quantities per unit length in the case of cylindrical aggregates, and quantities per unit area in the case of lamellae. The core volume V_C is calculated as the volumes of the A blocks, $V_C = gN_A v_A$. The concentrations of segments are assumed to be uniform in the core as well as in the corona, with φ_A standing for the volume fraction of the A segments in the core ($\varphi_A = 1$), and φ_B for the volume fraction of the B segments in the corona. If any two structural variables are specified, all remaining geometrical variables can be calculated through the relations given in Table 6. For convenience, R and D are chosen as the independent variables.

C. Free Energy of Micellization of Block Copolymers

An expression for $\Delta\mu_g^0$ is formulated by considering all the physicochemical changes accompanying the transfer of a singly dispersed copolymer molecule from the infinitely dilute solution state to an isolated micelle, also in the infinitely dilute solution state. First, the transfer of the singly dispersed copolymer to the micellar core is associated with changes in the state of dilution and in the state of deformation of the A block. Second, the B block of the singly dispersed copolymer is transferred to the corona region of the micelle, and this transfer process also involves changes in the states of dilution and deformation of the B block. Third, the formation of the micelle localizes the copolymer such that the A block is confined to the core while the B block is confined to the corona. Fourth, the formation of the micelle is associated with the generation of an interface between the micelle core made up of A blocks and the micelle corona consisting of solvent W and B blocks. Further, in the case of a BAB triblock copolymer, folding or loop formation of the A block occurs, ensuring that the B blocks at the two ends are in the aqueous domain while the folded A block is within the hydrophobic core of the micelle. This provides an additional free energy contribution. The overall free energy of micellization can be obtained as the sum of the above individual contributions:

$$(\Delta\mu_g^0) = (\Delta\mu_g^0)_{A,dil} + (\Delta\mu_g^0)_{A,def} + (\Delta\mu_g^0)_{B,dil} + (\Delta\mu_g^0)_{B,def} + (\Delta\mu_g^0)_{loc} + (\Delta\mu_g^0)_{int} + (\Delta\mu_g^0)_{loop} \quad (82)$$

One may observe that many of the above free energy contributions are analogous to those considered in Section IV.A for conventional surfactants. The A block dilution contribution is equivalent to the tail transfer free energy. The A block deformation is identical to the tail deformation energy. The B block dilution and deformation contributions are equivalent to head-group repulsions. The interfacial free energy is the same for both kinds of surfactants. Only the localization and looping free energy contributions are additions that had not been considered before. These two contributions are found to be less important relative to the other contributions. In essence, the free energy model for the block copolymer remains essentially the same as that for all self-assembling systems treated in this chapter. Expressions for each of the contributions appearing in Eq. (82) are formulated below.

1. Change in State of Dilution of Block A

In the singly dispersed state of the copolymer molecule in solvent, the A block is in a collapsed state, minimizing its interactions with the solvent. The region consisting of the collapsed A block with some solvent entrapped in it is viewed as a spherical globule, whose diameter $2R_{\infty A}$ is equal to the end-to-end distance of block A in the solvent. The volume of this spherical region is denoted by $V_{\infty A}$. The chain expansion parameter α_A describes the swelling of the polymer block A by the solvent W.

$$V_{\infty A} = \frac{4\pi R_{\infty A}^3}{3}, \qquad 2R_{\infty A} = \alpha_A N_A^{1/2} L_A, \qquad \alpha_A = \left(\frac{6}{\pi}\right)^{1/3} N_A^{-1/6} \phi_{A1}^{-1/3} \tag{83}$$

where φ_{A1} ($= N_A v_A / V_{\infty A}$) is the volume fraction of A segments within the monomolecular globule. The first equality in Eq. (83) follows from geometry, while the second equality is based on the definition of the chain expansion parameter α_A, taking $(N_A^{1/2} L_A)$ as the unperturbed end-to-end distance of block A. The third equality is obtained by combining the first two in conjunction with the definition for φ_{A1}. Applying the suggestion of de Gennes [58], the volume fraction φ_{A1} is calculated from the condition of osmotic equilibrium between the monomolecular globule treated as a distinct phase and the solvent surrounding it.

$$\ln(1 - \phi_{A1}) + \phi_{A1} + \chi_{AW} \phi_{A1}^2 = 0 \tag{84}$$

In Eq. (84), χ_{AW} is the Flory interaction parameter between the pure A polymer and solvent. In the micelle, the A block is confined to the core region where it is like a pure liquid. The difference in the dilution of block A from its singly dispersed state to the micellized state makes a free energy contribution given by the relation

$$\frac{(\Delta\mu_g^0)_{\mathrm{A,dil}}}{kT} = -N_{\mathrm{A}}\left[\frac{v_{\mathrm{A}}}{v_{\mathrm{W}}}\frac{1-\phi_{\mathrm{A1}}}{\phi_{\mathrm{A1}}}\ln(1-\phi_{\mathrm{A1}}) + \frac{v_{\mathrm{A}}}{v_{\mathrm{W}}}(1-\phi_{\mathrm{A1}})\chi_{\mathrm{AW}}\right] - \left(\frac{\sigma_{\mathrm{AW}}L_{\mathrm{A}}^2}{kT}\right)\frac{6N_{\mathrm{A}}^{1/2}}{\alpha_{\mathrm{A}}} \tag{85}$$

The first two terms account for the entropic and enthalpic changes associated with the removal of A block from its infinitely dilute state in the solvent to a pure A state. These terms are written in the framework of the Flory [53] expression for an isolated polymer molecule. The last term accounts for the fact that the interface of the globule of the singly dispersed A block disappears on micellization. This term is written as the product of the interfacial tension (σ_{AW}) between pure A and solvent W, the surface area of the globule ($4\pi R_{\infty \mathrm{A}^2}^2$), and the factor φ_{A1} (volume fraction of the polymer A in the globule) to account for the reduction in the contact area between the block A and solvent W caused by the presence of some solvent molecules inside the monomolecular globule. If the interfacial tension σ_{AW} is not available from direct measurements, it can be estimated using the relation $\sigma_{\mathrm{AW}} = (\chi_{\mathrm{AW}}/6)^{1/2}(kT/L^2)$, where $L = v_{\mathrm{W}}^{1/3}$. Such a relation is usually employed for the calculation of polymer–polymer interfacial tensions [132,133].

2. Change in State of Deformation of Block A

In the singly dispersed state of the copolymer, the conformation of the A block is characterized by the chain expansion parameter α_{A}, which is the ratio between the actual end-to-end distance and the unperturbed end-to-end distance of the polymer block. The free energy of this deformation is written using the Flory [53] expression derived for an isolated polymer molecule. Within the micelle the A block is stretched nonuniformly, with the chain ends occupying a distribution of positions within the core while ensuring that the core has a uniform concentration. The free energy contribution allowing for nonuniform chain deformation is calculated using the analysis of chain packing pioneered by Semenov [46] and discussed earlier in detail in Section IV.A. In the case of a BAB triblock copolymer, the A block deformation is calculated by considering the folded A block of size N_{A} to be equivalent to two A blocks of size $N_{\mathrm{A}}/2$. On this basis, one obtains

$$\frac{(\Delta\mu_g^0)_{\mathrm{A,def}}}{kT} = \left[q\left(\frac{p\pi^2}{80}\right)\frac{R^2}{(N_{\mathrm{A}}/q)L_{\mathrm{A}}^2}\right] - \left(\frac{3}{2}(\alpha_A^2 - 1) - \ln\alpha_{\mathrm{A}}^3\right) \tag{86}$$

where $q = 1$ for an AB diblock copolymer and $q = 2$ for a BAB triblock copolymer having a middle hydrophobic block. The parameter p is dependent on aggregate shape and has the value of 3 for spherical micelles, 5 for

cylinders, and 10 for lamellae (see Section IV.A). In Eq. (86), the first term represents the A block deformation free energy in the micelle while the second term corresponds to the deformation free energy in the singly dispersed copolymer.

3. Change in State of Dilution of Block B

In the singly dispersed state of the copolymer, the polymer block B is swollen with the solvent. As mentioned before, N_B denotes the size of the B block for the AB diblock copolymer, while for a symmetric BAB triblock copolymer, the end blocks are of equal size $N_B/2$. We consider this swollen B block to be a sphere whose diameter $2R_{\infty B}$ is equal to the end-to-end distance of isolated block B in the solvent. The volume of this spherical region is denoted by $V_{\infty B}$, while φ_{B1} [$= (N_B/q)v_B/V_{\infty B}$] is the volume fraction of B segments within the monomolecular globule;

$$V_{\infty B} = \frac{4\pi R_{\infty B}^3}{3}, \qquad 2R_{\infty B} = \alpha_B (N_B/q)^{1/2} L_B \tag{87}$$

The second equality in Eq. (87) is based on the definition of the chain expansion parameter α_B, which can be estimated using the expression developed by Flory (53). In the Flory expression for α_B, Stockmayer (134) has suggested decreasing the numerical coefficient by approximately a factor of 2 to ensure consistency with the results obtained from perturbation theories of excluded volume. Consequently, one can estimate α_B as the solution of

$$\alpha_B^5 - \alpha_B^3 = 0.88(1/2 - \chi_{BW})(N_B/q)^{1/2} \tag{88}$$

where χ_{BW} is the Flory interaction parameter between the B block and water.

In the micelle, the B blocks are present in the corona region of volume V_S. This region is assumed to be uniform in concentration with φ_B ($= gN_B v_B/V_S$) being the volume fraction of the B segments in the corona. The free energy of the corona region can be written using the Flory [53] expression for a network swollen by the solvent. Therefore, the difference in the states of dilution of the B block on micellization provides the following free energy contribution:

$$\begin{aligned}\frac{(\Delta\mu_g^0)_{B,dil}}{kT} = {} & N_B\left[\frac{v_B}{v_W}\frac{1-\phi_B}{\phi_B}\ln(1-\phi_B) + \frac{v_B}{v_W}(1-\phi_B)\chi_{BW}\right] \\ & - N_B\left[\frac{v_B}{v_W}\frac{1-\phi_{B1}}{\phi_{B1}}\ln(1-\phi_{B1}) + \frac{v_B}{v_W}(1-\phi_{B1})\chi_{BW}\right]\end{aligned} \tag{89}$$

The first two terms in Eq. (89) describe the entropic and enthalpic contributions to the free energy of swelling of the B block by the solvent in the

corona region of the micelle, while the last two terms refer to the corresponding contributions in the singly dispersed copolymer molecule.

4. Change in State of Deformation of Block B

In the singly dispersed state the B block has a chain conformation characterized by the chain expansion parameter α_B. In the micelle the B block is stretched nonuniformly over the micelle corona so as to ensure that the concentration in the corona region is uniform. Semenov [46] has shown that the estimate for the chain deformation energy assuming that the termini of all B blocks lie at the distance D from the core surface is not very different from that calculated assuming a distribution of chain termini at various positions within the corona. This has already been applied to the case of surfactants with oligomeric ethylene oxide headgroups in Section IV. We use that expression here also:

$$\frac{(\Delta \mu_g^0)_{B,def}}{kT} = \left[q\frac{3}{2}\frac{L_B R}{(a/q)\phi_B}P\right] - q\left[\frac{3}{2}(\alpha_B^2 - 1) - \ln \alpha_B^3\right] \tag{90}$$

where a is the surface area per molecule of the micelle core, $q = 1$ for AB diblock and 2 for BAB triblock, as mentioned before, and P is a shape-dependent function given by $P = (D/R)/[1 + (D/R)]$ for spheres, $P = \ln[1 + (D/R)]$ for cylinders, and $P = (D/R)$ for lamellae. The first term in Eq. (90) represents the free energy of deformation of the B block in the micellar corona, while the second term denotes the corresponding free energy in the singly dispersed copolymer molecule.

5. Localization of the Copolymer Molecule

On micellization, the copolymer becomes localized in the sense that the joint linking blocks A and B in the copolymer are constrained to remain in the interfacial region rather than occupying all the positions available in the entire volume of the micelle. The entropic reduction associated with localization is modeled using the concept of configurational volume restriction [135]. Thus, the localization free energy is calculated on the basis of the ratio between the volume available to the A–B joint in the interfacial shell of the micelle (surrounding the core and having a thickness L_B) and the total volume of the micelle:

$$\frac{(\Delta \mu_g^0)_{loc}}{kT} = -q \ln\left[\frac{d L_B}{R(1 + D/R)^d}\right] \tag{91}$$

Here, d refers to the dimensionality of aggregate growth and is 3 for spherical micelles, 2 for cylinders, and 1 for lamellae.

6. Formation of Micellar Core–Solvent Interface

When a micelle forms, an interface is generated between the core region consisting of the A block and the corona region consisting of the B block and the solvent W. The free energy of formation of this interface is estimated as the product of the surface area of the micellar core and an interfacial tension characteristic of this interface. The appropriate interfacial tension is that between a pure liquid of block A in the micelle core and a solution of block B and solvent W in the micellar corona. Because the corona region is often very dilute in block B, the interfacial tension can be approximated as that between the solvent W and the A block in the micelle core. Denoting the polymer A–solvent W interfacial tension by σ_{AW}, the free energy of generation of the micellar core–solvent interface is calculated from

$$\frac{(\Delta \mu_g^0)_{\text{int}}}{kT} = \frac{\sigma_{\text{agg}}}{kT} a, \qquad \sigma_{\text{agg}} = \sigma_{AW} \tag{92}$$

7. Backfolding or Looping in Triblock Copolymer

The backfolding of the middle block in a BAB triblock copolymer contributes an entropic term to the free energy of solubilization. This contribution is absent for the case of a diblock copolymer. Jacobson and Stockmayer [136] show that the reduction in entropy for the condition that the ends of a linear chain of N segments are to lie in the same plane or on one side of a plane is proportional to $\ln N$. Therefore, the assumption that the backfolding of the middle block in the micelle follows the same functional form is made. Hence, the backfolding entropy makes the following contribution in the case of a BAB copolymer:

$$\frac{(\Delta \mu_g^0)_{\text{loop}}}{kT} = \frac{3}{2} \beta \ln(N_A) \tag{93}$$

Here β is an excluded volume parameter that is equal to unity when the excluded-volume effects are negligible and larger than unity when these effects become important. In our calculations, β is taken to be unity. The difference in the estimate for β in the case of ABA and BAB triblock copolymers may be important for explaining any observed differences between these two kinds of triblock copolymers having the same overall molecular weight and composition.

D. Predicted Aggregation Behavior of Block Copolymers

Illustrative calculations have been carried out for the diblock copolymers, polystyrene-polyisoprene (PS-PI) and polyethylene oxide-polypropylene

oxide (PEO-PPO, denoted E_XP_Y), and for the triblock copolymer PEO-PPO-PEO (denoted $E_XP_YE_X$). One may note that for PS-PI block copolymers, the micellization is examined in n-heptane, which is a selective solvent for the PI blocks and is a nonsolvent for the PS block. For the other two block copolymers, the calculations have been done in water as the solvent with PEO being the hydrophilic and PPO the hydrophobic blocks.

1. Estimation of Model Parameters

To facilitate quantitative calculations, the values of molecular constants appearing in the free energy expressions are needed. The molecular volumes (v_A and v_B) of the repeating units appearing in the different polymer blocks are $0.1612\,nm^3$ for styrene, $0.0943\,nm^3$ for butadiene, $0.01257\,nm^3$ for isoprene, $0.0965\,nm^3$ for propyleneoxide, and $0.0646\,nm^3$ for ethyleneoxide [135]. The molecular volume of water is $0.030\,nm^3$ and of n-heptane is $0.2447\,nm^3$. Given the molecular weight M of the copolymer and the block composition (M_A/M), the number of repeating units N_A and N_B in blocks A and B can be calculated, knowing the segmental molecular weights. The characteristic length L is calculated knowing the molecular volume of the solvent. For polyisoprene–heptane the solvent is practically a theta solvent at 25°C and, correspondingly, the interaction parameters χ_{BW} is taken to be 0.5 [130]. For polystyrene–heptane the solvent is a very poor solvent. The interaction parameter at 25°C is taken to be $\chi_{AW} = 1.9$ [130]. The corresponding interfacial tension between pure polystyrene and n-heptane is estimated from to be 5.92 mN/m [135]. For polyethyleneoxide–water and polypropyleneoxide–water systems, the interaction parameters were estimated from the experimental activity data available in the literature [54]. These data display a concentration dependence for the interaction parameters. Because the corona region is a dilute solution of polyethyleneoxide in water, the value for χ_{BW} is taken from the dilute concentration region of the activity data. Correspondingly, $\chi_{BW} = 0.21$. Because the core region is made of pure polypropyleneoxide, the value for χ_{AW} is taken from the concentrated region of the activity data. For this condition $\chi_{AW} = 2.1$. The corresponding value for the interfacial tension between water and polypropyleneoxide is calculated to be 25.9 mN/m. The estimation of these molecular constants are discussed in detail in Ref. [135].

2. Influence of Free Energy Contributions

The role of various free energy contributions in influencing micelle formation can be understood from their dependence on the aggregation number. The formation of micelles in preference to the singly dispersed state of the copolymer occurs because of the large negative free energy contribution

arising from a change in the state of dilution of the solvent incompatible A block. This free energy contribution is a constant independent of the size of the micelle and hence does not govern the aggregation number of micelle. The contribution favorable to the growth of the aggregates is provided by the interfacial energy. The geometrical relations dictate that the surface area per molecule of the micelle decrease with an increase in the aggregation number. Consequently, the positive interfacial free energy between the micellar core and the solvent decreases with increasing aggregation number of the micelle, and thus this contribution promotes the growth of the micelle. The changes in the state of deformation of the A and the B blocks and the change in the state of dilution of the B block provide positive free energy contributions that increase with increasing aggregation number of the micelle. Therefore, these factors are responsible for limiting the growth of the micelle. The free energy of localization and the free energy of back-folding or looping (in the case of BAB triblock copolymers) are practically independent of g and thus have little influence over the determination of the equilibrium aggregation number. The net free energy of formation of the micelle per molecule is negative and shows a minimum at the equilibrium aggregation number.

3. Predicted Micellization Behavior

For the PS-PI copolymer, the calculated results have been compared against the measurements of Bahadur et al. [137] in Table 7. The tabulated experimental data have been derived from photon correlation spectroscopy and viscosity measurements, assuming that the micelle core is completely devoid of any solvent. The values for g, R, and D estimated from the measurements in this manner are compared against the model prediction and show reasonable agreement. Experimental observations using electron microscopy indi-

TABLE 7 Micellization Behavior of Polystyrene—Polyisoprene in n-Heptane at 25°C

M	M_A/M	R (Å) (Experiments)*	D/R	g	R (Å) (Predictions)	D/R	g
29,000	0.31	94	1.77	248	85	1.77	187
36,000	0.45	119	1.31	278	128	1.24	352
39,000	0.49	141	1.13	386	144	1.12	422
49,000	0.59	194	0.96	666	193	0.87	672
53,000	0.62	240	0.92	1113	211	0.80	778

*Source: Ref. 137.

cated that the micelles are practically monodispersed [137], which is also in agreement with the predictions.

Computed results for diblock copolymers of PEO-PPO are summarized in Table 8. The core radius, the corona thickness, the micelle aggregation number, and the calculated CMC (expressed as volume fraction ϕ_{CMC} in water) are all listed. The calculations have been carried out keeping the size M_A of the PPO block constant, the size M_B of the PEO block constant, the composition of the block copolymer M_A/M constant, and the overall molecular weight of the polymer M constant. In general, the PPO block plays a dominant role in determining the dimension of the core radius R, and hence the aggregation number g of the micelle, while the influence of the PEO

TABLE 8 Micellization Behavior of PEO–PPO Diblock Copolymers in Water

M	M_A/M	R (Å)	D/R	g	$-\ln \phi_{CMC}$
Results for constant $M_A = 3750$					
4,750	0.79	113	0.38	976	74.1
8,250	0.45	89	1.56	475	67.2
12,500	0.30	80	2.72	342	63.9
14,000	0.27	78	3.09	318	63.2
15,750	0.24	76	3.49	296	62.4
Results for constant $M_B = 8750$					
10.750	0.19	52	3.86	173	38.8
14,250	0.39	105	2.17	528	85.3
17,250	0.49	144	1.65	884	116.7
20.750	0.58	186	1.32	1354	148.3
28,750	0.70	275	0.92	2610	208.8
43,750	0.80	424	0.60	5491	298.1
Results for constant $M_A/M = 0.30$					
2,000	0.30	29	1.79	101	17.0
7,000	0.30	58	2.39	234	42.6
20,000	0.30	103	3.03	461	88.1
35,000	0.30	140	3.43	656	127.6
50,000	0.30	169	3.71	818	160.8
Results for constant $M = 12{,}500$					
12,500	0.75	189	0.58	1808	132.4
12,500	0.63	152	0.99	1143	114.2
12,500	0.50	122	1.50	736	95.7
12,500	0.40	100	2.02	512	80.3
12,500	0.20	59	3.79	208	46.0

block on R and g is comparatively smaller. The PEO block dominantly controls the corona dimension D, while the PPO block has only a marginal influence over it. In all cases the CMC is negligibly small because of the large size of the hydrophobic part of the block copolymer.

The relative importance of the PEO block (the headgroup) and the PPO block (the tail group) is quite different from that of conventional surfactant micelles. As seen in Section IV, the headgroup has a much more significant effect on the micellar properties for small surfactant molecules. This is because the headgroup interaction free energy is much more significant compared to the tail deformation free energy in the case of small surfactant molecules. Hence, the effect of the headgroup is dominant. In contrast, the tail deformation free energy can be comparable, if not larger, than the headgroup interaction energy in the case of block copolymers, depending on the relative sizes of the two blocks. Therefore, one sees the dominant role of the hydrophobic group in controlling the micelle size in the case of block copolymers.

4. Aggregate Shape Transitions

To investigate how the size and composition of the block copolymer affect the transition from one aggregate shape to another in the case of block copolymers, we have computed the aggregation properties of the family of Pluronic triblock copolymers, $E_XP_YE_X$. The calculated results are summarized in Table 9. The aggregate shape that yields the smallest free energy of aggregation is taken to be the equilibrium shape. Also given are the dimensions of the core (R) and the corona (D), and the aggregation number (g) in the case of spherical aggregates. The numerical values within brackets are some available experimental data (see details in Ref. [138]).

The calculations show that lamellar aggregates are favored when the ratio of PEO to PPO is small, whereas spherical aggregates are favored when the PEO to PPO ratio is large. Typically, for block copolymers containing 40 or more wt % PEO, only spherical aggregates form at 25°C. For block copolymers containing 30 wt % PEO, cylindrical aggregates are possible. Block copolymers containing 20 or less wt % PEO generate lamellae. This is analogous to the behavior of small-molecular-weight surfactants where the reduction in headgroup repulsions can cause a transition from spherical micelles to rodlike micelles and then to bilayers. In this sense the formation of block copolymer micelles is entirely analogous to the formation of conventional surfactant micelles.

One important difference that should be noted is connected to the tail transfer free energy contribution, which is negative and is the driving force for aggregation of surfactants and block copolymers. In

TABLE 9 Aggregation Behavior of PEO–PPO–PEO Triblock Pluronic Copolymers in Water

Name	Structure	R (nm)	D (nm)	g for Spheres	Shape
L62	$E_6P_{35}E_6$	0.75	1.92	—	Lamellae
L63	$E_9P_{32}E_9$	1.45	1.39	—	Lamellae
L64	$E_{13}P_{30}E_{13}$	3.41 (3.8 to 4.6)	1.66 (3.7 to 4.4)	57 (39 to 70)	Sphere
L65	$E_{19}P_{29}E_{19}$	3.07	2.21	43	Sphere
F68	$E_{77}P_{29}E_{77}$	2.13 (2.5)	5.1 (5.3)	15 (22)	Sphere
P84	$E_{19}P_{43}E_{19}$	4.22	2.25	75	Sphere
P85	$E_{26}P_{40}E_{26}$	3.63 (3.7)	2.83 (3.6)	53 (57, 37 to 78)	Sphere
F88	$E_{104}P_{39}E_{104}$	2.5	6.39	17	Sphere
F98	$E_{118}P_{45}E_{118}$	2.67	7.03	18	Sphere
P103	$E_{17}P_{60}E_{17}$	3.86	2.15	—	Cylinder
P104	$E_{27}P_{61}E_{27}$	5.1	2.98	94	Sphere
P105	$E_{37}P_{56}E_{37}$	4.39	3.73	65	Sphere
F108	$E_{133}P_{50}E_{133}$	2.83 (2.5)	7.66 (15.0)	20 (13)	Sphere
P123	$E_{20}P_{70}E_{20}$	4.21	2.44	—	Cylinder
F127	$E_{100}P_{64}E_{100}$	3.75	7.02	35 (15 to 45, 30)	Sphere

the case of conventional surfactants the negative free energy associated with the transfer of the tail is significant when water is the solvent and diminishes in magnitude when water is replaced by other polar organic molecules such as alcohols, glycerol, or formamide [139,140]. Therefore, the aggregation tendency is diminished when water is replaced by other solvents in the case of small-molecular-weight surfactants. In contrast, for block copolymers, the core-forming block can be incompatible with a wide variety of solvents, and therefore the tail transfer free energy contribution remains negative at appreciably large magnitude. Hence, significant aggregation of block copolymers is possible in a number of solvents. The aggregation phenomenon where entropy changes (hydrophobic effect) are important as in the case of conventional surfactants is replaced by an aggregation process where enthalpy effects are also very important in the case of block copolymer aggregates.

VIII. CONCLUSIONS

A quantitative approach to predicting micellar properties from the molecular structure of surfactant has been described in this chapter. No information derived from experiments on surfactant solutions is required for the predictive calculations. The approach combines the general thermodynamic principles of self-assembly with detailed molecular models for the various contributions to the free energy of micellization. Explicit analytical equations are developed for calculating each of these free energy contributions as a function of temperature. Methods for obtaining the few molecular constants appearing in these equations have been illustrated. A simple approach to calculating the aggregation properties via the maximum-term method, without having to perform detailed micelle size distribution calculations, is described. The quantitative approach is illustrated via predictive calculations performed on numerous surfactants, binary surfactant mixtures, and mixtures of surfactants with nonionic polymer. Surfactants having one or two tail groups, those possessing nonionic, anionic, cationic or zwitterionic headgroups, surfactants with fluorocarbon tails, and mixtures of hydrocarbon and fluorocarbon surfactants have been considered for the illustrative calculations. The formation of spherical micelles, globular micelles, rodlike micelles, and spherical bilayer vesicles have been investigated.

The quantitative approach has been extended also to block copolymer aggregates taking into account the polymeric nature of both the headgroups and the tail groups of the block copolymer. The behavior of block copolymers is seen as analogous to that of surfactants, but with broader aggregation capabilities in a variety of solvent systems. The quantitative approach

described in this chapter has a broad scope as demonstrated by its extension to treat other self-assembly phenomena such as micellization in polar non-aqueous solvents [139,140], solubilization of hydrocarbons in micelles [16,19], the formation of droplet-type and bicontinuous-type microemulsions [141], and micelle formation at solid–liquid interfaces [142,143]. An approach similar to that discussed in this chapter for calculating the aggregation behavior of surfactants and surfactant mixtures, but with some variations in the free energy expressions, has been discussed in a number of papers by Blankschtein and co-workers [39–41,144–147].

ACKNOWLEDGMENTS

Professor Ruckenstein has collaborated in many parts of the work discussed here as can be inferred from the cited references. The author has benefited from numerous discussions with him.

REFERENCES

1. C. Tanford. The Hydrophobic Effect. New York: Wiley, 1973.
2. C. Tanford. J. Phys. Chem., 78: 2469, 1974.
3. C. Tanford. In KL Mittal, ed. Micellization, Solubilization, Microemulsions. New York: Plenum Press, 1977, p 119.
4. K. Shinoda. ed. Solvent Properties of Surfactants. New York: Marcel Dekker, 1970.
5. P. Mukerjee. Adv. Colloid Interface Sci. 1:241, 1967.
6. P. Mukerjee. J. Phys. Chem., 73:2054, 1969.
7. P. Mukerjee. J. Phys. Chem., 76:565, 1972.
8. P. Mukerjee. J. Pharm Sci., 68:972, 1974.
9. P. Mukerjee. In KL Mittal, ed. Micellization, Solubilization, Microemulsions. New York: Plenum Press, 1977. p133
10. E. Ruckenstein and R. Nagarajan, J. Phys. Chem., 79:2622, 1975.
11. R. Nagarajan and E. Ruckenstein, J. Colloid Interface Sci., 60:221, 1977.
12. R. Nagarajan and E. Ruckenstein, In K.L. Mittal, ed. Micellization, Solubilization, Microemulsions. New York:Plenum Press, 1977. p 171.
13. R. Nagarajan and E. Ruckenstein, J. Colloid Interface Sci., 71:580, 1979.
14. E. Ruckenstein and R. Nagarajan, J. Phys. Chem., 85:3010, 1981.
15. R. Nagarajan. Adv. Colloid Interface Sci., 26:205, 1986.
16. R. Nagarajan and E. Ruckenstein, Langmuir, 7:2934, 1991.
17. H.V. Tartar. J. Phys. Chem., 55:1195, 1955.
18. J.N. Israelachvili, J.D. Mitchell, and B.W. Ninham. J. Chem. Soc. Faraday Trans. II, 72:1525, 1976.
19. R. Nagarajan and E. Ruckenstein. In J.V. Sengers, R.F. Kayser, C.J. Peters, and H.J. White, Jr, eds. Self-Assembled Structures. In Equations of State for Fluids and Fluid Mixtures. Amsterdam: Elsevier, 2000, Ch. 15, pp 589–749.

20. E. Ruckenstein and R. Nagarajan. J. Colloid Interface Sci., 57:388, 1976.
21. R. Nagarajan and E. Ruckenstein. J. Colloid Interface Sci., 91:500, 1983.
22. R. Nagarajan. Colloids Surfaces A:Physicochem Eng. Aspects, 71:39, 1993.
23. G.S. Hartley. Aqueous Solutions of Paraffin Chain Salts. Paris:Hermann, 1936.
24. D.G. Hall. J. Chem. Soc. Faraday Trans. I, 77:1121, 1981.
25. D.G. Hall. J. Chem. Soc. Faraday Trans. I, 81:885, 1985.
26. R. Nagarajan. Langmuir, 10:2028, 1994.
27. R. Nagarajan. J. Colloid Interface Sci., 90:477, 1982.
28. D.W.R. Gruen. Biochim. Biophys. Acta, 595:161, 1980.
29. D.W.R. Gruen. J. Colloid Interface Sci., 84:281, 1981.
30. D.W.R. Gruen. J. Phys. Chem., 89:146, 1985.
31. K.A. Dill and P.J. Flory. Proc. Natl. Acad. Sci. USA, 77:3115,1980.
32. K.A. Dill and P.J. Flory. Proc Natl. Acad. Sci. USA, 78:676, 1980.
33. K.A. Dill and R.S Cantor. Macromolecules, 17:380, 1984.
34. R.S. Cantor and K.A. Dill. Macromolecules, 17:384, 1984.
35. K.A. Dill, D.E. Koppel, R.S. Cantor, J.D. Dill, D. Bendedouch, and S.H. Chen. Nature, 309:42,1984.
36. A. Ben-Shaul, I. Szleifer, and W.M. Gelbart. Proc. Natl. Acad. Sci. USA, 81:4601, 1984.
37. A. Ben-Shaul, I. Szleifer, and W.M. Gelbart. J. Chem. Phys., 3:3597, 1985.
38. A. Ben-Shaul and W.M. Gelbart. Rev. Phys. Chem., 36:179, 1985.
39. S. Puvvada and D. Blankschtein. J. Chem. Phys., 92:3710, 1990.
40. S. Puvvada and D. Blankschtein. J. Phys. Chem., 96:5567,1992.
41. S. Puvvada and D. Blankschtein. In P.M. Holland and D.N. Rubingh, eds. Mixed Surfactant Systems. ACS Symposium Series 501, Washington DC: American Chemical Society, 1992, p 96.
42. R. Nagarajan. Langmuir, 18:31, 2002.
43. M.H. Abraham. J. Chem. Soc. Faraday Trans. I, 80:153, 1984.
44. M.H. Abraham and E. Matteoli. J. Chem. Soc. Faraday Trans. I, 84:1985, 1988.
45. P. Mukerjee and T. Handa. J. Phys. Chem., 85:2298, 1981.
46. A.N. Semenov. Soviet Phys. JETP, 61:733, 1985.
47. L.A. Girifalco and R.J. Good. J. Phys. Chem., 61:904, 1957.
48. R.J. Good and E. Elbing. Ind. Eng. Chem., 62:54,1970.
49. CRC Handbook of Chemistry, Physics, 60th ed. Boca Raton, FL:CRC Press Inc.
50. J.A. Beunen and E. Ruckenstein. J. Colloid Interface Sci., 96:469, 1983.
51. E. Ruckenstein and J.A. Beunen. Langmuir, 4:77, 1988.
52. D.F.. Evans and B.W. Ninham. J. Phys. Chem., 87:5025,1983.
53. P.J. Flory. Principles of Polymer Chemistry. Ithaca, NY: Cornell University Press, 1962.
54. G.N. Malcolm and J.S. Rowlinson, Trans. Faraday Soc., 53:921, 1957.
55. J. Sheu. Thermodynamics of Phase Separation in Aqueous Polymer-Surfactant-Electrolyte Solutions, Ph.D. Dissertation, The Pennsylvania State University, 1983.

56. R. Kjellander and E. Florin. J. Chem. Soc. Faraday Trans. I, 77:2053, 1981.
57. B.A. Mulley. In M.J. Schick, Ed. Nonionic Surfactants. New York: Marcel Dekker, 1967 Ch. 13.
58. P.G. de Gennes. Scaling Concepts in Polymer Physics. Ithaca, NY: Cornell University Press, 1979.
59. R. Defay, I. Prigogine, A. Bellemans, and D.H. Everett. Surface Tension, Adsorption. New York: Wiley, 1966.
60. K.S. Siow and D. Patterson. J. Phys. Chem., 77:356, 1973.
61. S. Wu. Polymer Interface, Adhesion. New York: Marcel Dekker, 1982.
62. I.V. Rao and E. Ruckenstein. J. Colloid Interface Sci., 119:211, 1987.
63. R.D. Dunlop and R.L. Scott, J. Phys. Chem., 66:631, 1962.
64. J.H. Hildebrand and J. Dymond. J. Chem. Phys., 46:624, 1967.
65. N. Funasaki and S. Hada. J. Phys. Chem., 87:342, 1983.
66. K. Shinoda, T. Yamanaka, and K. Kinoshita. J. Phys. Chem., 63:648, 1959.
67. K. Shinoda, T. Yamaguchi, and R. Hori. Bull. Chem. Soc. Japan, 34:237, 1961.
68. B. Focher, G. Savelli, G. Torri, G. Vecchio, D.C. McKenzie, D.F. Nicoli, and C.A. Bunton. Chem. Phys. Lett., 158:491, 1989.
69. K.W. Herrman, J. Colloid Interface Sci., 22:352, 1966.
70. P. Molyneux, C.T. Rhodes, and J. Swarbrick. Trans. Faraday Soc., 61:1043, 1965.
71. J. Swarbrick and J. Daruwala. J. Phys. Chem., 74:1293, 1970.
72. H.V. Tartar. J. Colloid Sci., 14:115, 1959.
73. J.F. Leibler and J. Jacobus. J. Phys. Chem., 81:130, 1977.
74. R.J. Williams, J.N. Philips, and K.J. Mysels. Trans. Faraday Soc., 51:728, 1955.
75. K.J. Mysels and L.H. Princen. J. Phys. Chem., 63:1696, 1959.
76. E.A.G. Aniansson, S.N. Wall, M. Almgren, H. Hoffmann, I. Kielmann, W. Ulbricht, R. Zana. J. Lang, and C. Tondre, J. Phys. Chem., 80:905, 1976.
77. Y. Moroi, N. Nishikido, H. Uehara, and R. Matuura. J. Colloid Interface Sci., 50:254, 1975.
78. V.A. Volkov. Colloid J. USSR, 38:610, 1976.
79. P.J. Missel, N. Mazer, M.C. Carey, and G.B. Benedek. J. Phys. Chem., 93:8354, 1989.
80. P. Becher. In M.J. Schick, ed. Nonionic Surfactants. New York: Marcel Dekker, 1967, Ch. 15.
81. P. Becher. In J.T.G. Overbeek, ed. Chemistry, Physics, Application of Surface Active Substances. New York: Gordon, Breach Science Publishers, 1964, p 621.
82. P. Becher and H. Arai. J. Colloid Interface Sci., 27:634, 1968.
83. K. Meguro, M. Ueno, and K. Esumi. In M.J. Schick, ed. Nonionic Surfactants—Physical Chemistry. New York: Marcel Dekker, 1987, p 109.
84. J.L. Woodhead, J.A. Lewis, J.N. Malcolm, and I.D. Watson. J. Colloid Interface Sci., 79:454, 1981.
85. M.J. Schick and A.H. Gilber, J. Colloid Interface Sci., 20:464, 1965.
86. K.N. Reddy, A. Foster, M.G. Styring, and C. Booth. J. Colloid Interface Sci., 136:588, 1990.
87. B.W. Barry and D.I.D. El-Aini. J. Colloid Interface Sci., 54:339, 1976.

88. B.W. Barry, D.I.D. El-Aini, and C.T. Rhodes. J. Colloid Interface Sci., 54:348, 1976.
89. P.H. Elworthy and C.B. Macfarlane. J. Chem. Soc., 537, 1962.
90. P.H. Elworthy and C.B. Macfarlane. J. Chem. Soc., 907, 1963.
91. C. Tanford, Y. Nozaki, and M.F. Rhode. J. Phys. Chem., 81:1555, 1977.
92. R. Ottewill, C.C. Storer, and T. Walker. Trans Faraday Soc., 63:2796, 1967.
93. R. Zana and C. Weill. J. Physique Lett., 46:L-953, 1985.
94. R. Nagarajan. Langmuir, 1:331, 1985.
95. R. Nagarajan. In P.M. Holland and D.N. Rubingh, eds. Mixed Surfactant Systems. ACS Symposium Series 501, Washington, DC:ACS, 1992, p 54.
96. I.V. Rao and E. Ruckenstein. J. Colloid Interface Sci., 113:375, 1986.
97. J.H. Hildebrand, J.M. Prausnitz, and R.L. Scott. Regular and Related Solutions. New York: Van Nostrand Reinhold Company, 1970.
98. J.M. Prausnitz. Molecular Thermodynamics of Fluid-Phase Equilibria. Englewood Cliffs, NJ: Prentice-Hall, 1969.
99. A.F.M. Barton. Handbook of Solubility Parameters, Other Cohesion Parameters. Boca Raton, FL:CRC Press, 1983.
100. P.M. Holland and D.N. Rubingh. J. Phys. Chem., 87:1984, 1983.
101. K.J. Mysels and R.J. Otter. J. Colloid Sci., 16:462, 1961.
102. L. Shedlowsky, C.W. Jakob, and M.B. Epstein. J. Phys. Chem., 67:2075, 1963.
103. I. Garcia-Mateos, M.M. Velazquez, and L.J. Rodriguez. Langmuir 6:1078, 1990.
104. K. Shinoda. J. Phys. Chem., 58:541, 1954.
105. S. Bucci, C. Fagotti, V. Degiorgio, and R. Piazza. Langmuir, 7:824, 1991.
106. A. Malliaris, W. Binana-Limbele, and R. Zana. J. Colloid Interface Sci., 110:114, 1986.
107. K.L. Stellner, J.C. Amante, J.F. Scamehorn, and J.H. Harwell. J. Colloid Interface Sci., 123:186, 1988.
108. E.W. Kaler, A.K. Murthy, B.E. Rodriguez, and J.A.N. Zasadzinsky. Science, 245:1371, 1989.
109. L.L. Brasher, K.L. Herrington, and E.W. Kaler. Langmuir, 11:4267, 1995.
110. M .Bergström. Langmuir, 12:2454, 1996.
111. Y. Kondo, H. Uchiyama, N. Yoshino, K. Nishiyama, and M. Abe. Langmuir, 11:2380, 1995.
112. Y. Wada, Y. Ikawa, H. Igimi, T. Makihara, S. Nagadome, and G. Sugihara. Fukuoka University Science Reports, 19:173, 1989.
113. J.C.T. Kwak, ed. PolymerSurfactant Systems. New York: Marcel Dekker, 1998.
114. E.D. Goddard. Colloid Surf., 19:255, 1986.
115. I.D. Robb. In E.H. Lucassen-Reynders, ed. Anionic Surfactants—Physical Chemistry of Surfactant Action. New York: Marcel Dekker, 1981, p 109.
116. S. Saito. In M.J. Schick, ed. Nonionic Surfactants. New York: Marcel Dekker, 1987, p 881.
117. E.D. Goddard and K.P. Ananthapadhmanabhan, eds. Interactions of Surfactants with Polymer and Proteins. Boca Raton, FL: CRC Press, 1993.

118. R. Nagarajan. ACS Polymer Preprints, 22:33, 1981.
119. R. Nagarajan and B. Kalpakci. ACS Polymer Preprints, 23:41, 1982.
120. R. Nagarajan. Colloids Surf., 13:1, 1985.
121. R. Nagarajan and B. Kalpakci. In P.L. Dubin, ed. Microdomains in Polymer Solutions. New York: Plenum Press, 1985, p 368.
122. E. Ruckenstein, G. Huber, and H. Hoffmann. Langmuir, 3:382, 1987.
123. R. Nagarajan. J. Chem. Phys., 90:1980, 1989.
124. R. Nagarajan. Langmuir, 9:369, 1993
125. Z. Tuzar and P. Kratochvil. Adv. Colloid Interface Sci., 6:201, 1976.
126. C. Price. In I. Goodman, ed. Developments of Block Copolymers I. London: Applied Science Publishers, 1982, p 39.
127. G. Riess, P. Bahadur, and G. Hurtrez. In Encyclopedia of Polymer Science and Engineering. New York: Wiley, 1985, p 324.
128. P.G. de Gennes. In J. Liebert, ed. Solid State Physics. New York: Academic Press, 1978, Suppl. 14, p 1.
129. L. Leibler, H. Orland, and J.C. Wheeler. J. Chem. Phys., 79:3550, 1983.
130. J. Noolandi and M.H. Hong. Macromolecules, 16:1443, 1983.
131. D. Whitmore and J. Noolandi. Macromolecules, 18:657, 1985.
132. E. Helfand and Y. Tagami. J. Polym. Sci. B, 9:741, 1971.
133. E. Helfand and A.M. Sapse. J. Chem. Phys., 62:1327, 1975.
134. W.H. Stockmayer. J. Polym. Sci., 15:595, 1955.
135. R. Nagarajan and K. Ganesh, J. Chem. Phys., 90:5843, 1989.
136. H. Jacobson and W.H. Stockmayer. J. Chem. Phys., 18:1600, 1950.
137. P. Bahadur, N.V. Sastry, S. Marti, and G. Riess. Colloids and Surf., 16:337, 1985.
138. R. Nagarajan. Colloids and Surf. B Biointerfaces, 16:55, 1999.
139. R. Nagarajan and Chien-Chung Wang. J. Colloid Interface Sci., 178:471, 1996.
140. R. Nagarajan and Chien Chung Wang. Langmuir, 16:5242, 2000.
141. R. Nagarajan and E. Ruckenstein. Langmuir, 16:6400, 2000.
142. R.A. Johnson and R. Nagarajan. Colloids and Surf. A. Physicochem. Eng. Aspects, 167:31, 2000..
143. R.A. Johnson and R. Nagarajan. Colloids and Surf. A Physicochem. Eng. Aspects, 167, 21, 2000.
144. A. Naor and D. Blankschtein, J. Phys. Chem., 96:7830, 1992.
145. Y.J. Nikas and D. Blankschtein. Langmuir, 10:3512, 1994.
146. N.J. Zoeller, D. Blankschtein. Ind. Eng. Chem. Res., 34:4150, 1995.
147. P.K. Yuet and D. Blankschtein. Langmuir, 12:3802, 3819, 1996.